A STUDY OF APPLICABLE ENCODING METHODS for a GEOSTATIONARY ORBITING EXPERIMENTAL SATELLITE

A REPORT

from the space science and engineering center
the university of wisconsin-madison
madison, wisconsin

A STUDY OF APPLICABLE ENCODING METHODS for a GEOSTATIONARY ORBITING EXPERIMENTAL SATELLITE

F. G. Stremler
G. R. Redinbo*
N. Chu
S. Iyengar
A. Sethuraman

This Work has been Performed
under
NATIONAL OCEANIC and ATMOSPHERIC ADMINISTRATION
NATIONAL ENVIRONMENTAL SATELLITE SERVICES

Contract 3-35372

The Space Science and Engineering Center
The University of Wisconsin
1225 W. Dayton Street
Madison, Wisconsin 53706

February, 1975

*On Leave: January 1, 1974 - June 30, 1974

Preliminary Copy Submitted to NOAA on July 1, 1974

TABLE OF CONTENTS

ACKNOWLEDGEMENTS

We wish to thank Ms. Priscilla Lu of the Department of Computer Science for performing the computer calculations for Appendix A in this report. The help of Eric Smith and Dennis Phillips of the Space Science and Engineering Center in adapting the WINDCO program and Gary Chatters in the use of the McIDAS system is sincerely appreciated.

LIST OF FIGURES

LIST OF TABLES

I.

INTRODUCTION

This report contains results in the analysis of several proposed encoding schemes for the high-resolution visual channels of a geostationary orbiting satellite. Distributions of intensity levels of photographs taken on the Apollo VI mission were studied in an attempt to obtain some guidance on the methods used and are summarized in an appendix. Considerations of any of the proposed methods were constrained by the permissible complexity involved for satellite experiments.

Our approach has been to avoid adaptive encoding techniques for satellite use in which the encoding methods depend on the individual characteristics of the particular scene being scanned. While some of these techniques appear to offer promise, we feel that the "hard-wired" approach is more practical for satellite instrumentation at this time. Some adaptive methods are under consideration and investigation in research programs elsewhere and are listed in the references. Some also provide guided research areas for our graduate students and will be reported later.

The discussion of the encoding methods proposed and discussed in this report is not intended to represent an overall survey of all methods available. It is intended to be a presentation of what we feel are the best choices for satellite scanners in the very near future,together with their relative advantages and disadvantages.

II
DPCM ENCODING STUDIES

From observations of histogram data (see Appendix A) of Apollo VI pictures,it would appear that considerable savings in bandwidth might be made by encoding the differences between adjacent brightness levels rather than encoding the levels themselves. Here we investigate two rather easily implemented methods of doing this using differential pulse code modulation (DPCM) - sometimes referred to as predictive quantization. Block diagrams of some DPCM systems are shown in Figure 2.1.

In the first method considered (hereafter referred to as first-order DPCM, but also known as zero-order predictive quantization) the entire level is encoded in the first sample of each scan line, and then only the difference between adjacent samples is sent at each sample point for the remainder of the scan line. (Note that in our application the first samples taken in each satellite revolution correspond to very low light levels and should be easy to encode accurately for a fixed number of levels.) Implementation of first-order DPCM requires only the addition of one unit of digital delay in the satellite and is easily alterable to a "normal" mode of operation for back-up. Based on studies of histogram data, as discussed in Appendix A, we felt it was reasonable to choose a 4-bit output (i.e., three bits plus sign bit) using this method.

Because our Apollo VI picture data are digitized to 8-bit accuracy, we have made some trial runs reducing the 8-bit picture data to 6-, 4-, and 2-bit output using first-order DPCM. (Note that one bit in each is reserved for sign, so 6-bit is really 5-bit plus sign.) As a fairly severe case study for cloud patterns, we chose the lower right quarter of Apollo AS6-2-877. (This photograph is shown in Figure 5.2a.)

The optics preceding the photomultiplier tube (PMT) in the visual scanner of the satellite acts as a spatial filter on the observed scene. The

response of this two-dimensional filter, based on measurement data, is discussed in Appendix B.

The output of the PMT in the visual scanner is applied to an electrical filter. The filter used in the synchronous meteorological satellite (SMS) placed into orbit in May 1974 uses a modified fifth-order Chebychev filter with a -3dB bandwidth B of 225 kHz. Thus the along-scan time resolution is on the order of:

$$t_r \approx 1/_{(2B)} = 2.22 \ \mu\text{-sec.}$$

The satellite spin rate is 100 rpm. For a satellite altitude of 19,360 n. mi. (22,300 statute miles), this gives a spatial resolution on the order of:

$$d_r \approx (2.22 \times 10^{-6}) \ (19360)(100)(2\pi/60) = 0.45 \text{ n. mi.}$$

The Apollo VI picture data are sampled in a 1024 x 1024 format so the spacing for each sample is about .08 n.mi. We can smooth each data scan line to a resolution of about 0.45 n.mi. by use of the SMS filter. Alternatively, we can smooth the Apollo VI data in two dimensions (along-scan and across-scan) to about 0.4 n.mi. in order to simulate the optical system. This subroutine is referred to in this report as "SMSOPT" and is described briefly in Appendix B. Filtering (whether electrical or optical) tends to smooth out the rapid fluctuations of the signal and makes the encoding problem easier. To make the input data correspond more closely to SMS data, we have also divided the Apollo data by four and truncated to simulate 6-bit (linearly quantized) data. Whenever this has been done, it is noted on the corresponding graph.

Some graphs of reconstructions using first-order DPCM and retaining 6-, 4-, and 2-bit (difference) accuracies are shown in Fig. 2.2. The scan line chosen for these comparisons is line no. 521, in the lower right quarter of Apollo AS6-2-877. The first plot in Fig. 2.2 shows the scan line, digitized to 8 bits, with reconstructions obtained by dropping 2-, 4-, and 6-bits. Note there is no error incurred, as expected, by dropping 2 bits. The second plot

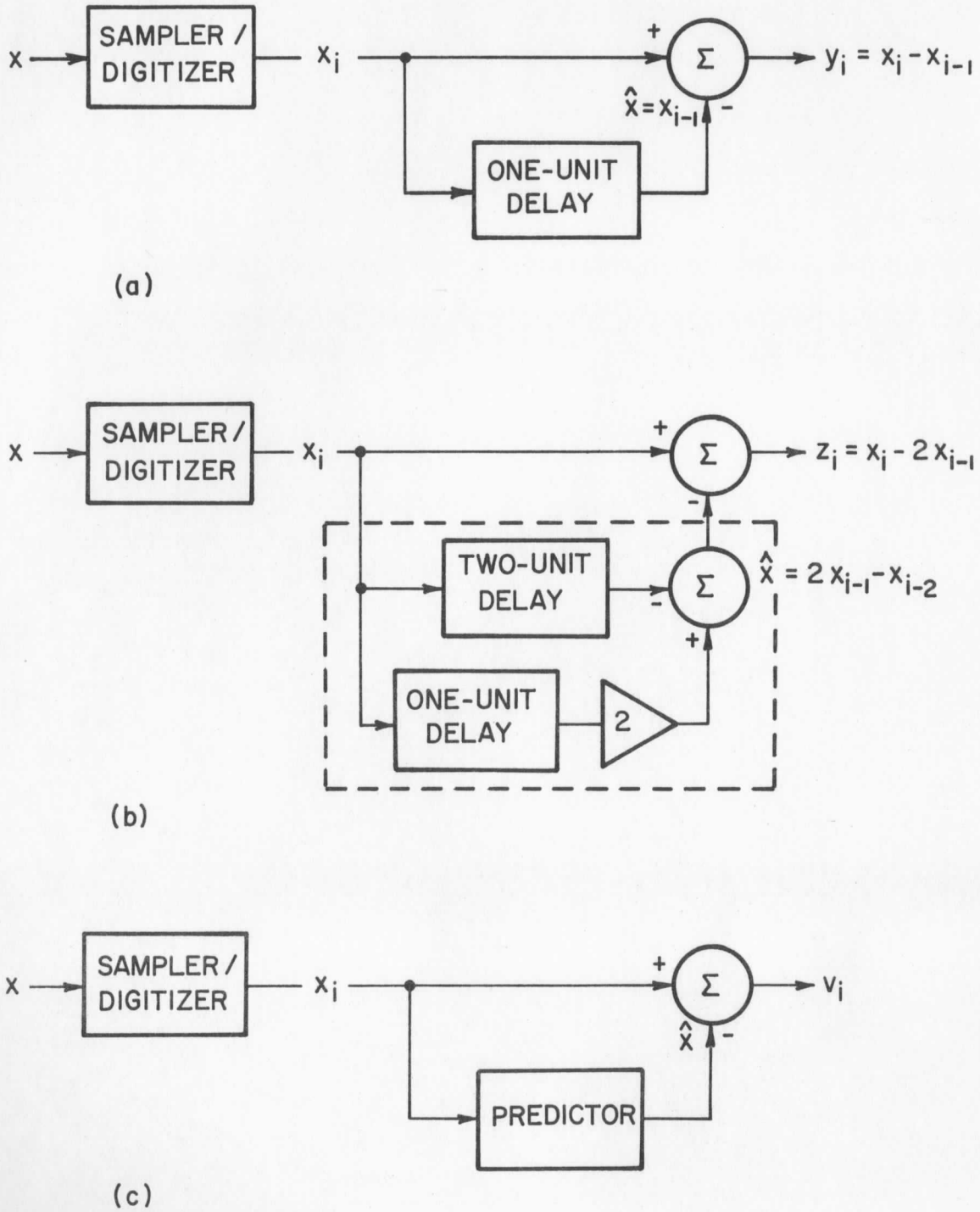

Figure 2.1. Block Diagrams of Some DPCM Systems:
(a) First-order DPCM (zero-order predictor);
(b) Second-order DPCM (first-order predictor);
(c) General DPCM (predictive quantizing).

is an expanded scale of the first half of the scan line. Plot 3 repeats using the current SMS filter to smooth the scan line first; plot 4 is the same reconstruction but plotted to an expanded scale. Note the dropping of two bits makes no noticeable difference in the reconstruction. It is interesting to note savings of about 2 bits/sample have been reported for high-quality television pictures using DPCM [4].

Plot 5 in Fig. 2.2 shows the same scan line after the optics filtering discussed in Appendix B. This plot demonstrates the effect of the optics smoothing for 8-bit input data.

In plots 6 and 7 the input picture data is first reduced to 6-bit accuracy. This reduces the reconstruction error in going to the 4-bit output accuracy without the optics filtering and eliminates the error with the optics filtering.

First-order DPCM is well-suited to situations in which the input data varies little from sample to sample. Large differences between samples, however, will tend to overflow the output accuracy and thus the decoder will incorrectly reconstruct the remainder of the scan line with a constant level error. In our case, that happens whenever a change greater than $2^3 = 8$ input levels occurs between adjacent samples in the data. When comparing against a constant output accuracy (in our case, 4-bits), quantizing the input data more coarsely and/or smoothing the input data with one- or two-dimensional filtering will reduce the overflow problem. The graphs in Fig. 2.2 illustrate this.

To investigate the overflow problem, we generated some statistics using first-order DPCM on the lower right quarter of Apollo AS6-2-877. The output accuracy was held to 4 bits (3 bits plus sign). With the possibility that the highest level (in our case, ±7) could be used as an overflow flag, we kept a count of: a) the number of times a "7" was used; b) the number of

overflows; c) the number of times an overflow occured twice consecutively; d) three times consecutively; and e) four times consecutively. These statistics are tabulated in Table 2.1.

Another encoding possibility is to use a second-order DPCM system (first-order predictive quantizer). Although the width or spread of the histogram data in Appendix A is not reduced as much going from first-differences to second-differences when compared to going from the levels to the first-differences, there is some reduction. The second-order DPCM system requires two units of digital delay, as shown in Fig. 2.1, and is almost as easy to implement as first-order DPCM. An advantage is it is well-suited to ramp-type input signals; a disadvantage is it will generate a ramp-type signal if an error is made. The lack of stability of a second-order DPCM system becomes a problem if adequate "damping" is not provided. Thus the possible increased efficiency comes with a possible stability penalty. In addition, of course, two initial conditions are required instead of one.

Some overflow statistics using second-order DPCM and a 4-bit output are shown in Table 2.1b. Note the number of overflows has been reduced drastically compared with the first-order system. However, each overflow is very detrimental, as will be seen shortly, if uncorrected.

Graphs showing both first- and second-order DPCM encoding/decoding retaining four bits (i.e., three plus sign) are shown in Fig. 2.3. Plot 2 is an expanded scale of plot 1; both demonstrate the instability of the second-order system. Plot 3 includes both SMSOPT and the current SMS filter. Note with the addition of the optics and filtering the second-order system is now stable and very accurate.

Beginning with plot 4, the input data is quantized linearly to 6-bits. Although improved, the second-order system again is not stable on the raw picture data. However, when the optics smoothing is added in plot 5, the

TABLE 2.1.

DPCM Overflow Statistics for the Lower Right Quarter of Apollo AS6-2-877 (2^{18} = 262,144 points). Four-bit code word (3 + sign); "7" used both for code and for overflow flag.

(a) First-order DPCM

Description	# overflow symbols	actual # of overflows	Seq. of 2	Seq. of 3	Seq. of 4
8-bit data, raw	88,461	82,366	47,780	26,572	15,430
8-bit data, filtered line-by-line by current SMS filter	33,592	29,638	24,044	15,936	9,230
8-bit data, filtered by SMSOPT	17,751	14,406	12,679	8,470	4,963
6-bit data, raw	12,999	10,758	3,725	544	92
6-bit data, filtered by SMSOPT	512	0	0	0	0

(b) Second-order DPCM

Description	# overflow symbols	actual # of overflows	Seq. of 2	Seq. of 3	Seq. of 4
8-bit data, raw	647	55	26	5	1

second-order DPCM system gives perfect reproduction on the scan line attempted (surpassing the performance of the first-order system).

The use of the SMSOPT smoothing without changing the sampling rate results in over-sampling. The optics smoothing reduces the picture resolution by a factor of almost five, so the sampling rate must be decreased by the same amount to obtain independent samples. The present SMS visual channel does just that. Therefore, to make a fair comparison, we have rerun the DPCM overflow statistics with the SMSOPT smoothing and then taken every fifth point. The results are shown in Table 2.2. Note now the performance of the second-order DPCM system is strictly inferior to that of the first-order DPCM system.

From these and other examples we have run, the statistical results of using the Apollo VI picture data directly or using the SMSOPT smoothing and then taking every fifth sample point are very similar. Thus, we shall prefer to use the Apollo VI data directly in our encoding studies in the remainder of this report.

Our conclusions here so far are that both first-order and second-order DPCM systems yield improved performance on 6-bit Apollo VI picture data when used with optics smoothing and 4-bit output. Both systems are relatively easy to implement. It appears the 6-bit to 4-bit reduction is reasonable and a safe assumption. Some further reductions are feasible and it all depends how safe a design one wishes. It appears, however, any further substantial bandwidth reduction is not very realistic using DPCM.

The above systems are quite straight-forward to implement and efficient when the data samples are highly correlated. If this is not the case, then dependence on the past values should not be weighted as high and, in the extreme case, be completely neglected. Therefore, an optimum DPCM system is adaptive and adjusts the difference encoding depending on the correlation of the samples. This type of system is illustrated in block-diagram form in

TABLE 2.2.

DPCM Overflow Statistics for Lower Right Quarter of Apollo AS-6-2-877.
[SMSOPT smoothing and SMS sampling rate (every fifth point); 10,404 sample points.]

(a) First-order DPCM

Description	# overflow symbols	actual # of overflows	Seq. of 2	Seq. of 3	Seq. of 4
8-bit to 4-bit	4856	4560	2990	1915	1237
6-bit to 4-bit	918	686	210	59	14
6-bit to 3-bit	3072	2476	1469	768	397

(b) Second-order DPCM

Description	# overflow symbols	actual # of overflows	Seq. of 2	Seq. of 3	Seq. of 4
8-bit to 4-bit	5715	5334	3835	2670	1925
6-bit to 4-bit	1596	1311	633	270	136

Fig. 2.1c. Essentially, this system contains an optimum predictor which acts on the past data to estimate the most probable present value. The difference between the two is sent. While more efficient, this system is also more difficult to build and maintain remotely. We have not considered systems which must compute correlation coefficients to optimize their encoding on board the satellite for this reason.

The tendency for DPCM systems to overflow is a severe disadvantage when the scan lines are long, as in the case of the SMS. Two picture reconstructions for first- and second-order DPCM with overflow problems are shown in Fig. 2.4 In Fig. 2.4a, a first-order DPCM system was used. In Fig. 2.4b, a second-order DPCM was used after SMS optics and electrical filtering, but every fifth point was taken so that the samples were independent.

The overflow problem can be reduced and even eliminated if the bit reduction is lessened or more stringent filtering is employed. Both were considered not viable alternatives and decrease the efficiency of this encoding method.

Another alternative is to detect the overflow condition and correct for it. We have developed an algorithm for doing this using a stand-by accumulator, as shown in Table 2.3.

TABLE 2.3

Algorithm of Accumulator Subroutine for First-Order DPCM

For sequence of data points IG(1), IG(2), IG(3), ..., IG (N):

1. Set: ACCUMULATOR = IG(1)
2. For k = 2 to N, DO:
   Set: BUFFER = IG(k)
   REMAINDER = BUFFER - ACCUMULATOR
   IF: REMAINDER $\leq$ 7, Go to Step 3
   OUTPUT = sign of REMAINDER times 7
   ACCUMULATOR = ACCUMULATOR + OUTPUT
   Go to Step 2 to repeat the DO loop
3. OUTPUT = REMAINDER
   ACCUMULATOR = BUFFER
   Go to Step 2 to repeat the DO loop

The accumulator scheme works as follows. A detector for the count of $2^3-1=7$ -- consisting of three AND gates -- is used to detect a potential overflow condition. If the "seven" detector is not activated, the system operates like a conventional DPCM system with the exception that the difference is always loaded in a buffer and held to the next sample point, then "dumped" and reloaded. When the "seven" detector activates, it disables the "dump" and the buffer acts like an accumulator. The system continues to take "sevens" out of the accumulator until the difference is less than seven, whereupon the system reverts to its normal mode of operation. Thus the accumulator system acts like a nonlinear low-pass filter and tends to round off the sharp edges of clouds, but only if the contrast is high. For lower contrast, all frequency components are transmitted.

Use of the stand-by accumulator with a first-order DPCM system is shown in Fig. 2.5 Note even though the system temporarily overflows, most noticeably when going from 8-bit data to 4-bit data, it always regains the correct operating levels. This is in direct contrast to first-order DPCM without the accumulator, where each overflow results in an operating level error which persists for the remainder of a scan line. Two possible configurations for implementing the stand-by accumulator are shown in block-diagram form in Fig. 2.6.

Summarizing, the use of first-order DPCM allows a decrease in bandwidth on Apollo VI picture data of about 33%. Use of second-order DPCM allows some additional decrease, but not enough to warrant the potential stability problems which may occur. The overflow problem is serious for long scan lines but can be remedied with a stand-by accumulator. This accumulator is simple and easily realized using reliable digital logic circuitry.

The use of delta modulation -- which is basically a one-bit (i.e., sign bit only) first-order DPCM system -- was also considered. This encoding system is extremely simple to implement and, if operated fast enough, has the desirable

features of DPCM with accumulator. However, just to match the intensity resolution of four-bit DPCM requires an increase in the clocking and multiplexing rates by a factor of eight. These speeds were judged excessive for a multiple-scanner system. Generally, it has also been found delta modulation requires slightly greater bandwidth than PCM for fairly high fidelity requirements.

FIGURE 2.2. PLOTS OF FIRST-ORDER DPCM ENCODING/DECODING COMBINATIONS FOR APOLLO AS6-2-877.

Notes:
1. Solid line indicates input data scan line (digitized to 8-bits unless marked otherwise).
2. Dashed lines represent dropping bits after subtraction, as indicated.
3. Input data accuracy is 8-bits (i.e., 256 levels) unless specified.
4. Scan line used is line # 521, elements 513-1024.

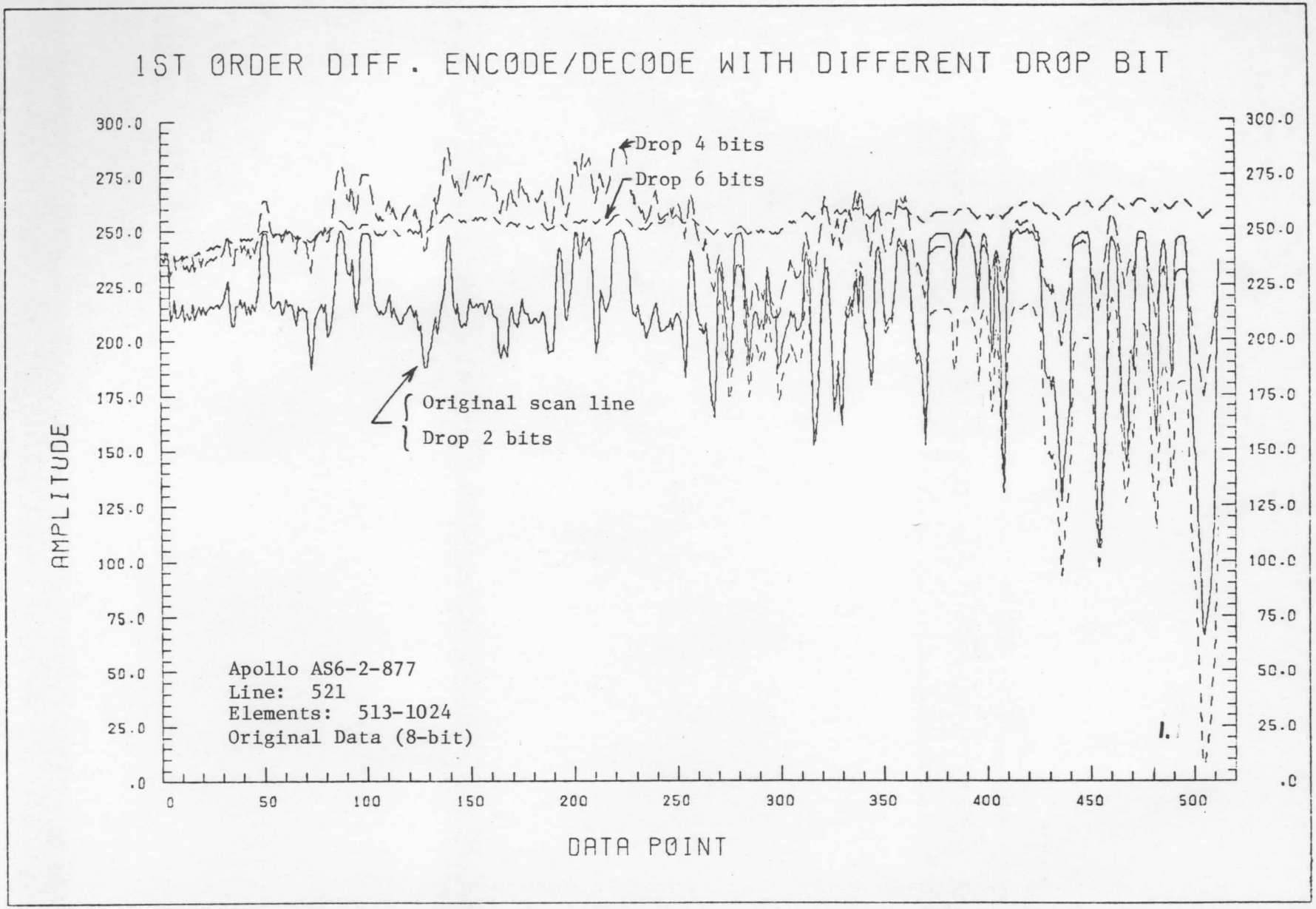
1ST ORDER DIFF. ENCODE/DECODE WITH DIFFERENT DROP BIT
Drop 4 bits
Drop 6 bits
Original scan line
Drop 2 bits
Apollo AS6-2-877
Line: 521
Elements: 513-1024
Original Data (8-bit)
AMPLITUDE
DATA POINT
300.0
275.0
250.0
225.0
200.0
175.0
150.0
125.0
100.0
75.0
50.0
25.0
.0
0
50
100
150
200
250
300
350
400
450
500

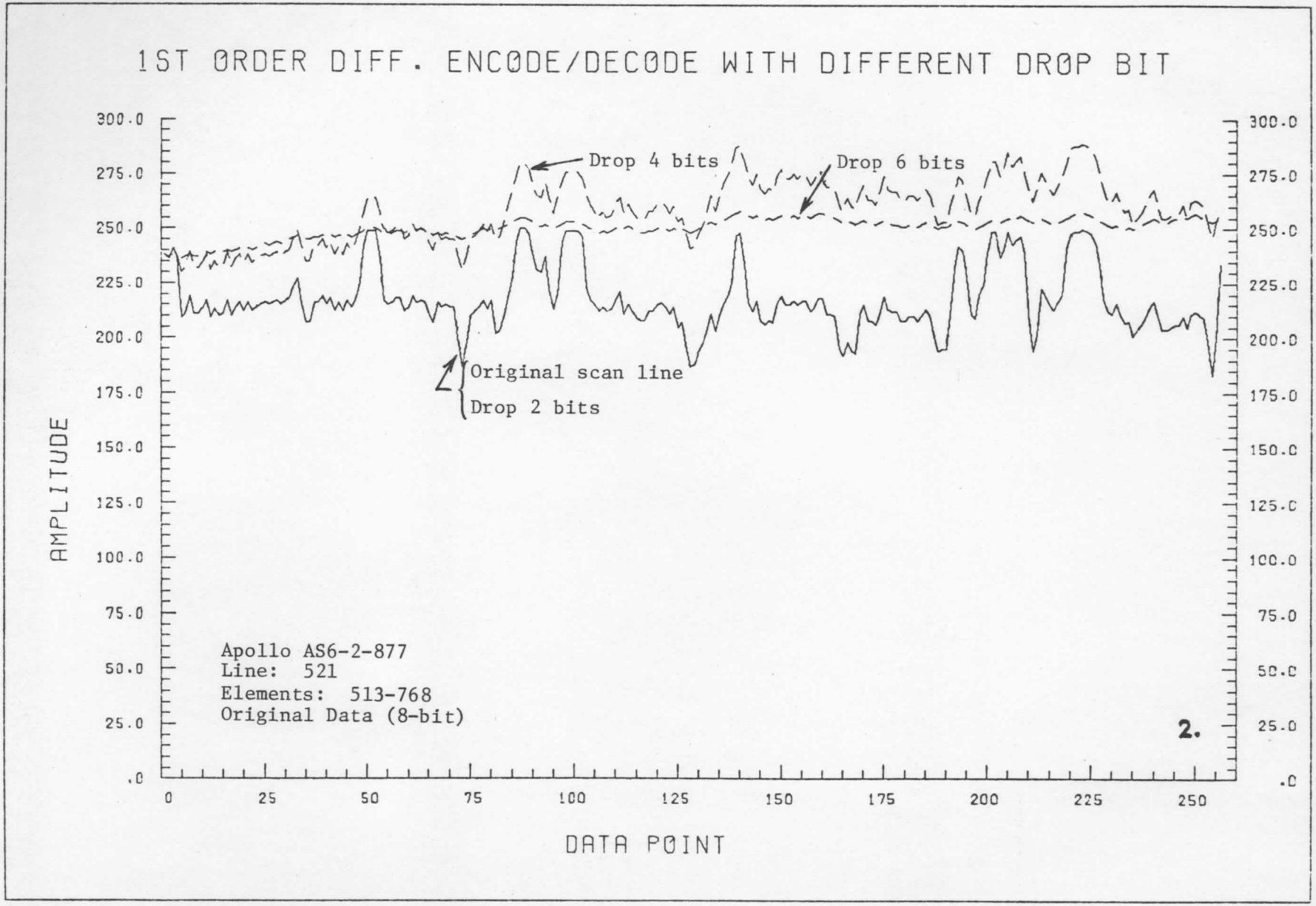
1ST ORDER DIFF. ENCODE/DECODE WITH DIFFERENT DROP BIT
Drop 4 bits
Drop 6 bits
Original scan line
Drop 2 bits
Apollo AS6-2-877
Line: 521
Elements: 513-768
Original Data (8-bit)
2.
AMPLITUDE
DATA POINT
300.0
275.0
250.0
225.0
200.0
175.0
150.0
125.0
100.0
75.0
50.0
25.0
.0
0
25
50
75
100
125
150
175
200
225
250

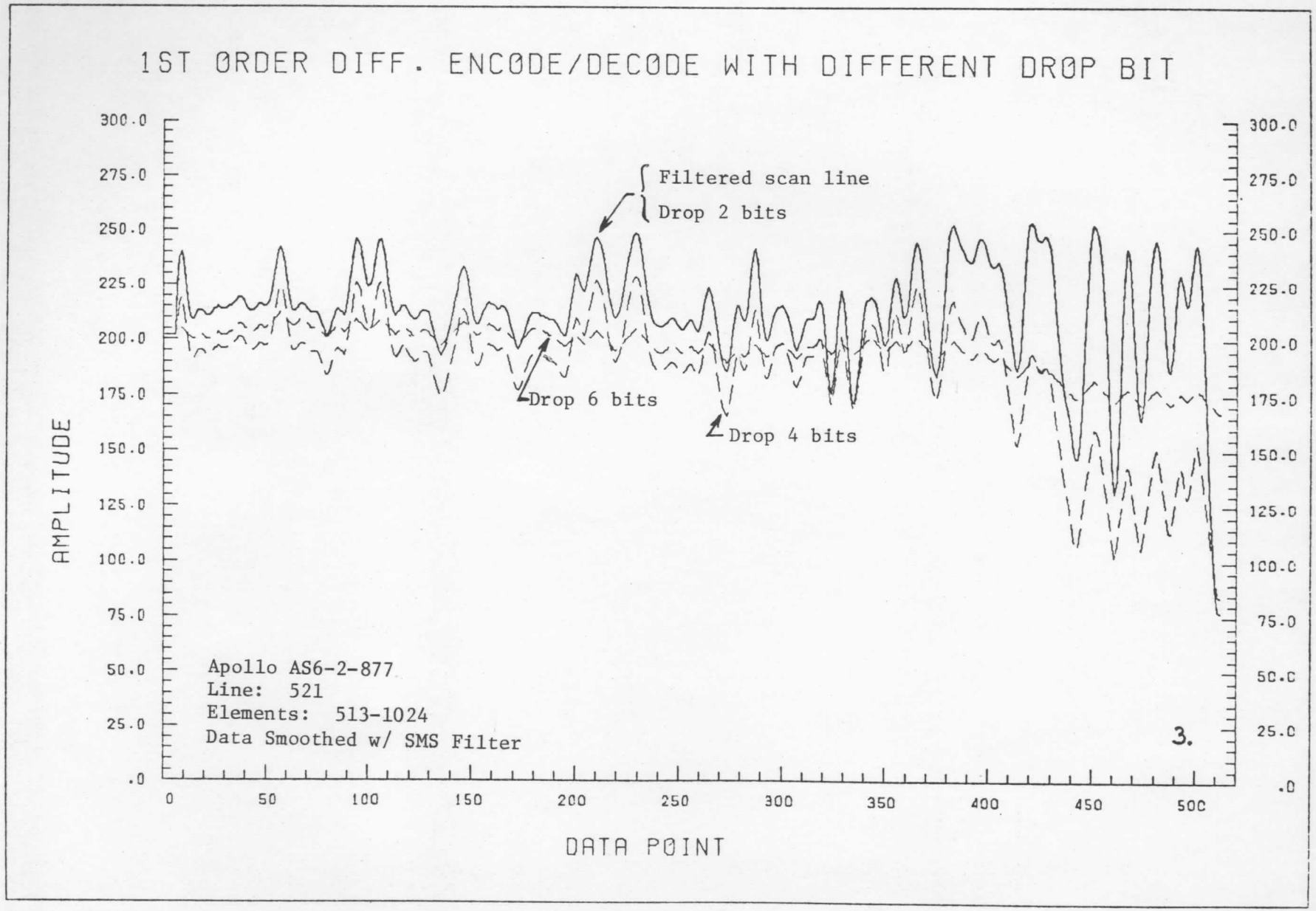
1ST ORDER DIFF. ENCODE/DECODE WITH DIFFERENT DROP BIT
AMPLITUDE
DATA POINT
300.0
275.0
250.0
225.0
200.0
175.0
150.0
125.0
100.0
75.0
50.0
25.0
.0
0
50
100
150
200
250
300
350
400
450
500
Filtered scan line
Drop 2 bits
Drop 6 bits
Drop 4 bits
Apollo AS6-2-877
Line: 521
Elements: 513-1024
Data Smoothed w/ SMS Filter
3.

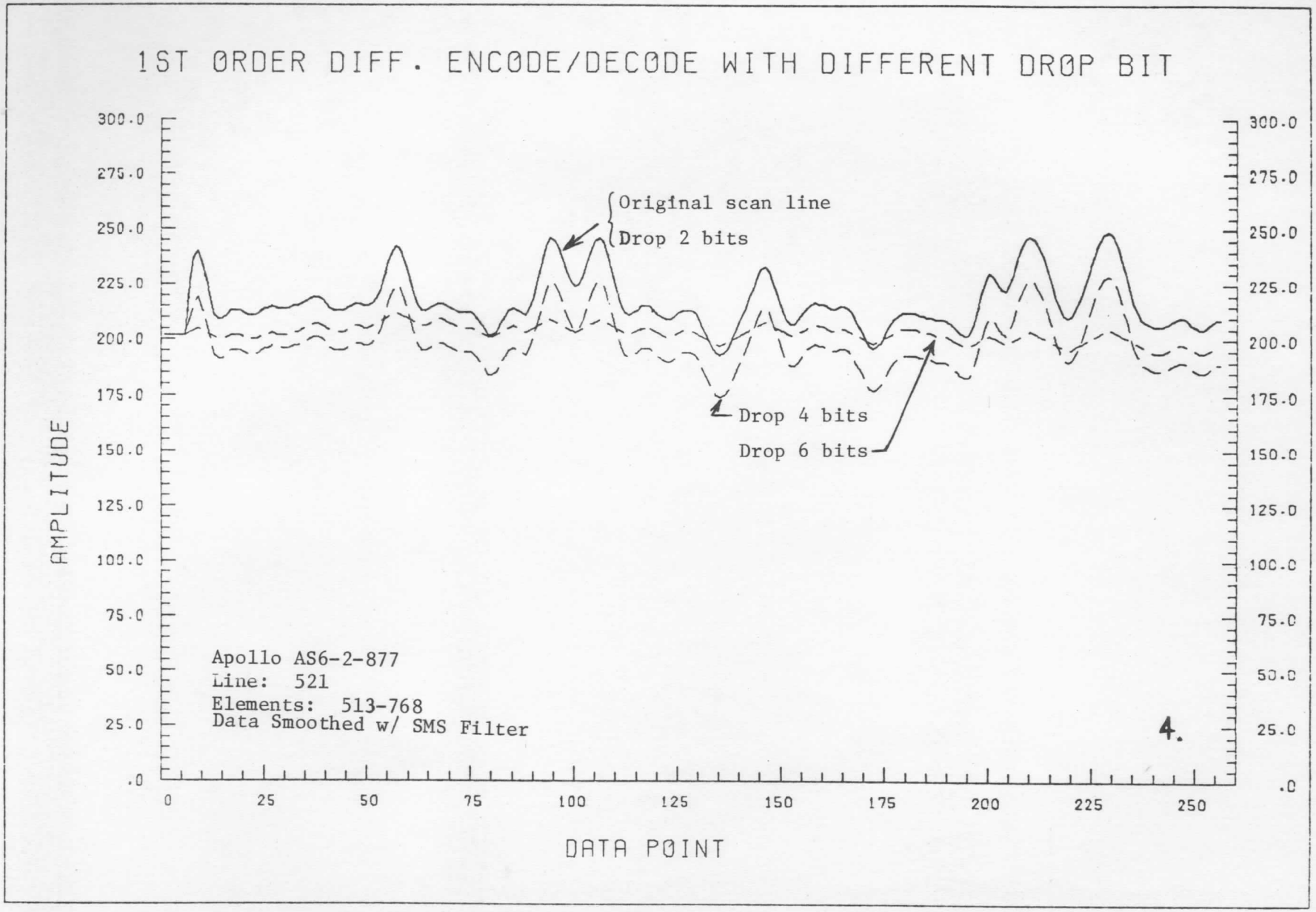
1ST ØRDER DIFF. ENCØDE/DECØDE WITH DIFFERENT DRØP BIT
AMPLITUDE
DATA PØINT
300.0
275.0
250.0
225.0
200.0
175.0
150.0
125.0
100.0
75.0
50.0
25.0
.0
0
25
50
75
100
125
150
175
200
225
250
Original scan line
Drop 2 bits
Drop 4 bits
Drop 6 bits
Apollo AS6-2-877
Line: 521
Elements: 513-768
Data Smoothed w/ SMS Filter
4.

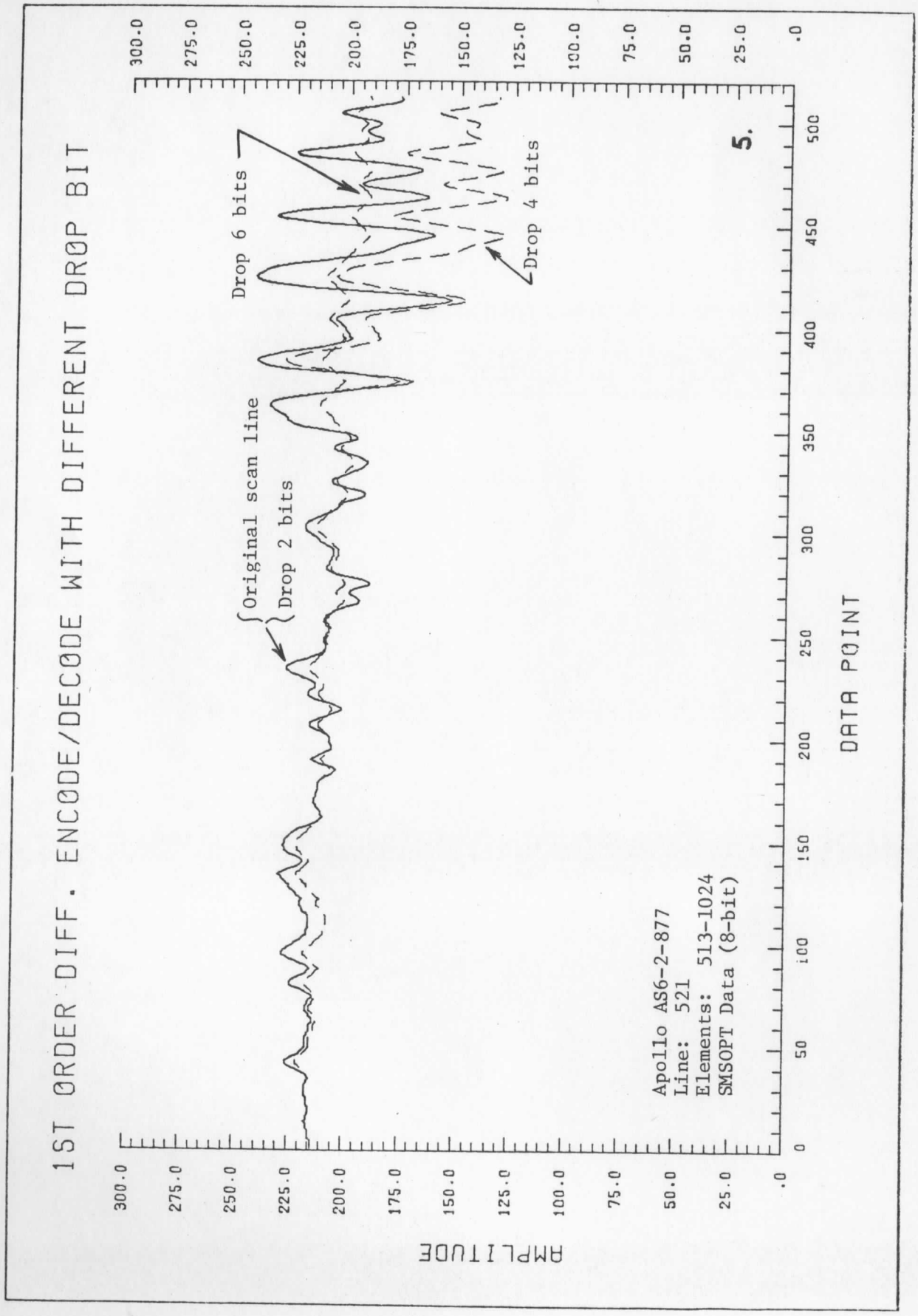
1ST ORDER DIFF. ENCODE/DECODE WITH DIFFERENT DROP BIT
Original scan line
Drop 2 bits
Drop 6 bits
Drop 4 bits
5.
Apollo AS6-2-877
Line: 521
Elements: 513-1024
SMSOPT Data (8-bit)
AMPLITUDE
DATA POINT
300.0
275.0
250.0
225.0
200.0
175.0
150.0
125.0
100.0
75.0
50.0
25.0
.0
0
50
100
150
200
250
300
350
400
450
500

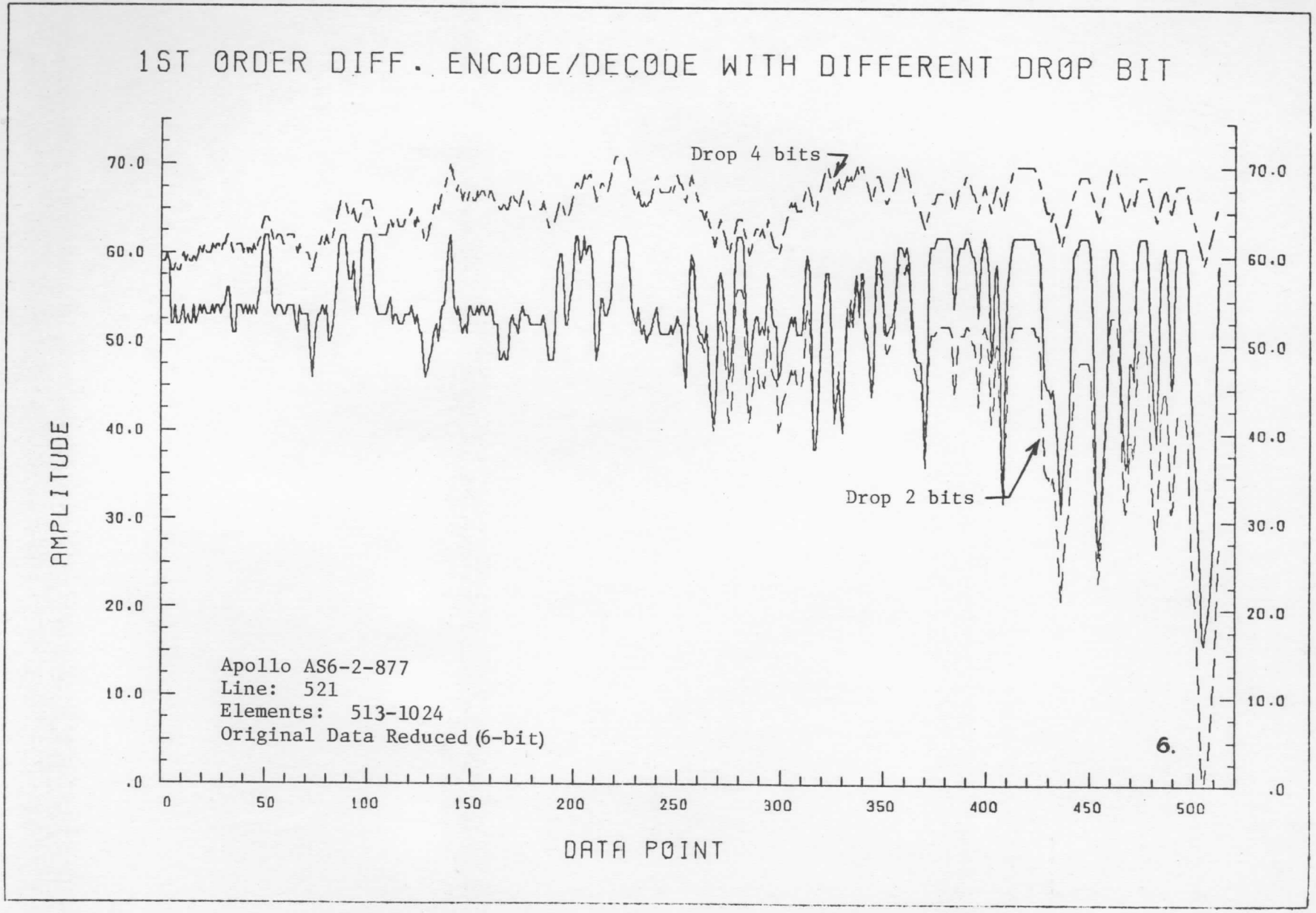
1ST ORDER DIFF. ENCODE/DECODE WITH DIFFERENT DROP BIT
Drop 4 bits
Drop 2 bits
AMPLITUDE
DATA POINT
70.0
60.0
50.0
40.0
30.0
20.0
10.0
.0
0
50
100
150
200
250
300
350
400
450
500
Apollo AS6-2-877
Line: 521
Elements: 513-1024
Original Data Reduced (6-bit)
6.

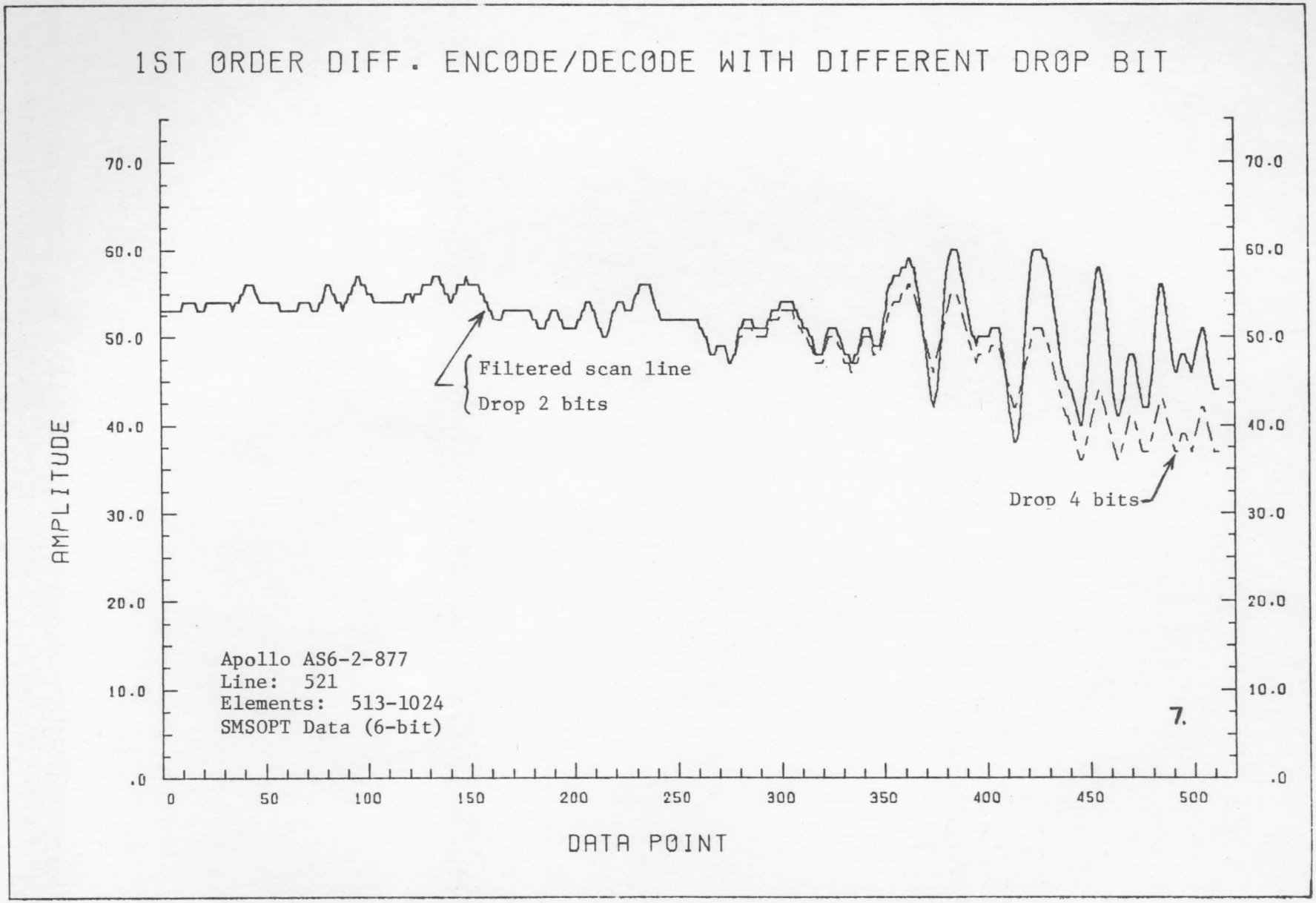
1ST ORDER DIFF. ENCODE/DECODE WITH DIFFERENT DROP BIT
AMPLITUDE
70.0
60.0
50.0
40.0
30.0
20.0
10.0
.0
0
50
100
150
200
250
300
350
400
450
500
DATA POINT
Filtered scan line
Drop 2 bits
Drop 4 bits
Apollo AS6-2-877
Line: 521
Elements: 513-1024
SMSOPT Data (6-bit)
7.

FIGURE 2.3. COMPARISON OF FIRST-ORDER AND SECOND-ORDER DPCM ENCODING/DECODING FOR APOLLO AS6-2-877.

Notes:
1. Solid line indicates input data scan line (digitized to 8-bits unless marked otherwise).
2. Dashed lines represent dropping bits after subtraction, as indicated.
3. Input data accuracy is 8-bits (i.e., 256 levels) unless specified.
4. Output fixed to 4-bits (i.e., 3 plus sign).

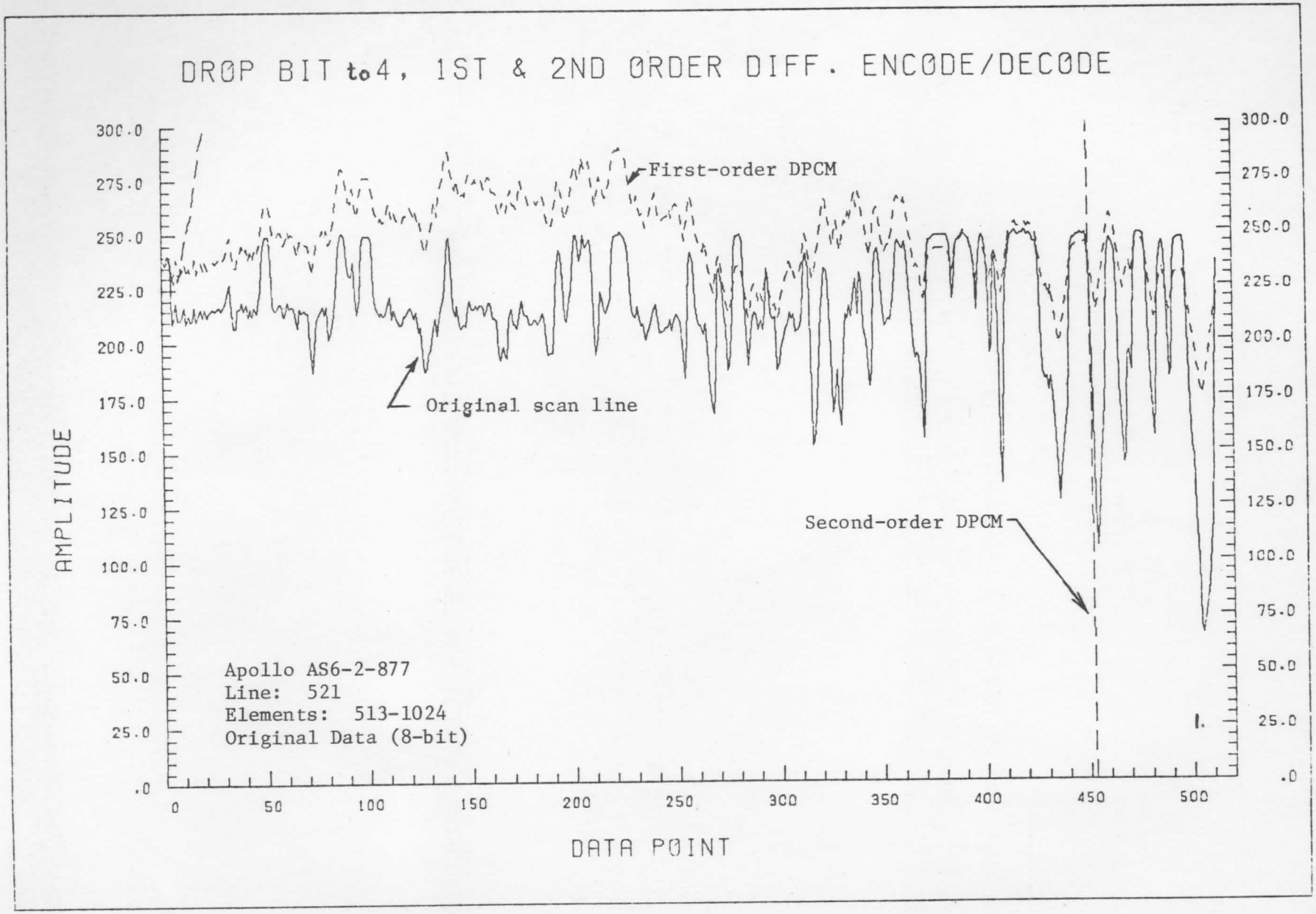
DROP BIT to 4, 1ST & 2ND ORDER DIFF. ENCODE/DECODE
First-order DPCM
Original scan line
Second-order DPCM
Apollo AS6-2-877
Line: 521
Elements: 513-1024
Original Data (8-bit)
AMPLITUDE
DATA POINT
300.0
275.0
250.0
225.0
200.0
175.0
150.0
125.0
100.0
75.0
50.0
25.0
.0
0
50
100
150
200
250
300
350
400
450
500

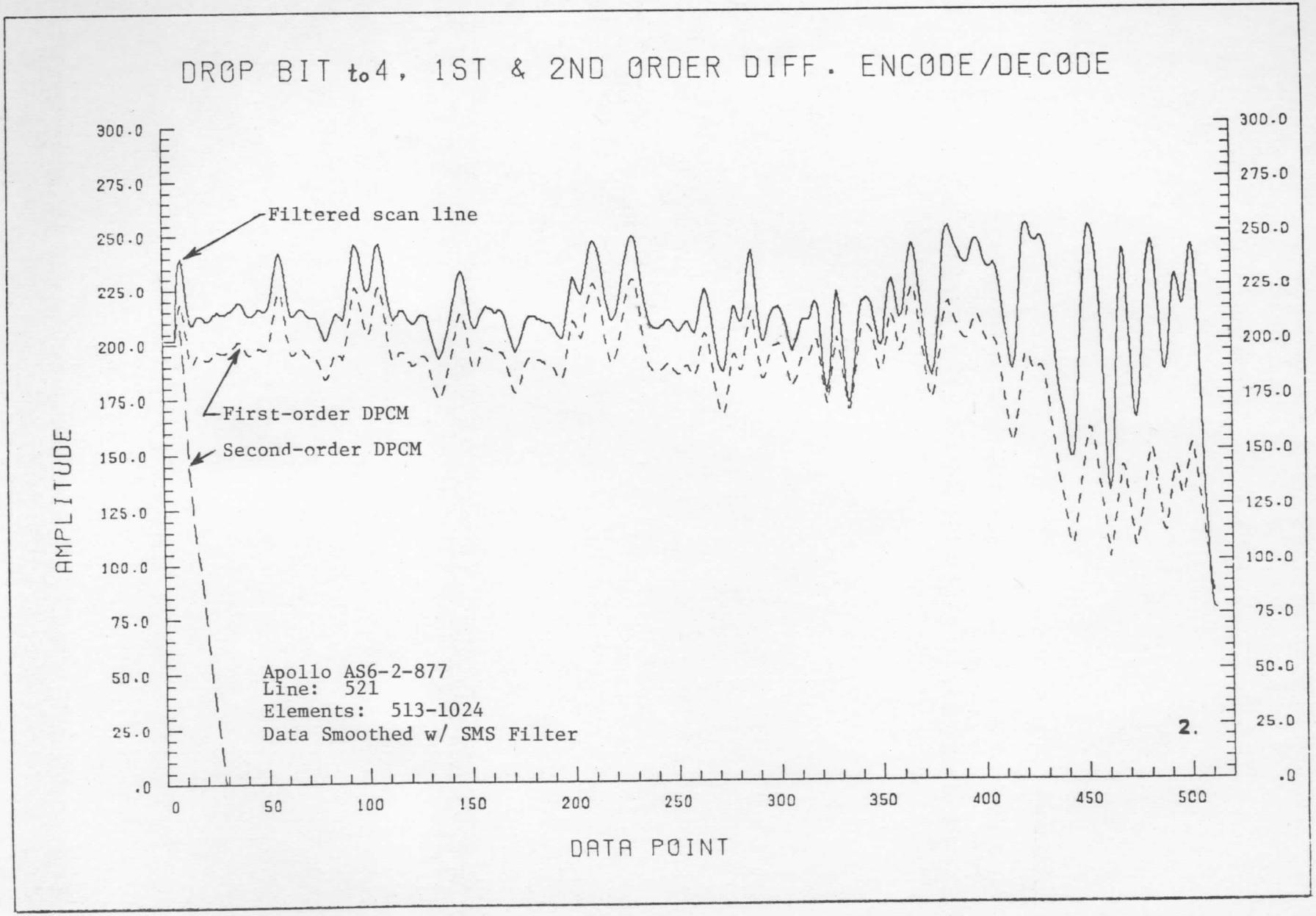
DROP BIT to 4, 1ST & 2ND ORDER DIFF. ENCODE/DECODE
AMPLITUDE
DATA POINT
Filtered scan line
First-order DPCM
Second-order DPCM
Apollo AS6-2-877
Line: 521
Elements: 513-1024
Data Smoothed w/ SMS Filter
2.
300.0
275.0
250.0
225.0
200.0
175.0
150.0
125.0
100.0
75.0
50.0
25.0
.0
0
50
100
150
200
250
300
350
400
450
500

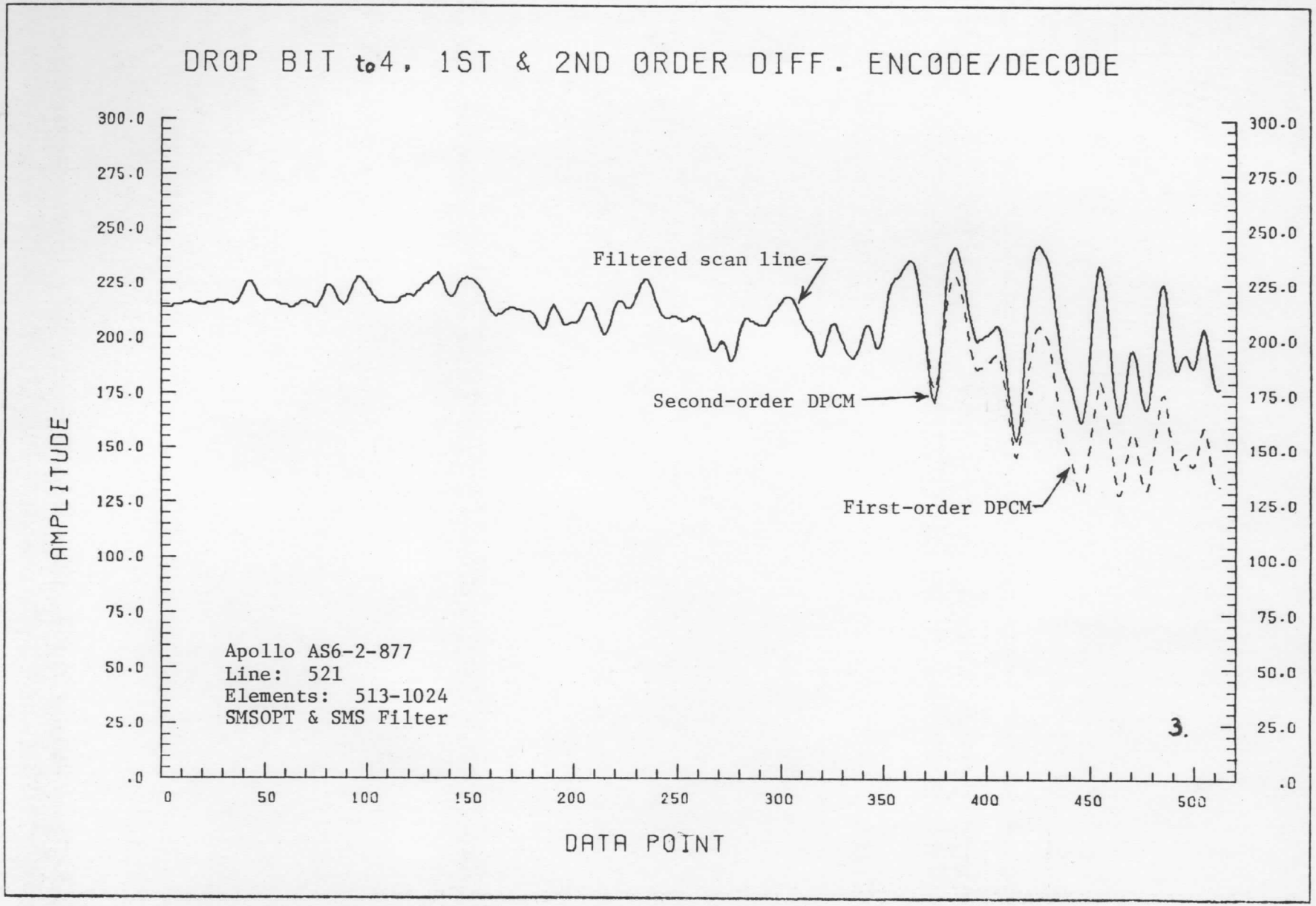
DROP BIT to4, 1ST & 2ND ORDER DIFF. ENCODE/DECODE
AMPLITUDE
DATA POINT
300.0
275.0
250.0
225.0
200.0
175.0
150.0
125.0
100.0
75.0
50.0
25.0
.0
0
50
100
150
200
250
300
350
400
450
500
Filtered scan line
Second-order DPCM
First-order DPCM
Apollo AS6-2-877
Line: 521
Elements: 513-1024
SMSOPT & SMS Filter
3.

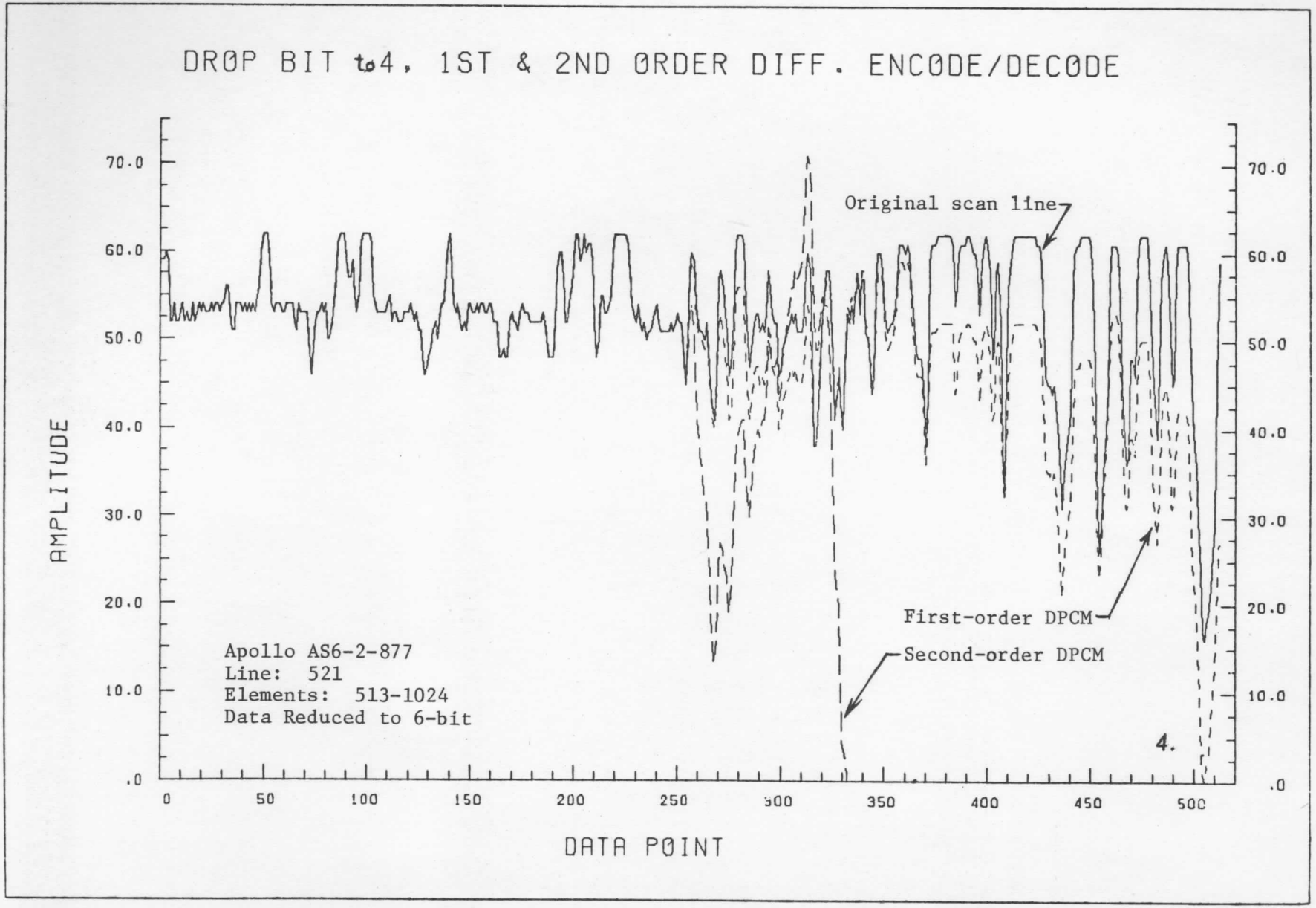
DROP BIT to4, 1ST & 2ND ORDER DIFF. ENCODE/DECODE
AMPLITUDE
70.0
60.0
50.0
40.0
30.0
20.0
10.0
.0
0
50
100
150
200
250
300
350
400
450
500
DATA POINT
Original scan line
First-order DPCM
Second-order DPCM
Apollo AS6-2-877
Line: 521
Elements: 513-1024
Data Reduced to 6-bit
4.

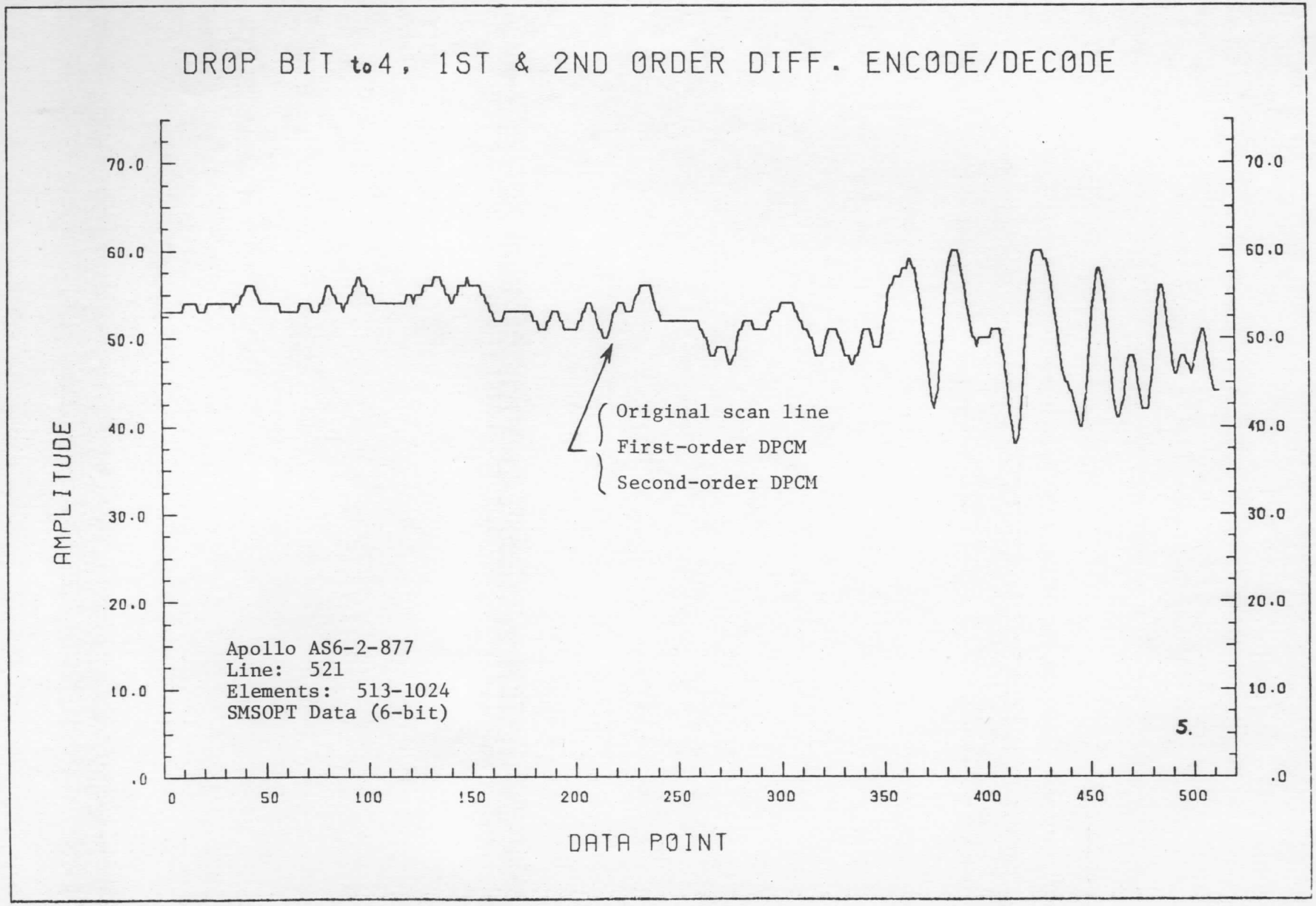
DROP BIT to4, 1ST & 2ND ORDER DIFF. ENCODE/DECODE
AMPLITUDE
70.0
60.0
50.0
40.0
30.0
20.0
10.0
.0
0
50
100
150
200
250
300
350
400
450
500
DATA POINT
Original scan line
First-order DPCM
Second-order DPCM
Apollo AS6-2-877
Line: 521
Elements: 513-1024
SMSOPT Data (6-bit)
5.

(a)

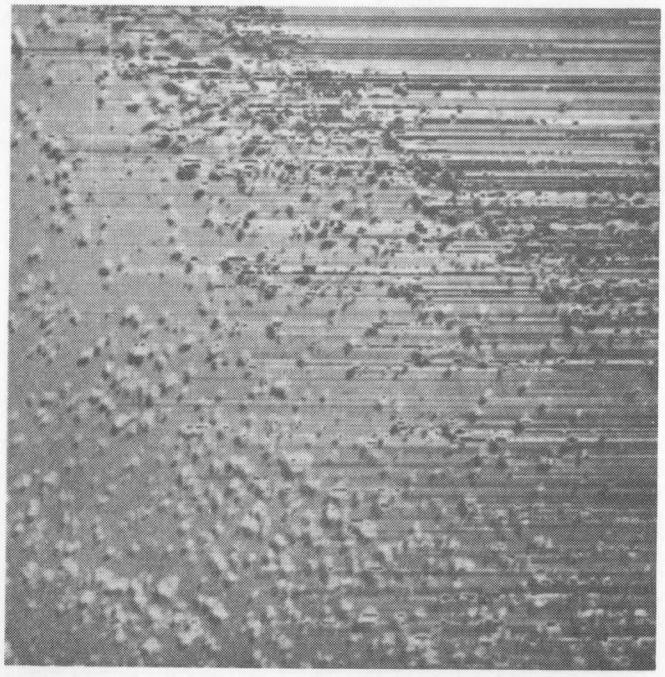

(b)

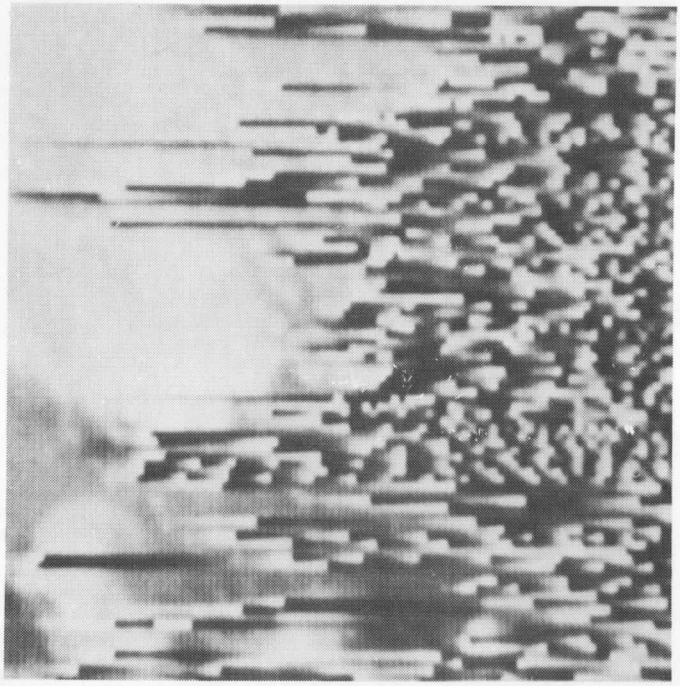

Figure 2.4. Picture Reconstructions for Two DPCM Systems with Overflow.
(a) First-order DPCM on Apollo AS6-2-877 (URQ);
(b) Second-order DPCM on Apollo AS6-2-877 (LRQ); SMSOPT and SMS filtering; every fifth point sampled.

FIGURE 2.5. PLOTS OF FIRST-ORDER DPCM ENCODING/DECODING FOR APOLLO AS6-2-877 USING A STAND-BY ACCUMULATOR.

Notes: 1. Solid line indicates input data scan line (digitized to 6-bits).

2. Dashed lines represent reconstruction, dropping bits after differencing as indicated.

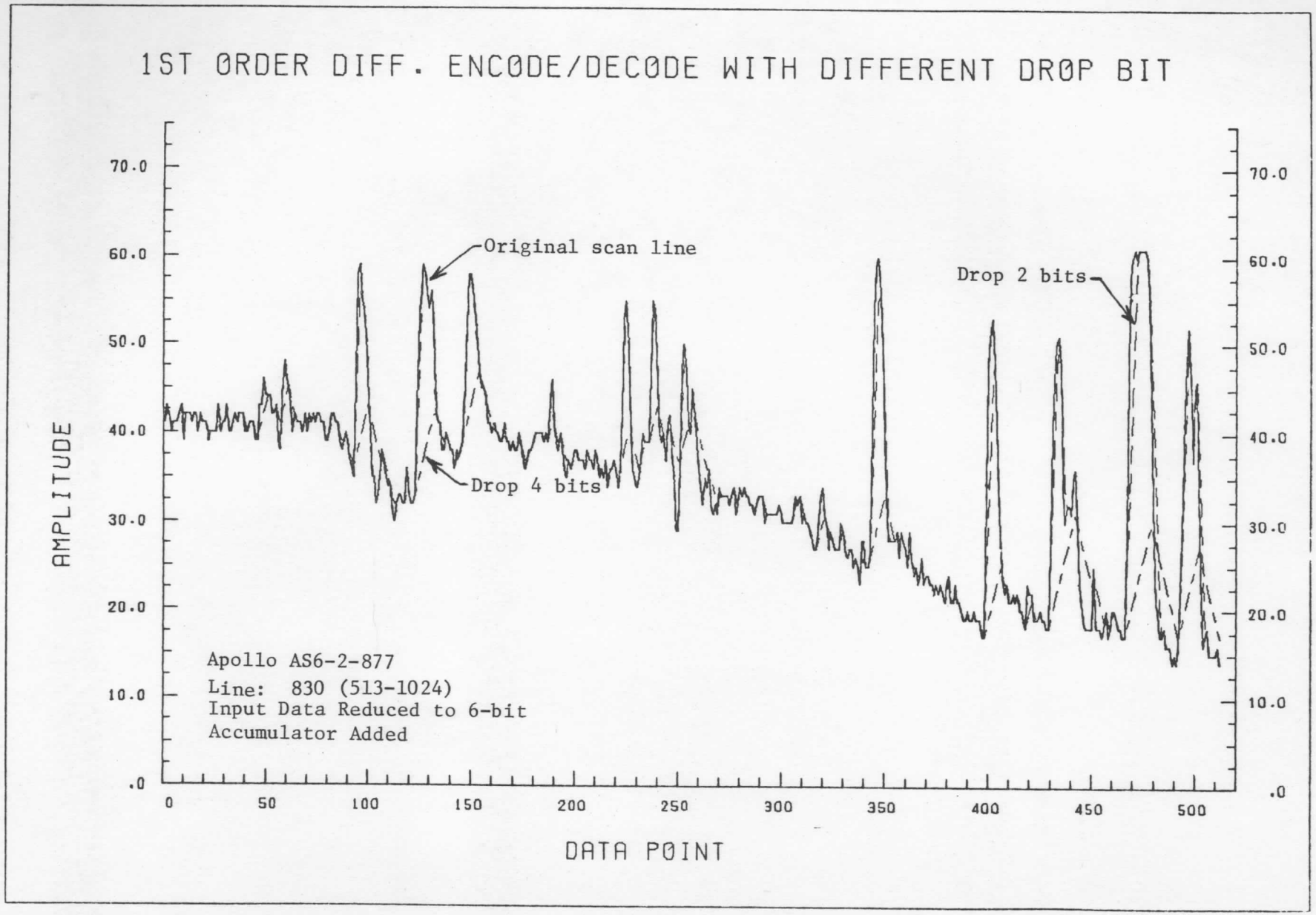
1ST ORDER DIFF. ENCODE/DECODE WITH DIFFERENT DROP BIT
AMPLITUDE
70.0
60.0
50.0
40.0
30.0
20.0
10.0
.0
Original scan line
Drop 2 bits
Drop 4 bits
Apollo AS6-2-877
Line: 830 (513-1024)
Input Data Reduced to 6-bit
Accumulator Added
0
50
100
150
200
250
300
350
400
450
500
DATA POINT

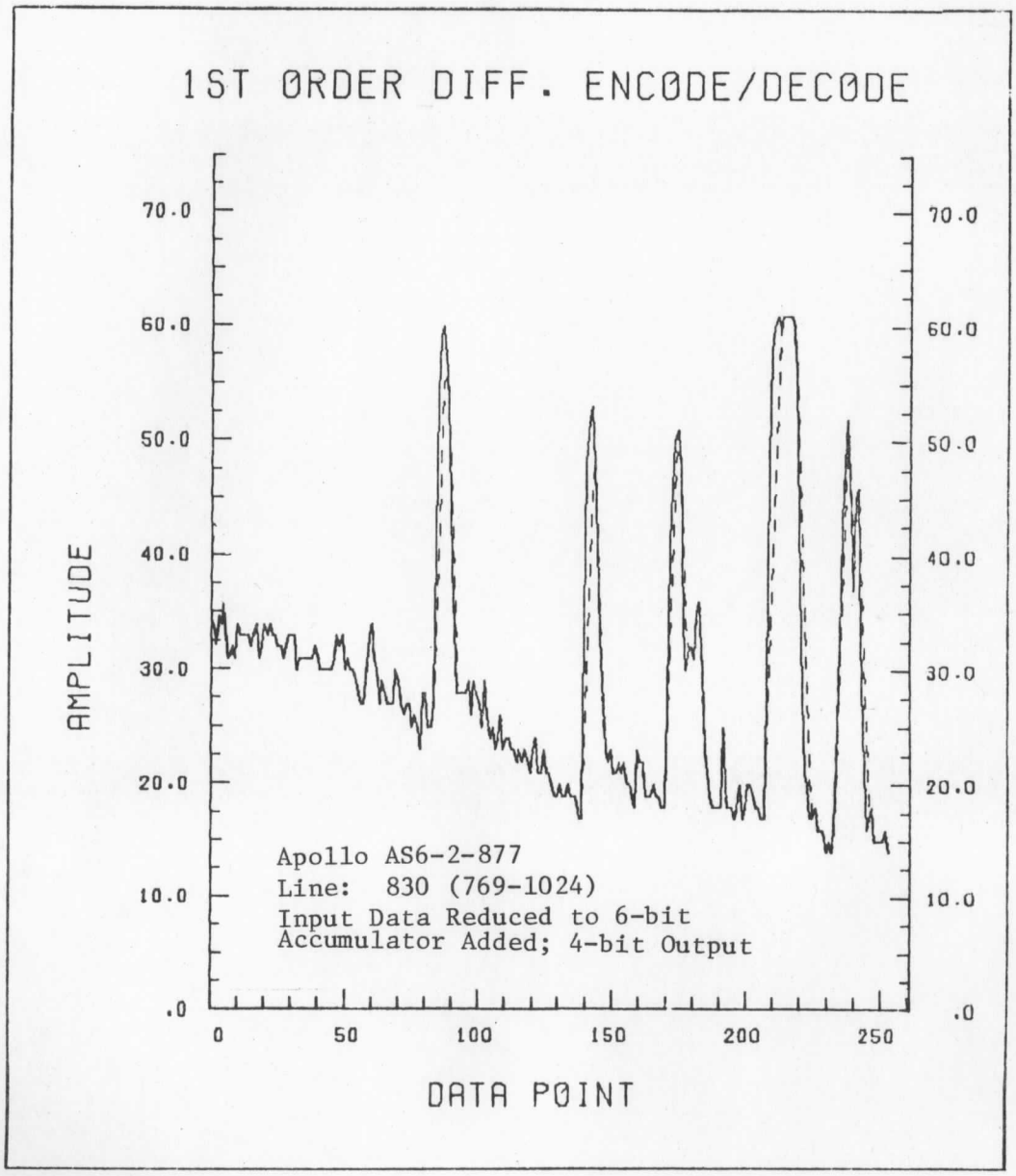
1ST ØRDER DIFF. ENCØDE/DECØDE
AMPLITUDE
70.0
60.0
50.0
40.0
30.0
20.0
10.0
.0
0
50
100
150
200
250
DATA PØINT
Apollo AS6-2-877
Line: 830 (769-1024)
Input Data Reduced to 6-bit
Accumulator Added; 4-bit Output

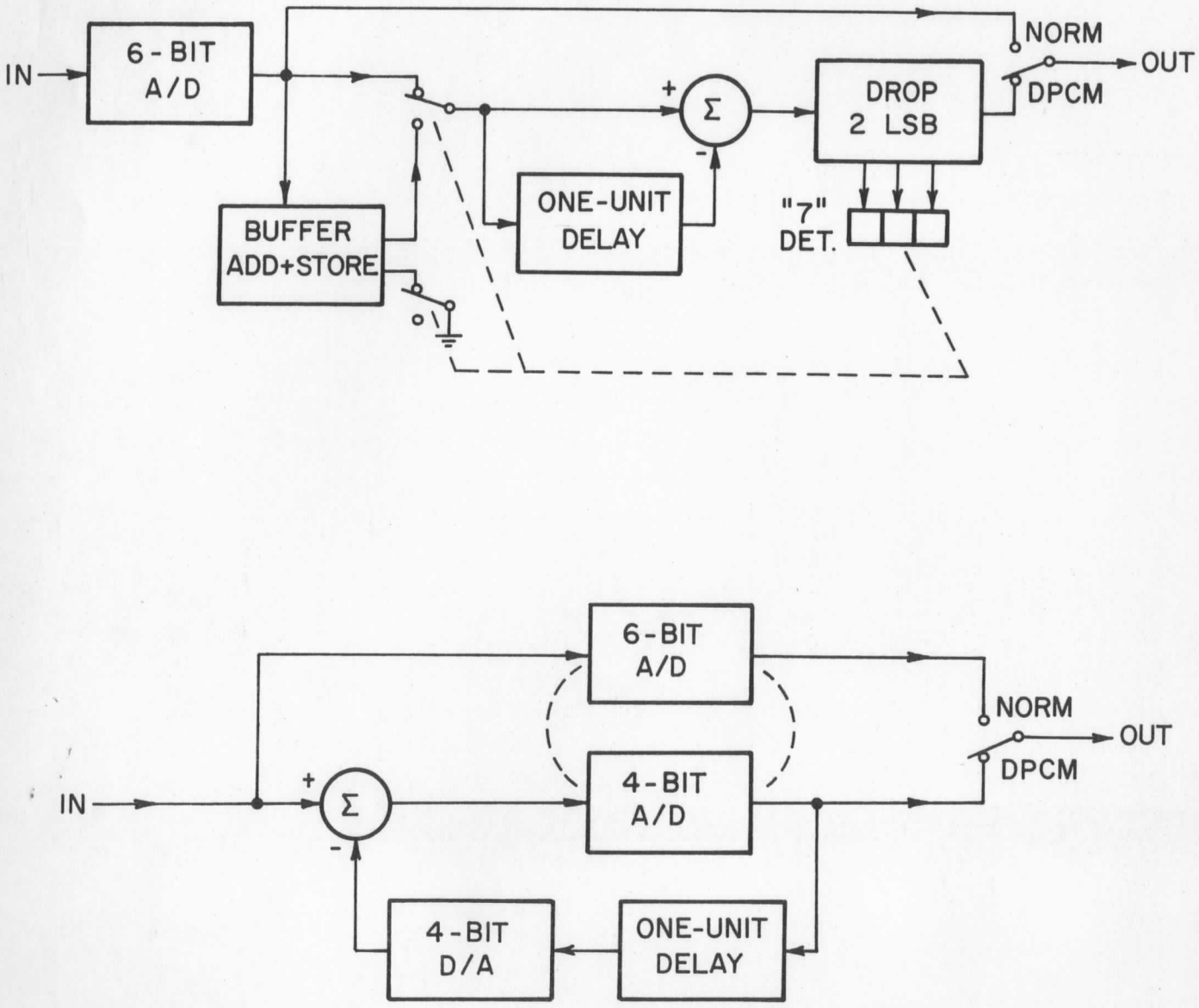

Figure 2.6. Two Possible DPCM Systems with Accumulation which would be Suitable for a Geostationary Orbiting Satellite Experiment.

III
INTERPOLATIVE ENCODING

The discussion in the preceding chapter centered on the use of uniform time sampling and encoding. There is a class of encoding techniques which makes use of nonuniform sampling methods for bandwidth compression. When made adaptive, some of these techniques have reported factors as high as four in satellite simulation studies [6]. A closely allied method is that of interpolative encoding [7]. The advantage of the interpolative encoder for satellite work is it is not adaptive and the algorithm can be preset. A disadvantage in both is it is difficult to efficiently multiplex several channels.

We have investigated the use of both first-order and second-order interpolative encoding on the Apollo VI picture data. The algorithms for the first- and second-order interpolative encoders are shown in Tables 3.1 and 3.2.

Reconstructions of line #521 in the lower right quarter of Apollo AS6-2-877 were run using both the first- and second-order interpolator and are shown in Fig. 3.1. The original data was 8-bit and the sample tolerance accuracies (ξ) were run at 6-bits and 4-bits, as noted on the graphs. The 4-bit sample tolerance accuracies resulted in appreciable errors, but the 6-bit accuracies yielded very acceptable reconstructions.

As an example of the data compression realized for the 512-point line shown in Fig. 3.1, the first-order interpolator required 375 data points for 6-bit tolerance accuracy and 191 data points for the 4-bit accuracy. The second-order interpolator required 128 data points for 6-bit tolerance accuracy and 88 data points for the 4-bit accuracy.

TABLE 3.1. ALGORITHM FOR THE FIRST-ORDER INTERPOLATOR

Transmission

1. Let x_k be the last sample value set and x_j be the present data point from the Apollo VI data.
2. Truncate as required (preset).
3. If x_j is the first sample value of a scan line, send that sample value and go to 6.
4. For each data point, form:

$$|x_j - x_k| < \xi$$

where ξ is an arbitrary bound (specified).

5. Increase j until the inequality is exceeded; let this point be: i + 1; then:
6. Send the sample value x_i.
7. Let: k = i and repeat.

Reconstruction

1. Hold the present sample level until a new sample value is received.
2. Let: k = i and repeat.

TABLE 3.2. ALGORITHM FOR THE SECOND-ORDER INTERPOLATOR

Transmission

1. Let x_k be the last sample value sent, x_i the present sample value in the sequence considered, and x_j be an intermediate sample value ($k<j<i$).

2. If x_i is the first sample value in a scan line, send that sample value and go to 3.

3. For each data point, form:

$$\left| \left(\frac{x_i - x_k}{i-k} \right) (j-k) \ (x_k - x_j) \right| \leq \xi$$

where ξ is an arbitrary bound (specified).

4. For each i, test over all $k < j < i$.

5. Increase i until the inequality is exceeded for some j; let this point be: $\ell + 1$.

6. Send the sample value x_ℓ.

7. Let $k = \ell$ and repeat.

Reconstruction

1. If x_i is the first sample value in a scan line, hold that level until the next sample is received.

2. Hold the slope: $(x_i - x_k / i-k)$ until the next sample is received.

3. Let: $k = i$ and repeat.

Summarizing, these sample reconstructions show a first-order interpolator using 6-bit accuracy is roughly equivalent in bandwidth compression to DPCM. In contrast, the second-order interpolator yields savings on the order of a factor of four and is clearly superior in this regard to DPCM.

The above comparisons have been made on a scan-line-by-scan-line basis. However, several channels are used in the visual channels of modern geo-stationary orbiting satellites. This presents a multiplexing problem because the interpolative encoders are not uniform time samplers. The full savings in their use is not realized, therefore, unless a uniform time sampling rate conversion is made, and this comes at the cost of buffer storage.

A compromise would probably be to use some buffer storage (say, an 8x8 array for an 8-channel system) and "strobe" the output sample values by a rate reduced by about a factor of 2-3 below the input sample data rate. It is possible to set up such a system simulation and make a statistical study of the percentage time there will be an overflow, although we have not attempted to do so.

In conclusion, interpolative encoding offers significant bandwidth compression, but at the expense of some multiplexing problems for efficient multiple-channel use.

FIGURE 3.1. GRAPHS OF A RECONSTRUCTED SCAN LINE FROM APOLLO AS6-2-877 USING INTERPOLATIVE ENCODING

Notes: 1). Solid line is the original scan line (8-bit data, unsmoothed).

2). Dashed lines are the line reconstructions using 6-bit and 4-bit sample accuracies, as noted.

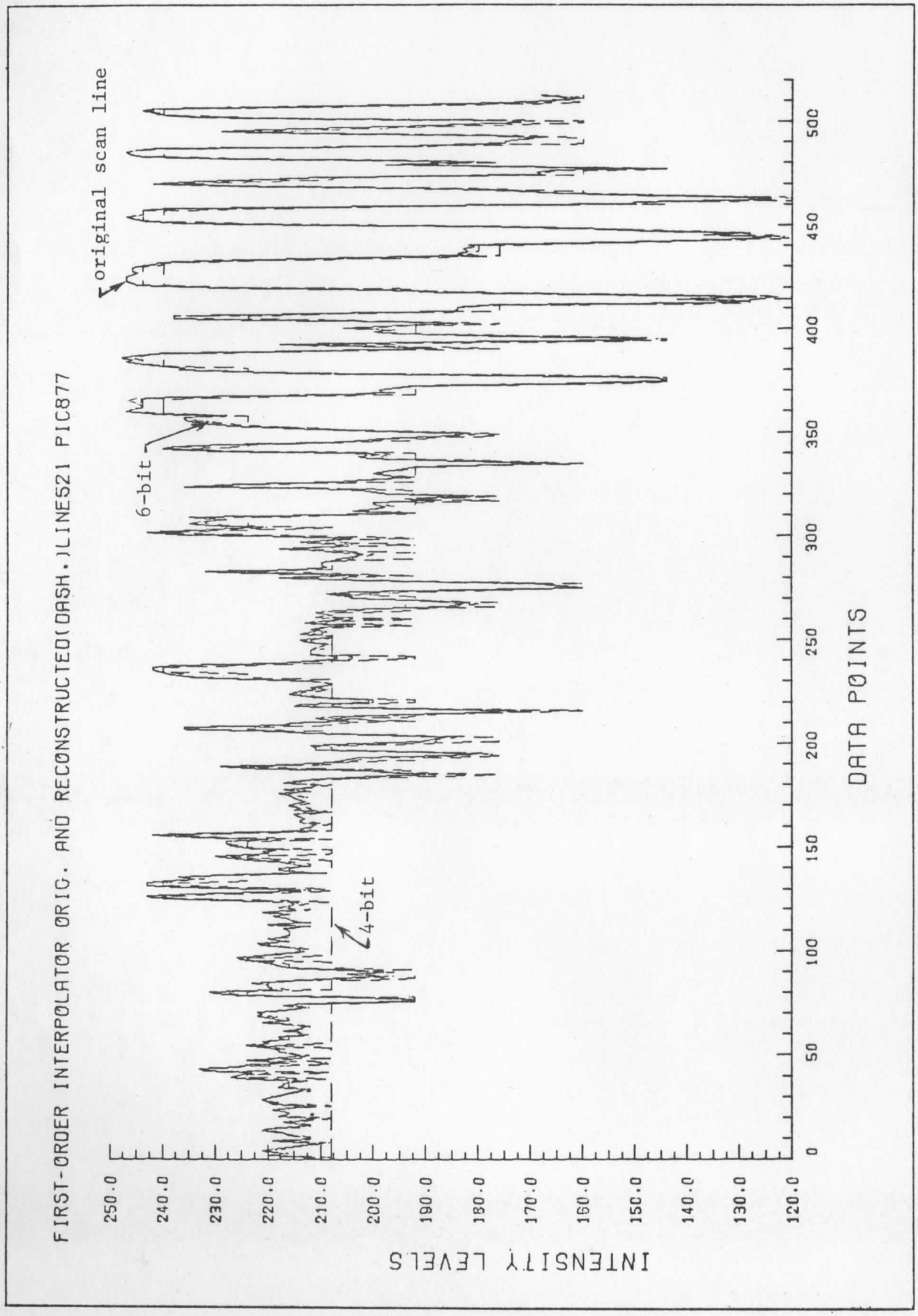
FIRST-ORDER INTERPOLATOR ORIG. AND RECONSTRUCTED(OASH.JLINE521 PIC877
original scan line
6-bit
4-bit
INTENSITY LEVELS
DATA POINTS
250.0
240.0
230.0
220.0
210.0
200.0
190.0
180.0
170.0
160.0
150.0
140.0
130.0
120.0
0
50
100
150
200
250
300
350
400
450
500

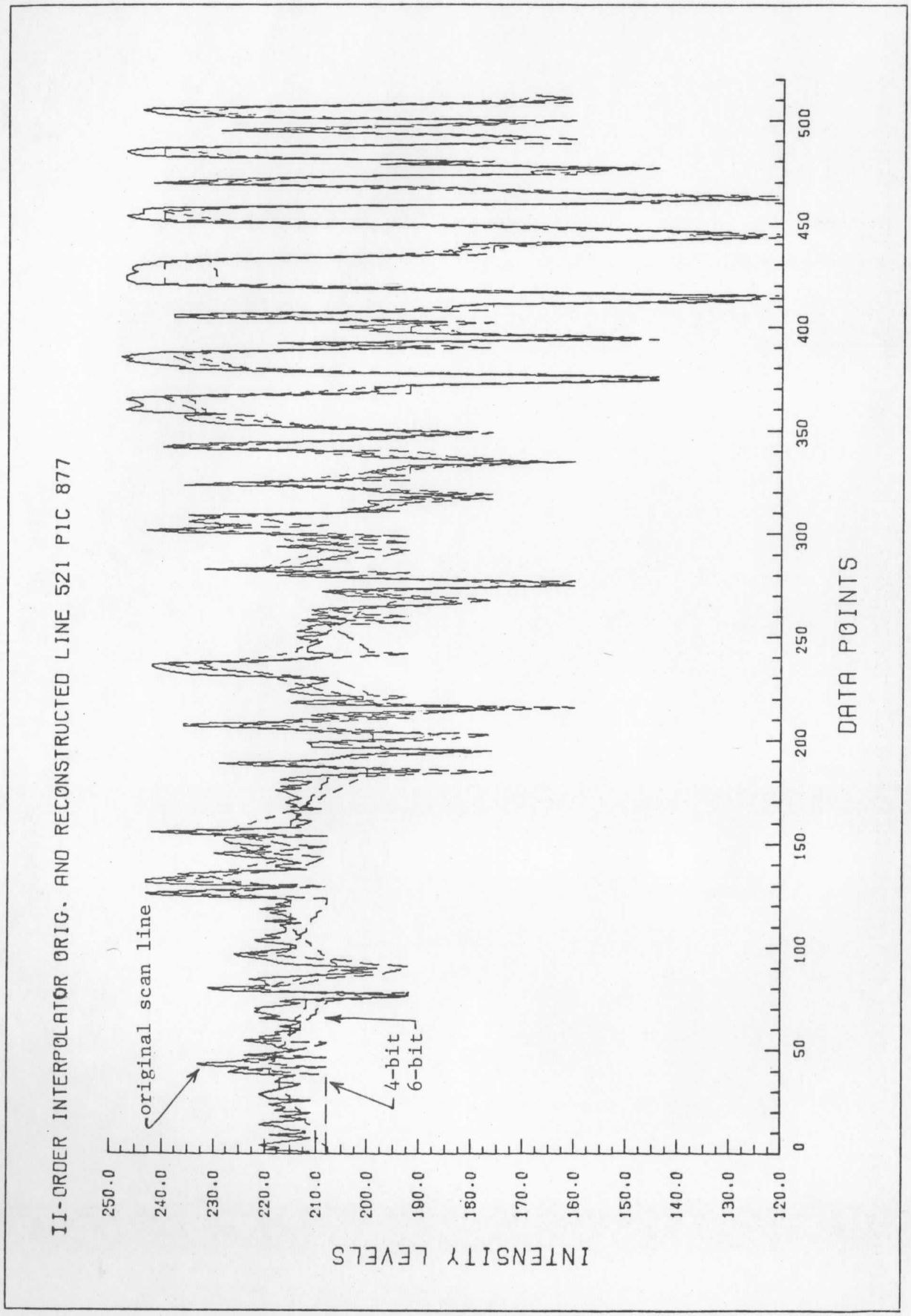
II-ORDER INTERPOLATOR ORIG. AND RECONSTRUCTED LINE 521 PIC 877
original scan line
4-bit
6-bit
INTENSITY LEVELS
DATA POINTS
250.0
240.0
230.0
220.0
210.0
200.0
190.0
180.0
170.0
160.0
150.0
140.0
130.0
120.0
0
50
100
150
200
250
300
350
400
450
500

IV.
TWO-DIMENSIONAL ENCODING

Our criteria for judging picture quality obtained for meteorological uses are the spatial and intensity level accuracy needed for visual interpretation and the spatial and intensity level accuracy needed for wind measurements (these are discussed in Chapter V). Criteria for the former use are fairly subjective, whereas the latter is based on two-dimensional correlation techniques.

In judging picture quality for both uses, a two-dimensional array of points is involved; yet we have assumed in the previous chapters that signal processing be performed only in the along-scan direction. Here we consider two-dimensional methods in hope of gaining more substantial reductions in required bandwidth. Theoretical considerations show reductions on the order of a factor of about three (3) might be expected when compared to line-by-line processing [9].

Many different data processing methods could be considered here. For example, the DPCM and interpolative methods discussed in the previous chapters can be extended to two dimensions. To be efficient, however, these methods require a computation of the two-dimensional correlation coefficients [3]. Our aversion to adaptive systems has led us to consider other systems.

An attractive two-dimensional method is transform coding. This method involves the storage of a two-dimensional array of sample points, a computation of the coefficient array, and the quantization and transmission of selected coefficients. At the receiver, the coefficient data is assembled in an array and an inverse transform is taken to yield the reconstructed scan lines. An advantage is the picture data are treated in small two-dimensional "packets", corresponding to the way the data are to be used. A disadvantage is the data must be handled in an array, requiring storage. Part of the problem is solved in a visual scanner which has several parallel channels; because of the

8-channel configuration of the visual channels in the SMS, we have chosen an 8x8 array. Some reported work along these lines has been done by Landau and Slepian [10] on television data using a 4x4 array.

Use of the well-known Fourier transform for this purpose was quickly ruled out as a result of computational complexity. A transform which lends itself to logic-type computation is that using Walsh functions [11,12]. While having some drawbacks for large-array computations, they were chosen here mainly for their computational simplicity and favorable qualities for small-array computations [17]. These functions form an orthonormal set using the levels +1, -1. The first eight Walsh functions are shown in Fig.4.1. We have restricted our choice to eight because the visual scanner on the SMS has eight parallel channels.

The Hadamard matrix used to represent the Walsh functions is ordered with respect to the number of sign changes in each row (sequency ordering). For an 8x8 array, this is:

$$\begin{bmatrix} + & + & + & + & + & + & + & + \\ + & + & + & + & - & - & - & - \\ + & + & - & - & - & - & + & + \\ + & + & - & - & + & + & - & - \\ + & - & - & + & + & - & - & + \\ + & - & - & + & - & + & + & - \\ + & - & + & - & - & + & - & + \\ + & - & + & - & + & - & + & - \end{bmatrix}$$

where "+" indicates "+1" and "-" indicates "-1".

The computed Walsh coefficients are arranged in an 8x8 array and indexed as shown in Fig. 4.2a.

The method of indexing the coefficients (i,j) in Fig. 4.2a is by the zero

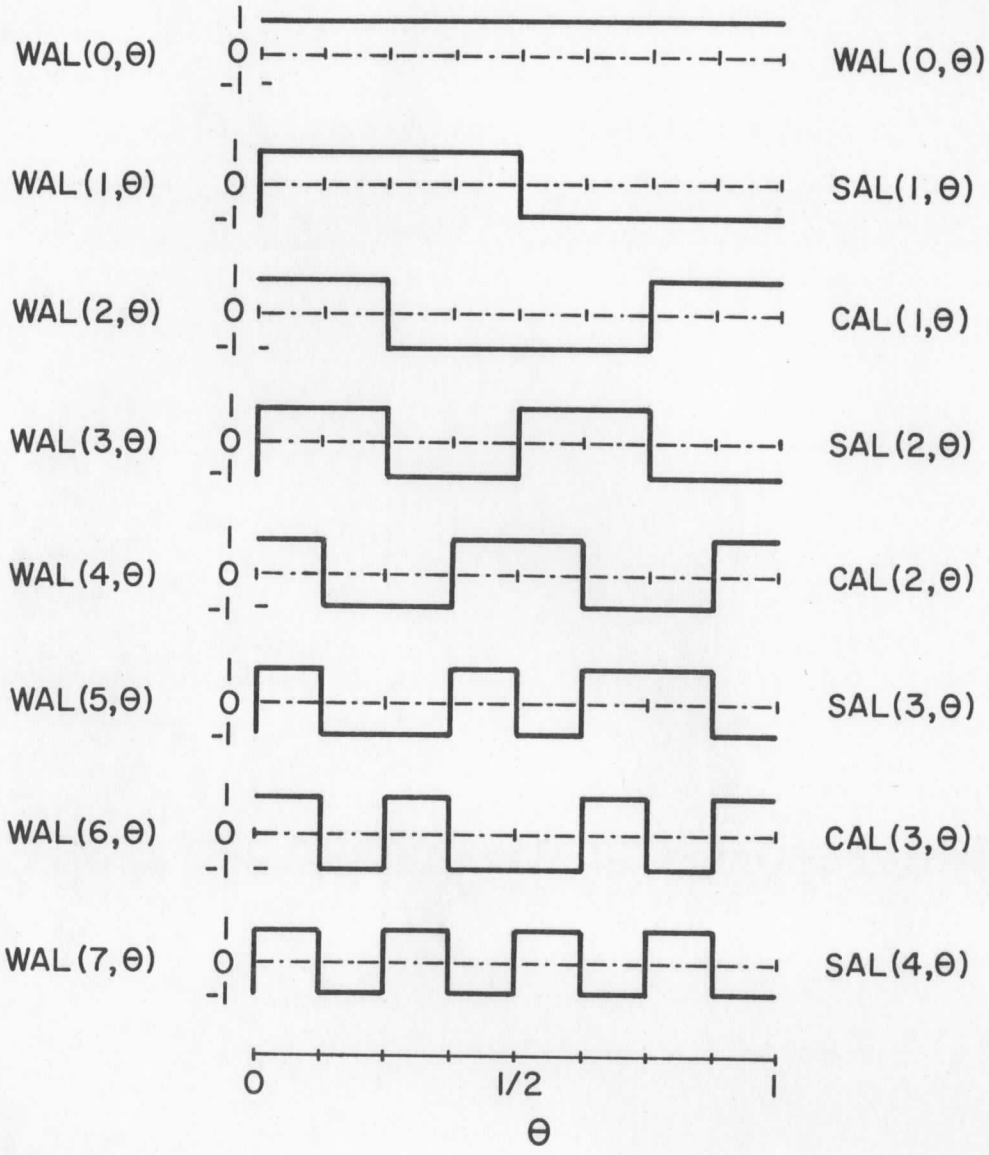

NOTATION:

θ: NORMALISED INDEPENDENT VARIABLE

WAL(i,θ): Walsh Function With i=No. of zero crossings excluding any at θ=0

SAL(j,θ): Walsh Function of sequency j with odd symmetry about θ=1/2 (ignore θ=0)

SEQUENCY: One-half the average No. of zero-crossings in the interval

CAL(j,θ): Similar to SAL(j,θ), but even symmetry about θ=1/2

FIGURE 4.1. GRAPHS OF THE FIRST EIGHT WALSH FUNCTIONS.

crossings in the vertical and horizontal coordinates respectively. The sequency can be found from:

vertical sequency = [i/2] = greatest integer obtained after division of i by 2;

horizontal sequency = [j/2] = greatest integer obtained after division of j by 2.

Thus for $i \neq 1$; $j \neq 1$, the sequency of the term with the general indexing (i,j) is: ([i/2],[j/2]). The description in terms of sequency is not unique, however. For example, (2,2), (2,3), (3,2), and (3,3) all have vertical sequency of one and horizontal sequency of one, but they have differing spatial shifts ("phase shifts"). (The analogy with sines and cosines at a given frequency are the "sal" and "cal" functions at a given sequency as shown in Fig. 4.1.) Note the first coefficient (i=1, j=1) corresponds to the "D.C." or average value of the 8x8 data block, whereas the coefficient (i=8, j=8) corresponds to the most rapid fluctuations in the selected picture sub-area.

Based on coefficient computations for Apollo AS6-2-877, we select 25 or 16 of the 64 coefficients as being the most important, as shown in Fig. 4.2b. All others are set equal to zero before the coefficient array is transmitted. The selection is predetermined so the satellite hardware can be designed to only compute the desired coefficients, resulting in appreciable savings. The selected coefficient values are quantized and transmitted at a reduced data rate.

The choice of the coefficients selected depends to some extent on the type of picture content being transmitted. This is being studied and a report of work to date is included in Appendix C.

Investigation of this type of encoding using the closely-related Hadamard basis functions has been investigated rather recently and reported in the literature [10,13,14]. With the exception of the work by Landau and Slepian [10], this has been confined to relatively few pictures. The techniques employed

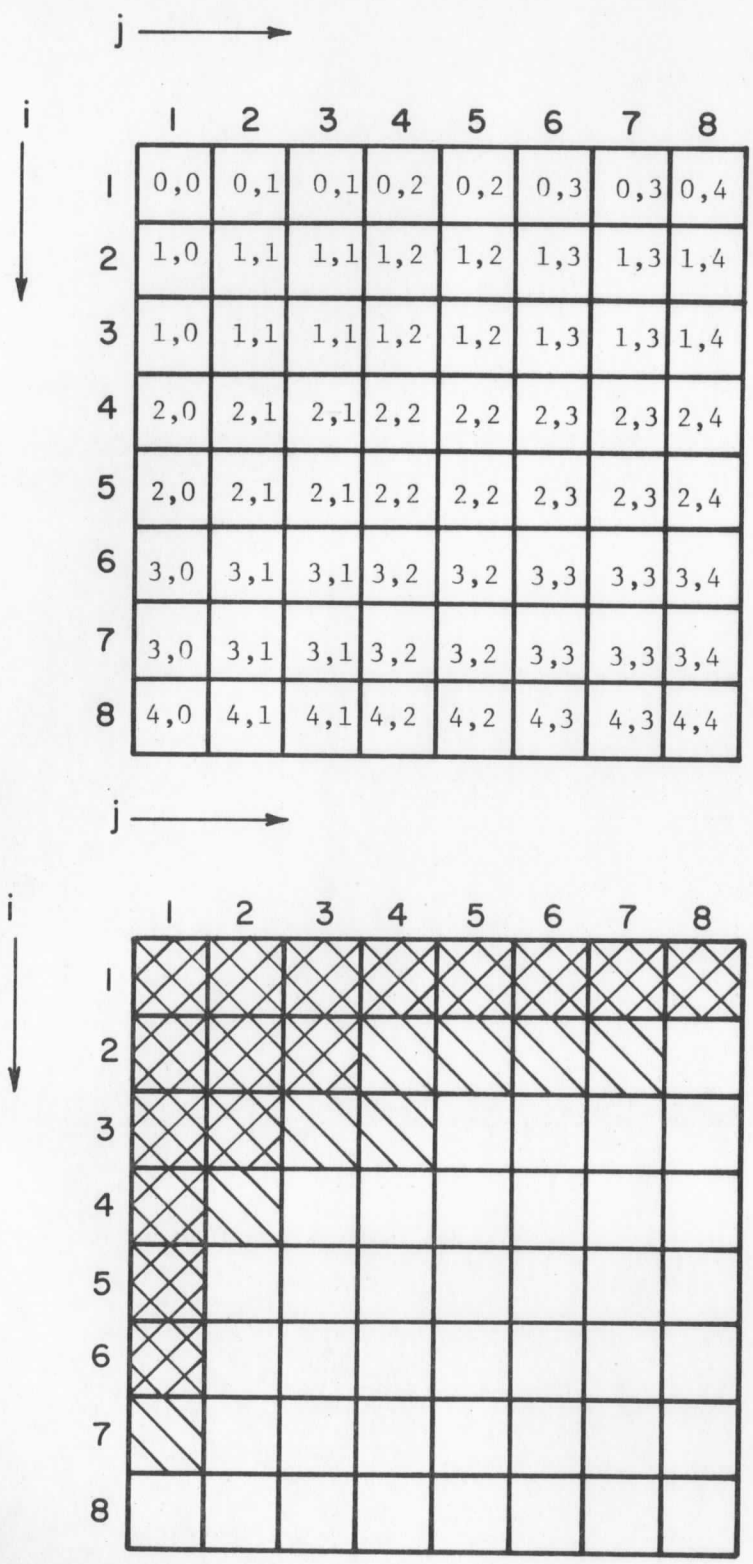

Figure 4.2. a). Diagram of Sequency and Matrix Notation of an 8×8 Walsh Coefficient Array; b). Selection Rule for Walsh Coefficients for Apollo AS6-2-877 (diagonal lines indicate the 25 retained; crosshatched indicate the 16 retained).

have been to optimize the selection of coefficients by first investigating the variances of the coefficients for a given picture. Because we prefer not to use an adaptive system, we have been investigating ways to make the choices a priori based on our studies of representative cloud photographs.

To implement the simulation studies, a fast Walsh transform (FWT) subroutine was written using a modification of the fast Fourier transform (FFT) [15]. Some sample runs were made of various picture content and the tables of coefficients were studied [2]. From observations of these results and comparisons with others analyzing ERTS data using these techniques [16], we have chosen to retain either 25 or 16 of the 64 coefficients for Apollo AS6-2-877. This selection rule has been modified later, as described in Appendix C, to accomodate a wider range of Apollo VI picture data.

The effort in computing a Walsh transform is almost trivial when compared to the Fourier transform. It consists in multiplying the data by plus or minus one over increasingly smaller increments and forming sums. Both operations are easy to implement with logic-type circuitry. In analogy with the use of the term "frequency" in the Fourier transform, a measure of how rapidly the Walsh functions vary over a given interval is called "sequency".

A problem which arises in transform coding is that of a proper choice of quantization rule for the transmission of the coefficients retained. This has received some attention in the recent literature. The problem is that the low-sequency terms in picture data can be very large and rapidly varying while the higher sequency terms are very small and vary slowly between adjacent "blocks" of data. One approach is to use a non-linear quantizer which is matched to a gaussian probability density [13]. (This is similar to a bipolar version of the present non-linear SMS quantizer.) Another approach is to use an adaptive quantization rule based on a computation of picture

statistics [14]. We have ruled out the later choice as impractical for satellite use at this time. If the computation of coefficients is performed using analog methods, then an analog non-linear quantizer can be used that is similar to the one now employed in the SMS. If the computation of coefficients is performed digitally, then a read-only memory (ROM) can be employed to perform the non-linear conversion.

In order to make the quantization rather straightforward, we adopted the following rule based on observations of picture data. The zero-sequency term, which corresponds to the average value, is divided by a factor of 50 and the coefficients of terms of other sequencies are divided by a factor of 5. Then a 6-bit linear quantization is used on all the coefficients retained. Because the zero- and first-sequency terms can be quite large in picture data, this choice avoids excessive overloads. It is a rather crude three-step approximation to the gaussian quantization rule cited above. (Based on more studies of Apollo VI picture data, we have altered the numbers slightly, as discussed in Appendix C.)

Fig. 4.3 shows plots of a set of two reconstructed lines from the right side of Apollo AS6-2-877 using the above procedure. The input data used is 8-bit data and no optics smoothing was used. In the eight-line run (i.e., 8×2^9 points)-- of which we are showing only two lines--there were only three overflows in the 6-bit linear quantizer. Note, in contrast to DPCM, the effect of an overflow error is distributed over 64 picture elements (8×8 data block) and does not affect picture elements in adjacent data blocks. The results given in Fig. 4.3 are very encouraging, so we tried a few runs retaining only 16 of the 64 coefficients. The effects of quantization become more and more noticeable as the number of coefficients retained is lowered. Fig. 4.4 shows a reconstructed scan line using input data which has first been

smoothed by the SMSOPT (optics) subroutine. The first plot retains full computer accuracy on the coefficients, but the second uses the modified coefficient quantizer described above.

As mentioned in the previous chapter, the use of the SMSOPT smoothing routine without reducing the sampling rate is not quite fair because all the samples are no longer independent. Because the rms resolution of the SMSOPT routine is 4.65 samples, we can reduce the sampling rate by a factor of five to obtain independent samples. Figure 4.4 shows a reconstructed scan line using input data which has first been smoothed by the SMSOPT routine and then sampled every fifth sample and every fifth line. The first plot retains full computer accuracy on the coefficient values but the second uses the 6-bit modified linear quantizer. Note the choice of the quantizer becomes more critical in this case.

Implementation of this technique will probably require two 8x8 arrays of data storage, one of these used for a buffer storage. Computations can be performed using logic-type circuitry and 16- or 32-bit buffer can be used for serial readout. Recent advances in charge-coupled and surface-wave acoustic delay lines make sampled analog operations feasible [18]. Completely digital operation is also a possibility, and these choices would have to be investigated [19]. Note the system is self-multiplexing, i.e., a separate multiplexer is not required for the eight lines.

Our conclusions indicate transform coding using the two-dimensional Walsh transform can reduce the bandwidth required by a factor of about 3-4 at the expense of some added complexity. More can be gained if the choice of coefficients and their quantization can be made adaptive. The discussion in Appendix C summarizes our work on the coefficient selection and quantization over an ensemble of the Apollo VI picture data.

FIGURE 4.3. GRAPHS OF TWO RECONSTRUCTED LINES FROM APOLLO AS6-2-877 USING AN 8×8 WALSH TRANSFORM.

Notes: 1). Solid line is the original scan line (8-bit data, unsmoothed).

2). Dashed line is the reconstructed line after quantizing 24 of the 64 coefficients to 6-bits and then taking the inverse Walsh transform.

3). Scan lines taken from the right half of picture; scan lines are noted.

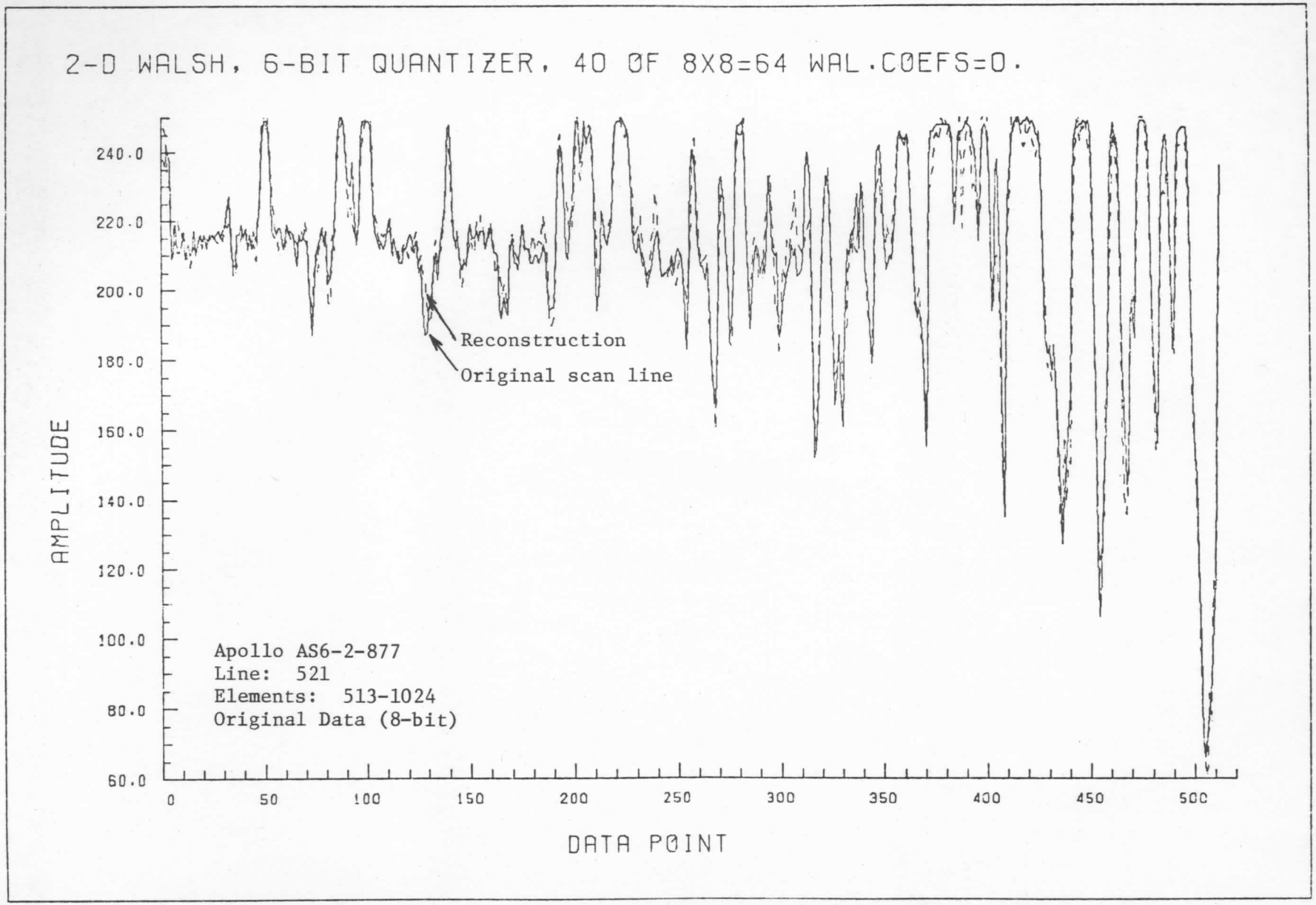
2-D WALSH, 6-BIT QUANTIZER, 40 OF 8X8=64 WAL.COEFS=0.
240.0
220.0
200.0
180.0
160.0
140.0
120.0
100.0
80.0
60.0
AMPLITUDE
Reconstruction
Original scan line
Apollo AS6-2-877
Line: 521
Elements: 513-1024
Original Data (8-bit)
0
50
100
150
200
250
300
350
400
450
500
DATA POINT

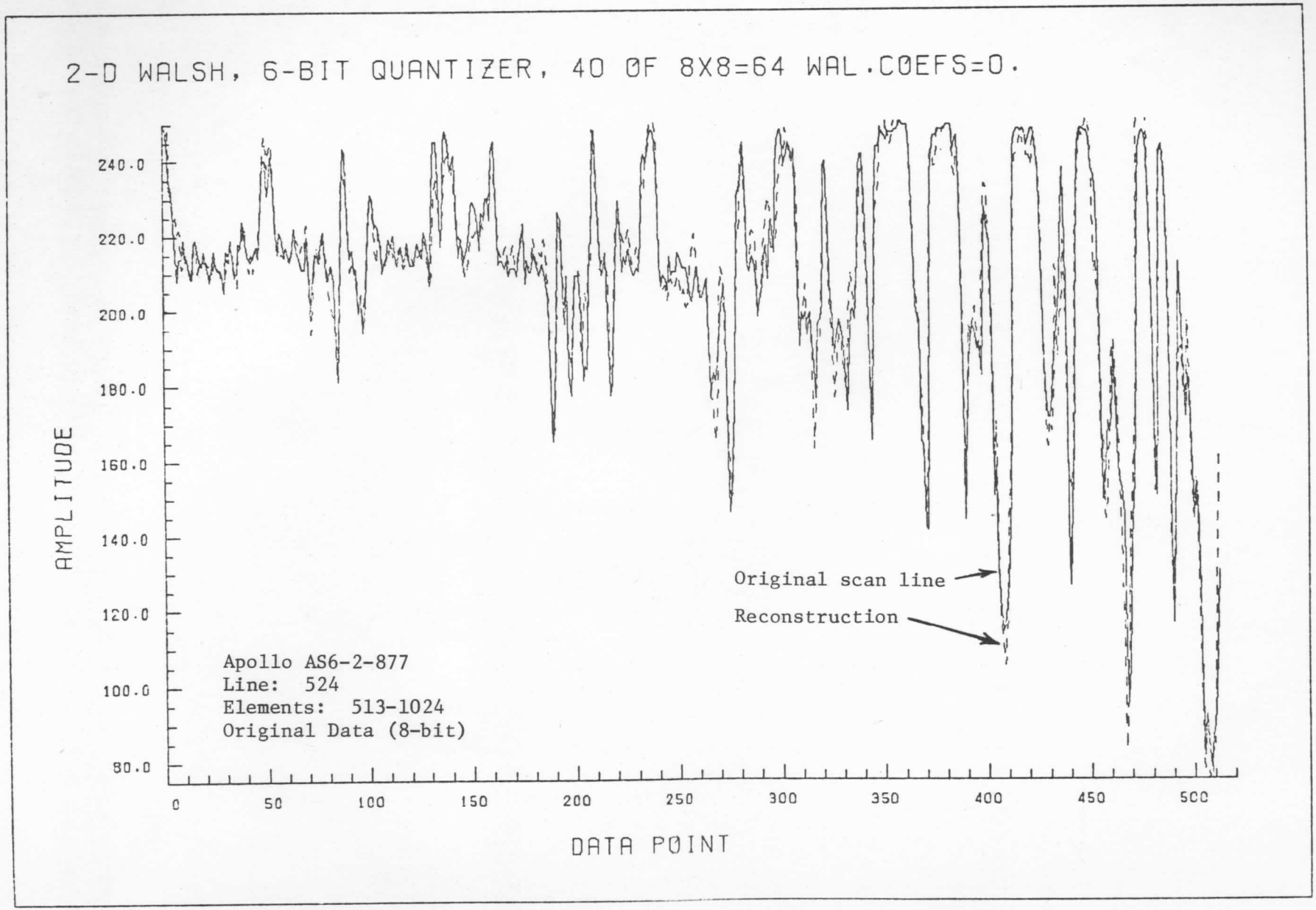
2-D WALSH, 6-BIT QUANTIZER, 40 OF 8X8=64 WAL.COEFS=0.
AMPLITUDE
240.0
220.0
200.0
180.0
160.0
140.0
120.0
100.0
80.0
0
50
100
150
200
250
300
350
400
450
500
DATA POINT
Original scan line
Reconstruction
Apollo AS6-2-877
Line: 524
Elements: 513-1024
Original Data (8-bit)

FIGURE 4.4. GRAPHS SHOWING EFFECTS OF QUANTIZATION IN THE 8×8 WALSH TRANSFORM.

Notes: 1). Solid line is the original scan line (8-bit data, smoothed with SMSOPT).

2). Dashed line in the first graph is the reconstructed line after retention of 16 of the 64 coefficients and then taking the inverse Walsh transform.

3). Dashed line in the second graph is the reconstructed line after quantizing 16 of the 64 coefficients to 6 bits and then taking the inverse Walsh transform.

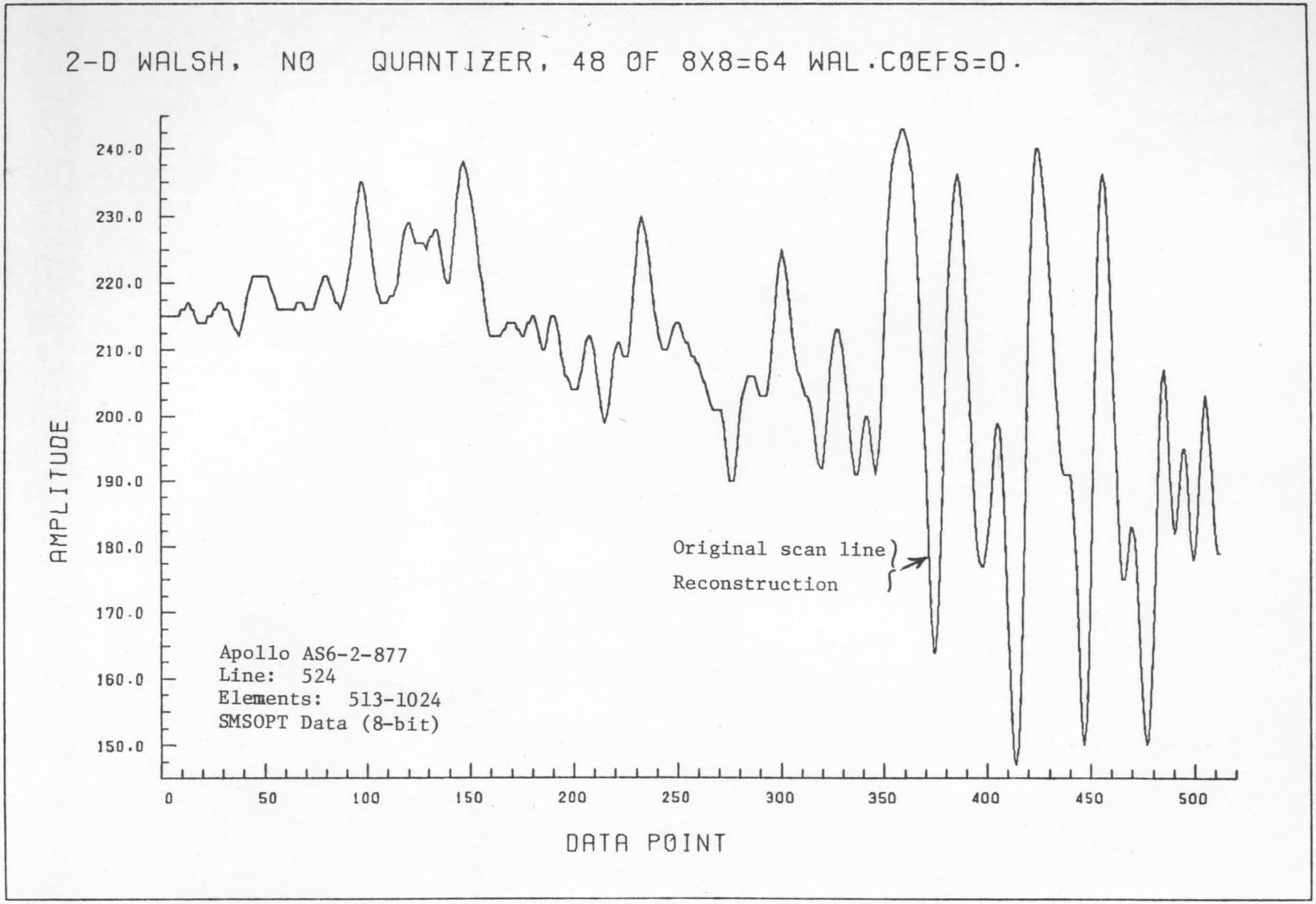
2-D WALSH, NO QUANTIZER, 48 OF 8X8=64 WAL.COEFS=0.
AMPLITUDE
240.0
230.0
220.0
210.0
200.0
190.0
180.0
170.0
160.0
150.0
0
50
100
150
200
250
300
350
400
450
500
DATA POINT
Original scan line
Reconstruction
Apollo AS6-2-877
Line: 524
Elements: 513-1024
SMSOPT Data (8-bit)

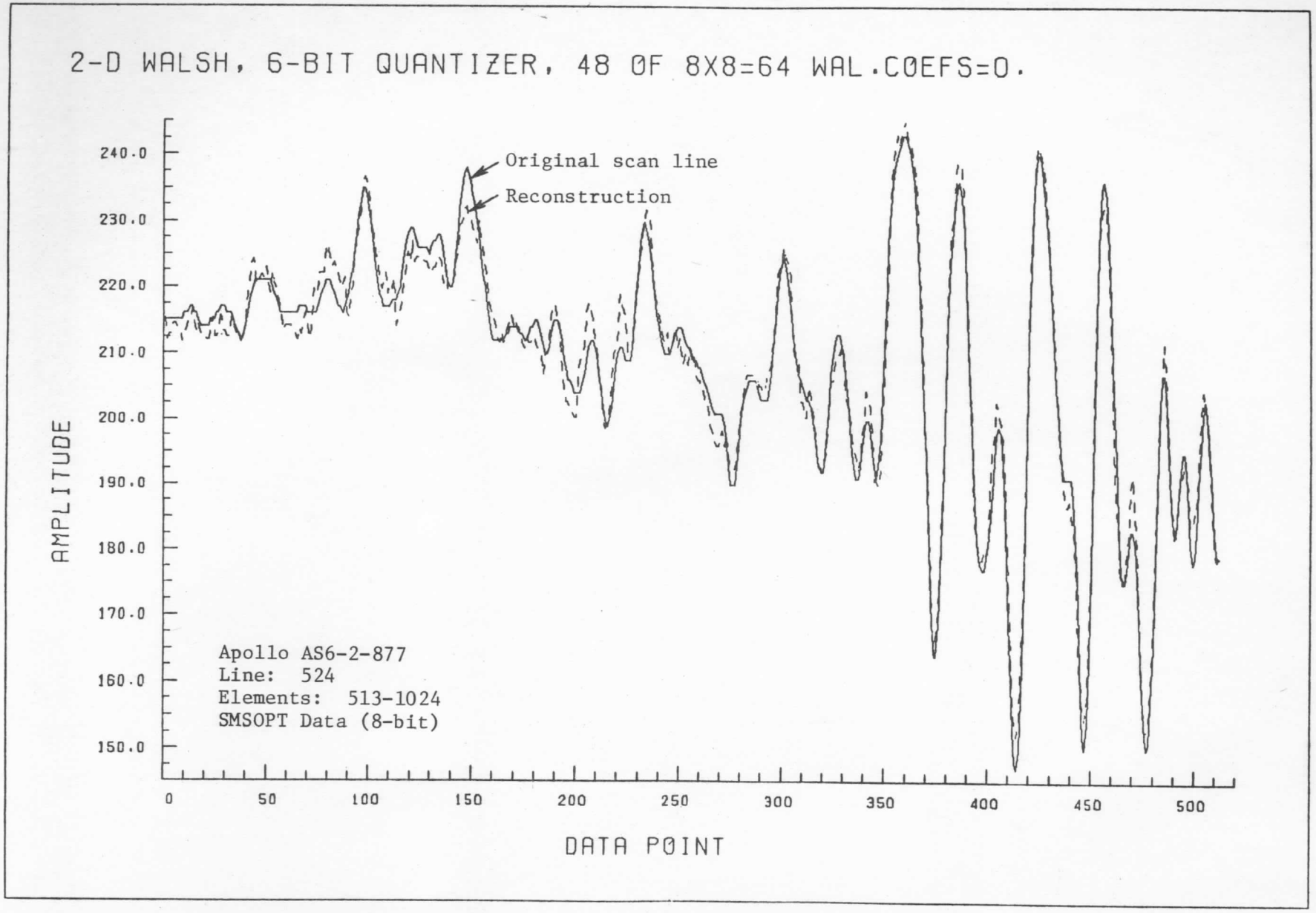
2-D WALSH, 6-BIT QUANTIZER, 48 OF 8X8=64 WAL.COEFS=0.
Original scan line
Reconstruction
AMPLITUDE
240.0
230.0
220.0
210.0
200.0
190.0
180.0
170.0
160.0
150.0
0
50
100
150
200
250
300
350
400
450
500
DATA POINT
Apollo AS6-2-877
Line: 524
Elements: 513-1024
SMSOPT Data (8-bit)

FIGURE 4.5. GRAPHS SHOWING EFFECTS OF QUANTIZATION IN 8×8 WALSH TRANSFORM WHEN SAMPLING RATE IS REDUCED BY FACTOR OF FIVE.

Notes:

1). Solid line is the original scan line (8-bit data, smoothed with SMSOPT).

2). Data has been sampled at every fifth point and every fifth line.

3). Dashed line in the first graph is the reconstructed scan line after retention of 16 of the 64 coefficients and then taking the inverse Walsh transform.

4). Dashed line in the second graph is the reconstructed line after quantizing 16 of the 64 coefficients to 6 bits, setting the rest to zero, and then taking the inverse Walsh transform.

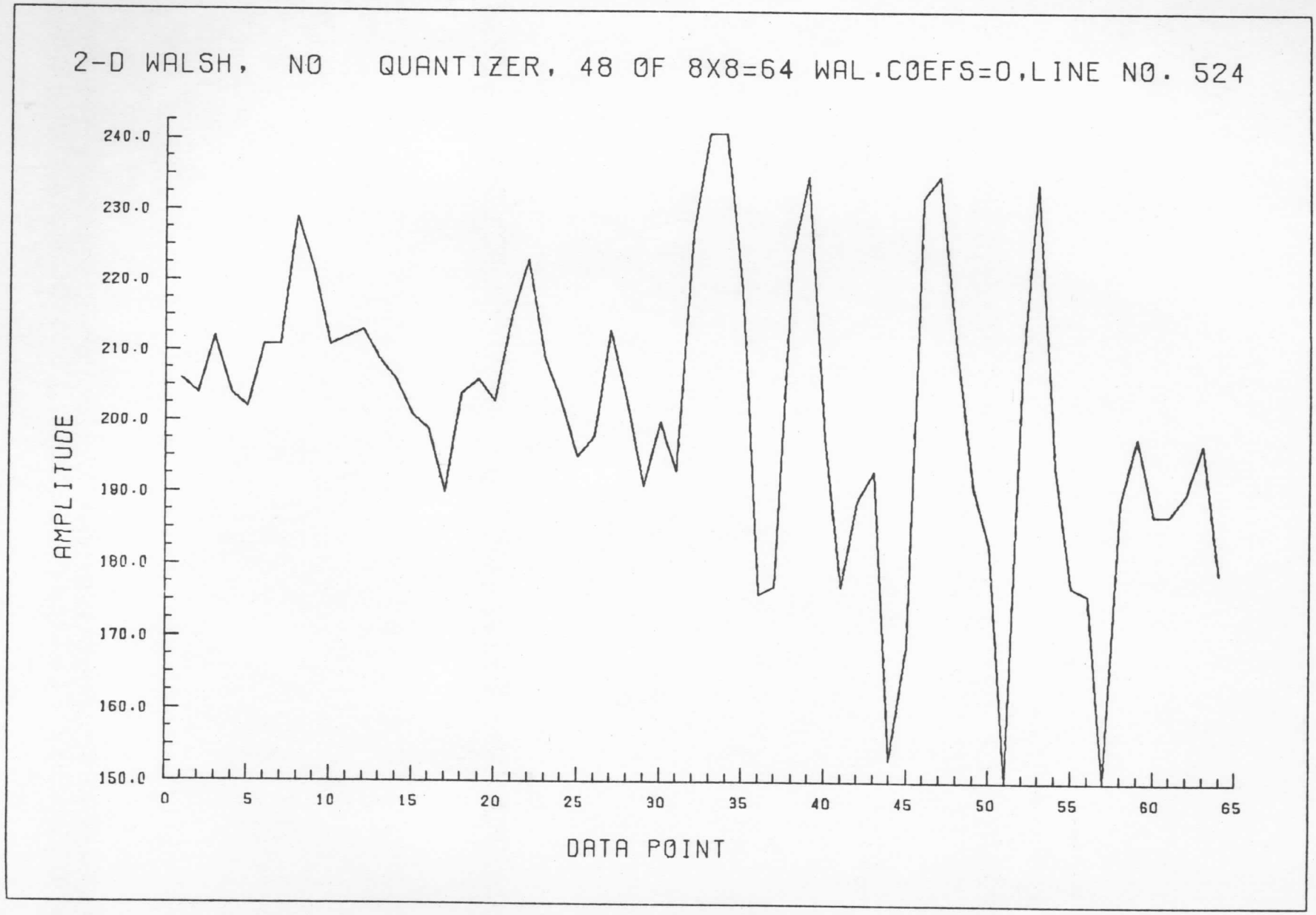
2-D WALSH, NO QUANTIZER, 48 OF 8X8=64 WAL.COEFS=0,LINE NO. 524
AMPLITUDE
240.0
230.0
220.0
210.0
200.0
190.0
180.0
170.0
160.0
150.0
0
5
10
15
20
25
30
35
40
45
50
55
60
65
DATA POINT

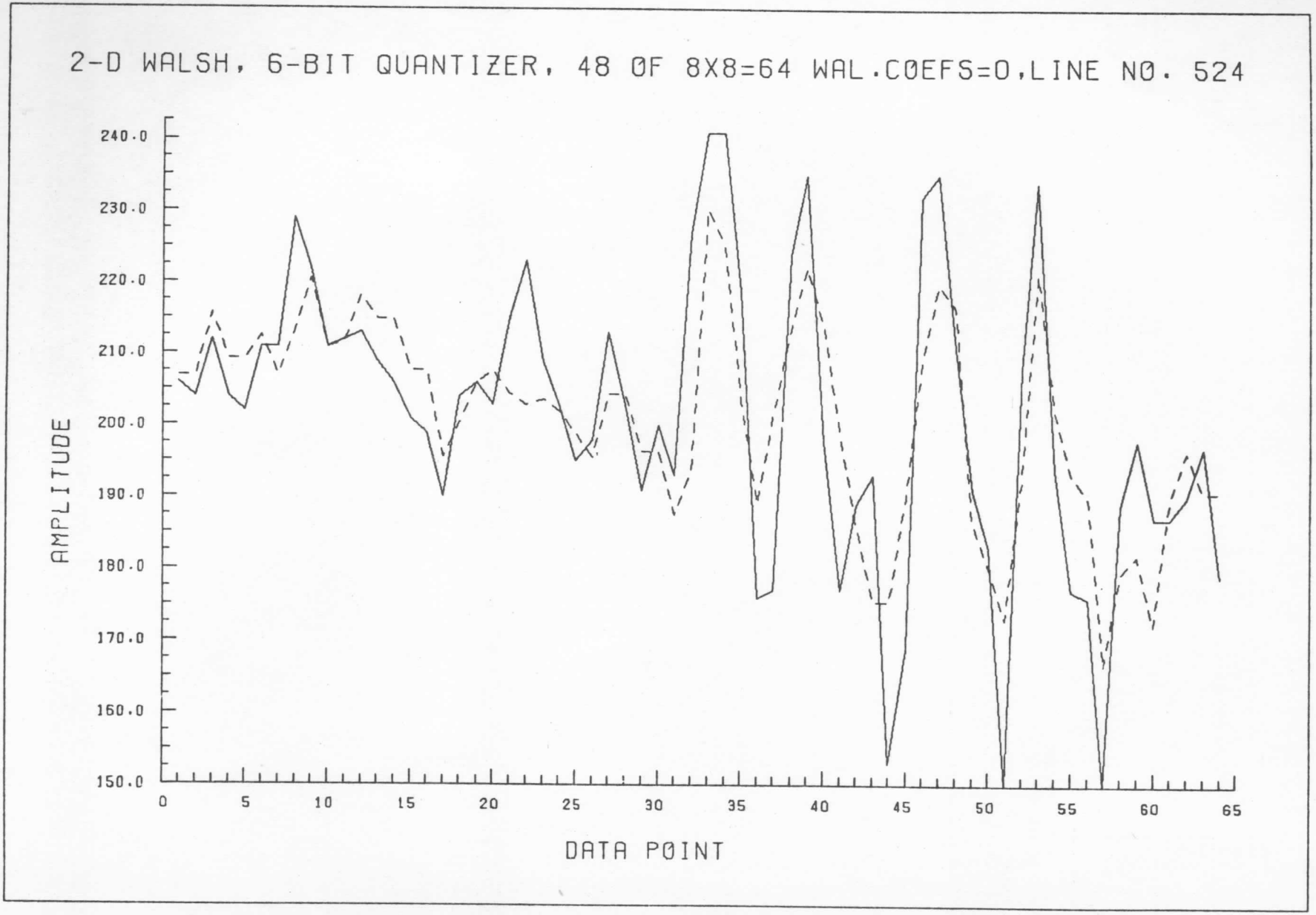
2-D WALSH, 6-BIT QUANTIZER, 48 OF 8X8=64 WAL.COEFS=0,LINE NO. 524
AMPLITUDE
240.0
230.0
220.0
210.0
200.0
190.0
180.0
170.0
160.0
150.0
0
5
10
15
20
25
30
35
40
45
50
55
60
65
DATA POINT

V
COMPARISONS IN PERFORMANCE

We have chosen two criteria for the performance of possible encoding methods. The first is that of the wind measurement surfaces which yield an estimate on the possible accuracy of determining winds from successive cloud pictures. The second criterion is reconstructed picture quality. Because both are rather difficult to measure quantitatively (the latter more so than the former) we present the plots and photographs here together with our interpretation.

5.1 Wind Measurement Surfaces

Through the courtesy of Eric Smith and Dennis Phillips of the U.W. Space Science and Engineering Center, the WINDCO program developed earlier for generation of wind measurement surfaces of ATS data [20] was adapted to the Apollo picture data. This program was run on the McIDAS display system at the U.W. Space Science and Engineering Center for the different encoding systems and the results are shown here.

In the WINDCO program, a 32x32-point matrix array is moved at varying lags across a 64x64-point array. A metric is chosen and the resulting surfaces are displayed in a three-dimensional frame of reference. The peak can be used as a wind measurement accuracy indicator and the secondary peaks and surfaces as an indicator of possible erroneous measurements.

Several different metrics can be chosen. For these studies we have used a "magnitude-error" sum. This means the magnitude of the differences are summed to give the measurement surfaces. Other possible criteria are magnitude-squared-error and cross-correlation. The magnitude-error criterion was chosen to minimize the McIDAS computing time. It also generally gives higher secondary peaks and measurement surfaces which are of interest in the comparison. Some

plots using the much longer correlation program were run on the Univac 1108 for the same Apollo VI data and are included in Appendix D for reference.

The input data for making these measurements does not include effects of optics, PMT noise, or filtering, and therefore are tests of the encoding methods themselves.

In Fig. 5.1a, several picture samples taken from the lower right quarter of Apollo AS6-2-877 were run against themselves as an idealized case. The picture locations are given; note the small bright clouds give excellent wind measurement surfaces.

In the succeeding graphs in Fig. 5.1, the outputs of different encoding systems were run against the original data for the same picture locations. (No attempt was made to line up the pictures exactly so the peaks in the wind measurement surfaces are not always at zero.)

Many more computations were run than those which correspond to the plots shown. Some areas, particularly those where the cloud patterns vary little over the 32x32-point array size, show little change with various encoding choices. The plots shown here are representative of some of the sharply-defined cloud patterns and show marked differences.

From the results of Fig. 5.1, we conclude the 4-bit first-order DPCM system is very good in making wind measurements, both from the width of the measurement peak and in the relative attenuation of the sidelobe levels. Both the 8x8 Walsh with 24 coefficients and the 6-bit second-order interpolator provide poorer wind measurement surfaces. The trend is fairly consistent over all four surfaces displayed.

FIGURE 5.1. WIND MEASUREMENT SURFACE PLOTS FOR SELECTED AREAS IN APOLLO AS6-2-877

Notes:

1). A photograph of Apollo AS6-2-877 (LRQ) is shown in Fig. 5.2a.

2). The centers for the plots, assuming that the upper left corner of Apollo AS6-2-877 (LRQ) is at (0,0), are:

(1). Line 52, element 152;
(2). Line 112, element 152;
(3). Line 352, element 152;
(4). Line 412, element 152.

The plot numbers correspond to the above listings.

3). Matrix sizes used were: 32x32, 64x64.

4). Encoding methods are noted on graphs.

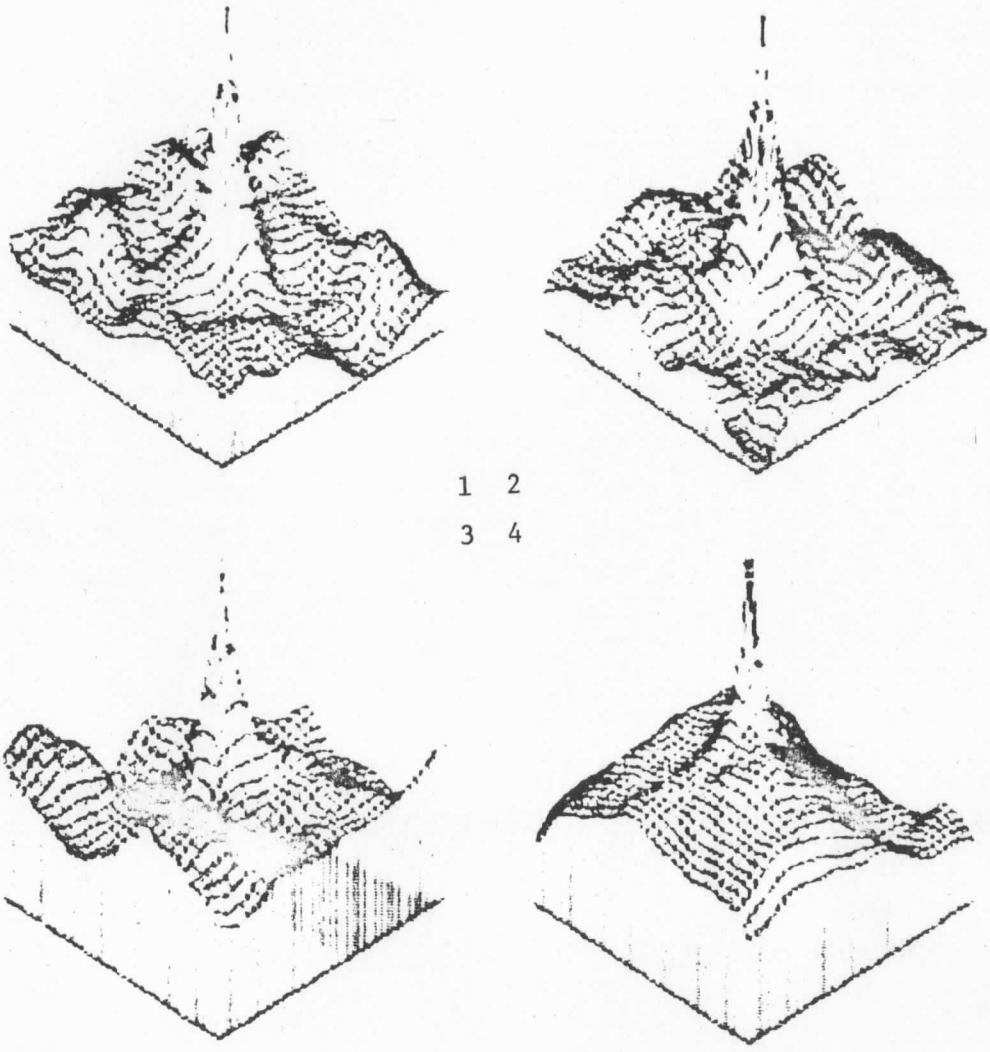

1 2

3 4

Apollo AS6-2-877; LP1 metric

Original data

8-bit linear code

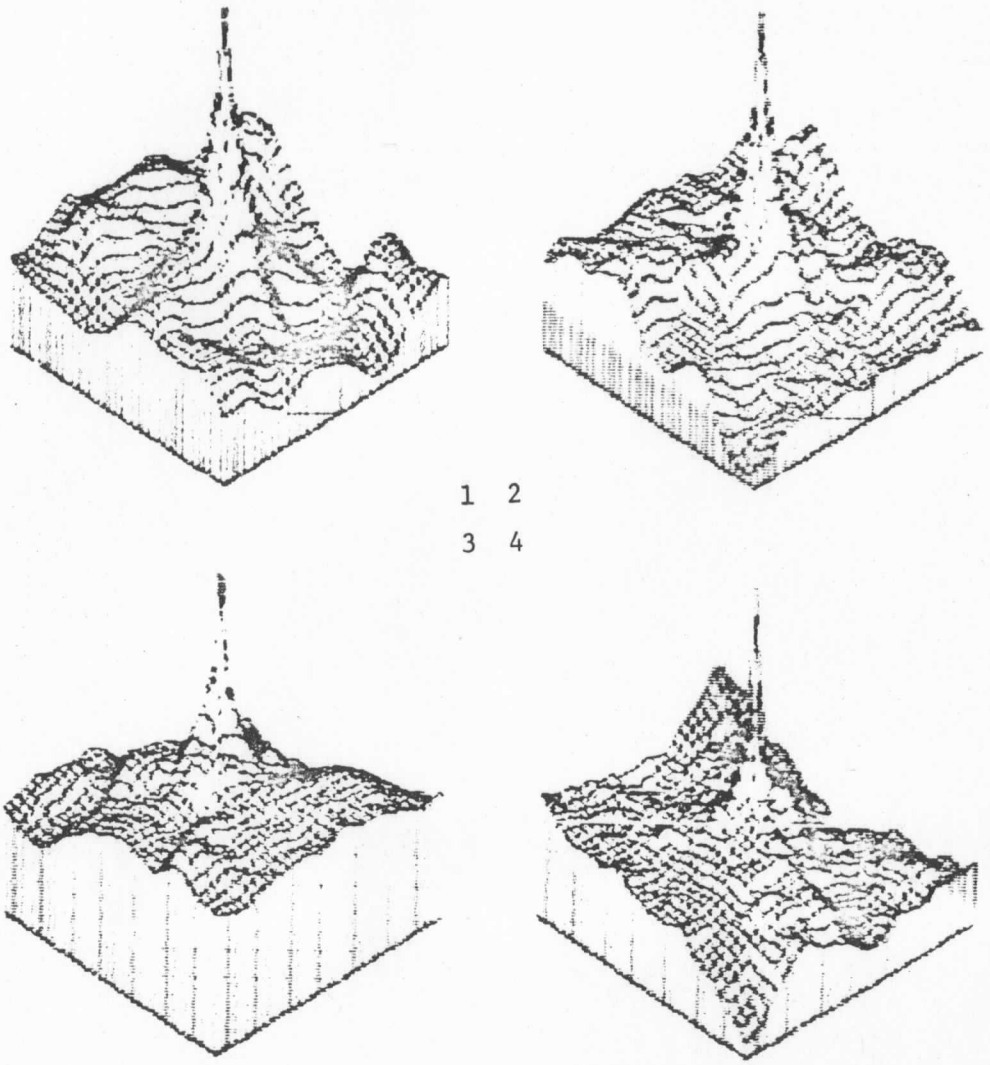

1 2

3 4

Apollo AS6-2-877; LP1 metric
First-order DPCM w/accumulator
4-bit linear output code

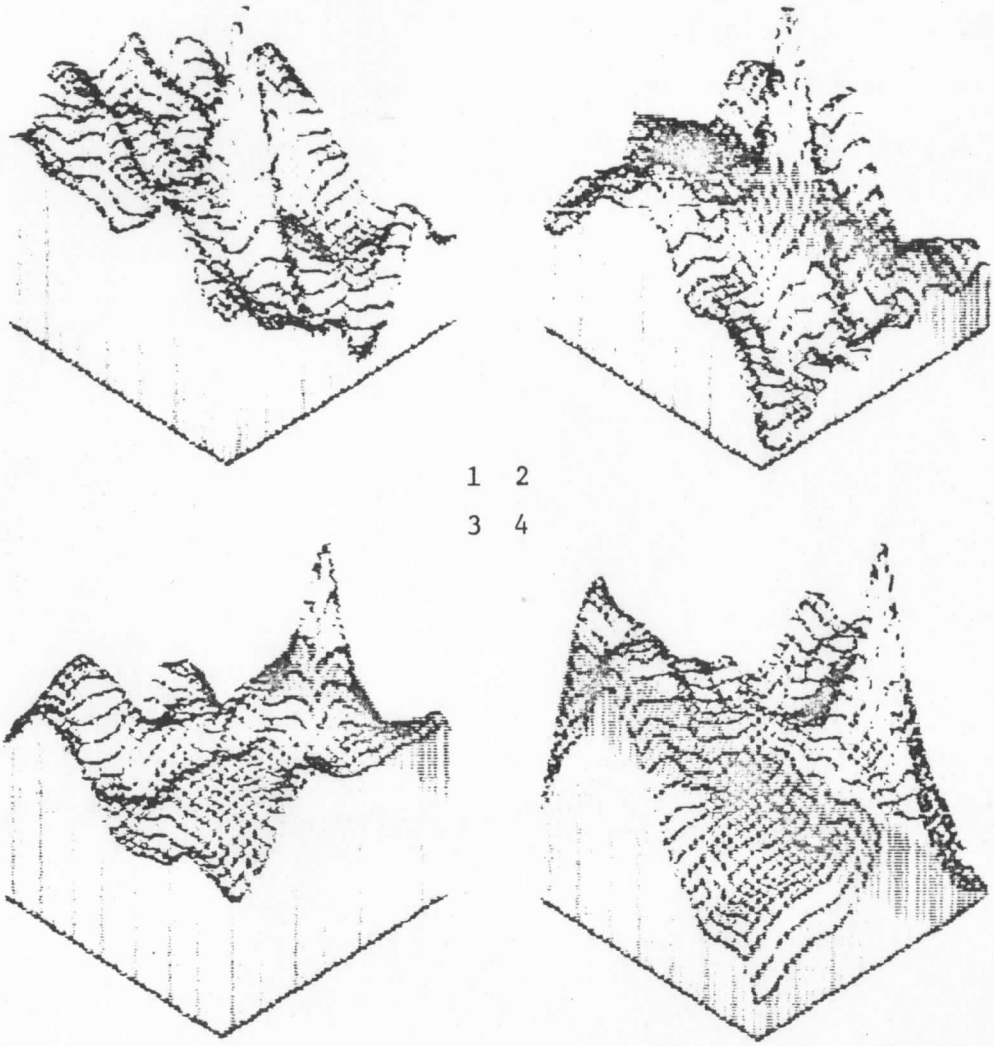

1 2

3 4

Apollo AS6-2-877; LP1 metric
Second-order Interpolator
6-bit linear output code

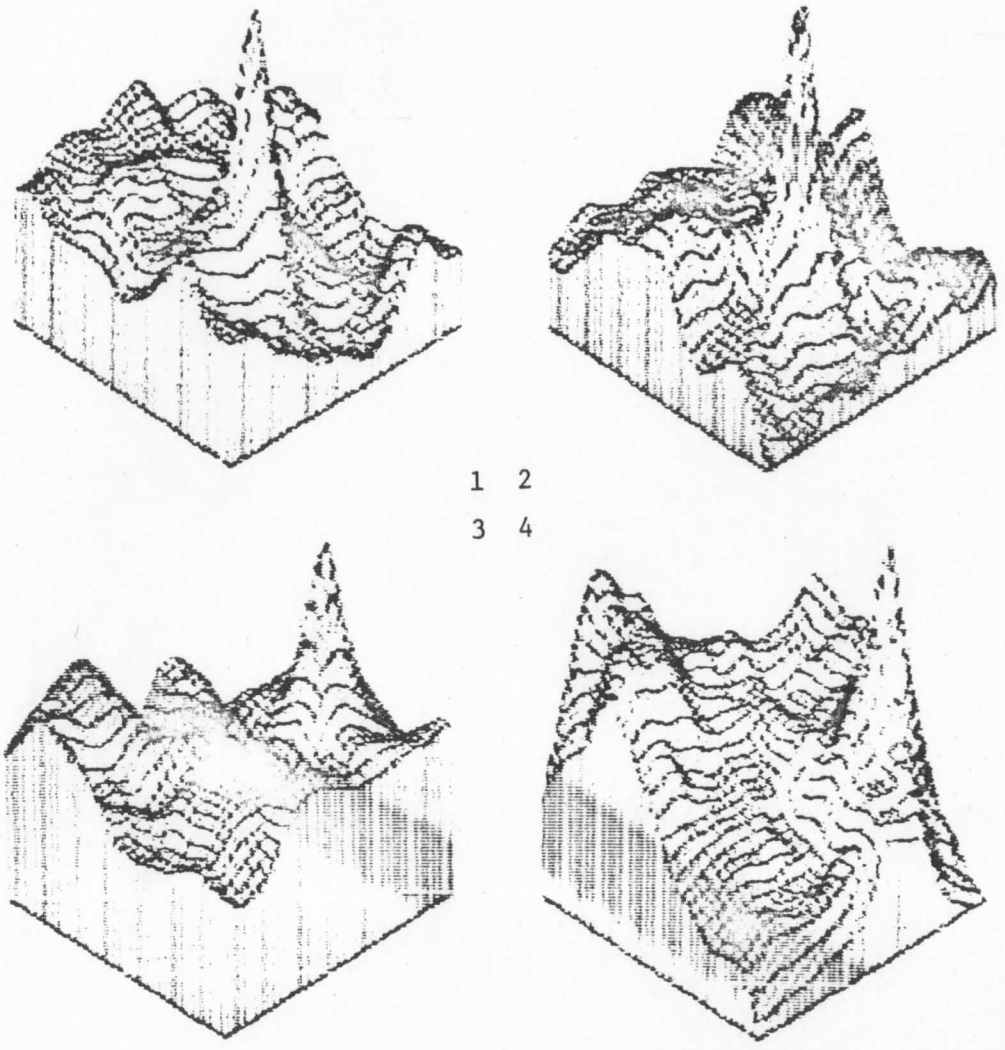

1 2

3 4

Apollo AS6-2-877; LP1 metric
8x8 Walsh, 24 coefficients
6-bit piecewise linear code

5.2 Picture Reconstruction

A second criterion for judging the performance is how well each encoding method reproduces a given picture. Picture quality is somewhat of a subjective criterion, so we have reproduced four representative quarter-pictures from the Apollo VI mission for each encoding method. Because the selection rule for the Walsh coefficients varied slightly in our various simulations, we include a diagram, shown in Fig. 5.2., of the selection rule used in these picture simulations.

Fig. 5.3a shows the original lower right quarter of Apollo AS6-2-877 as sampled and reconstructed and is included for reference. Fig. 5.3b shows the same quarter-picture after it has been passed through a simulation of the present SMS optics system (see Appendix B). The optics program has not been used in any of the encoding method studies, so picture degradation can be attributed directly to the encoding method. This one reproduction using the SMS optics program is included for reference. If the same optics were used, the encoding errors would add to the degradation already introduced.

Fig. 5.4 shows four picture reconstructions using each of the three main encoding methods discussed in this report. Note all three give acceptable reconstructions. Observing the detail carefully does disclose some differences, however, and the first-order DPCM system has a favorable edge on performance. The Walsh method exhibits some 8×8 "block" effect, most noticeably in the lower right corner of #877. This can probably be minimized by assigning a longer code to the "D.C." term in each 8×8 block. Coefficient selection for the 8×8 Walsh encoding used a symmetrical version of the rule discussed in Chapter 4 and is shown in Fig. 5.2. In proportion to the bandwidth efficiency, however, the 8×8 Walsh encoding does a remarkably good job of picture reconstruction.

The second-order interpolator, while having the same bandwidth efficiency in these studies as the 8×8 Walsh, definitely exhibits inferior performance. The one-dimensional scan lines are clearly evident and some picture detail is obscured.

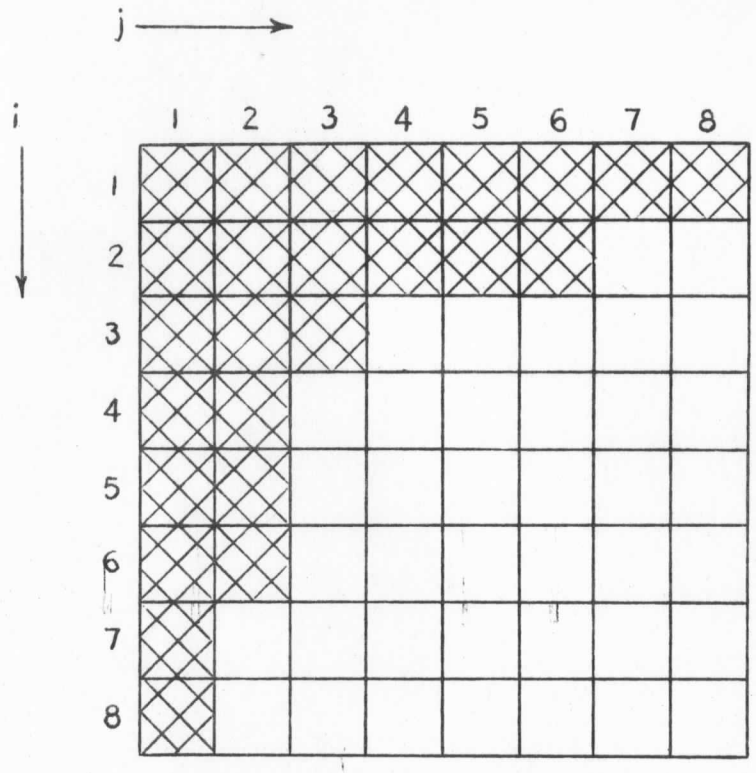

Figure 5.2. Diagram of Walsh Coefficient Array used for Picture Reconstruction of Apollo AS6-2-877, -934, -1430, -1469.

FIGURE 5.3. A RECONSTRUCTION OF APOLLO AS6-2-877 (LRQ) AND EFFECTS OF SATELLITE OPTICS.

Notes: 1. Data is 8-bit in a 512×512 format.

2. Data sampling is 0.08 n.mi/sample.

3. See Appendix B for explanation of SMSOPT.

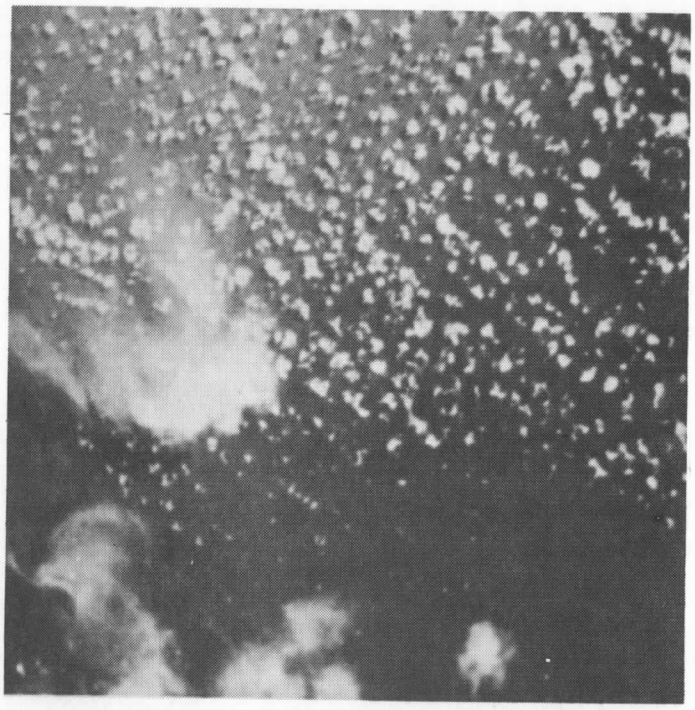

Apollo AS6-2-877 (LRQ)
Original Data
8-bit linear code

Apollo AS6-2-877 (LRQ)
SMSOPT data
8-bit linear code

FIGURE 5.4. APOLLO PICTURE RECONSTRUCTIONS USING DIFFERENT ENCODING METHODS

Notes:
1. Data is in 512×512 format.
2. Encoding method is as indicated.
3. Picture scaling is normally 40 n.mi. x 40 n.mi.

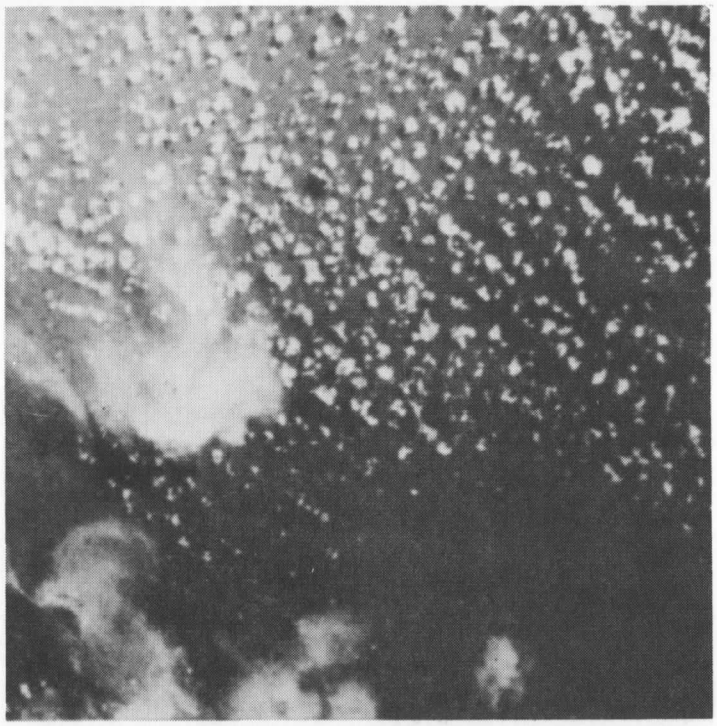

Apollo AS6-2-877 (LRQ)
First-order DPCM w/accumulator
4-bit linear output code

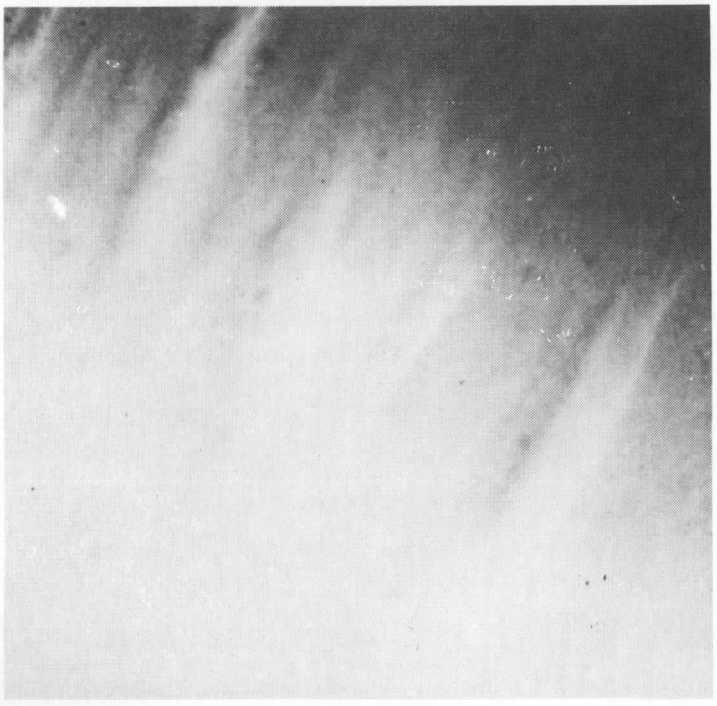

Apollo AS6-2-934 (URQ)
First-order DPCM w/accumulator
4-bit linear output code

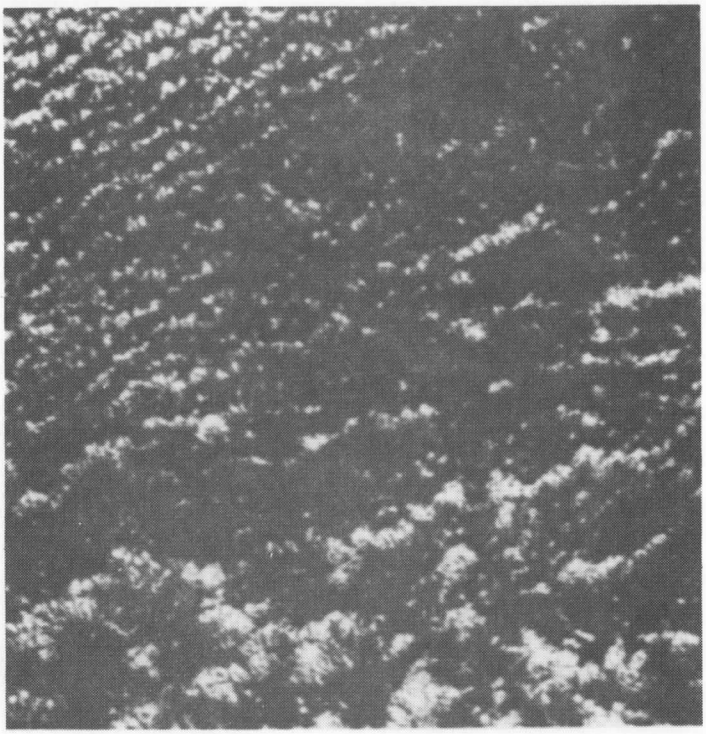

Apollo AS6-2-1430 (CRQ)
Fist-order DPCM w/accumulator
4-bit linear output code

Apollo AS6-2-1469 (LRQ)
First-order DPCM w/accumulator
4-bit linear output code

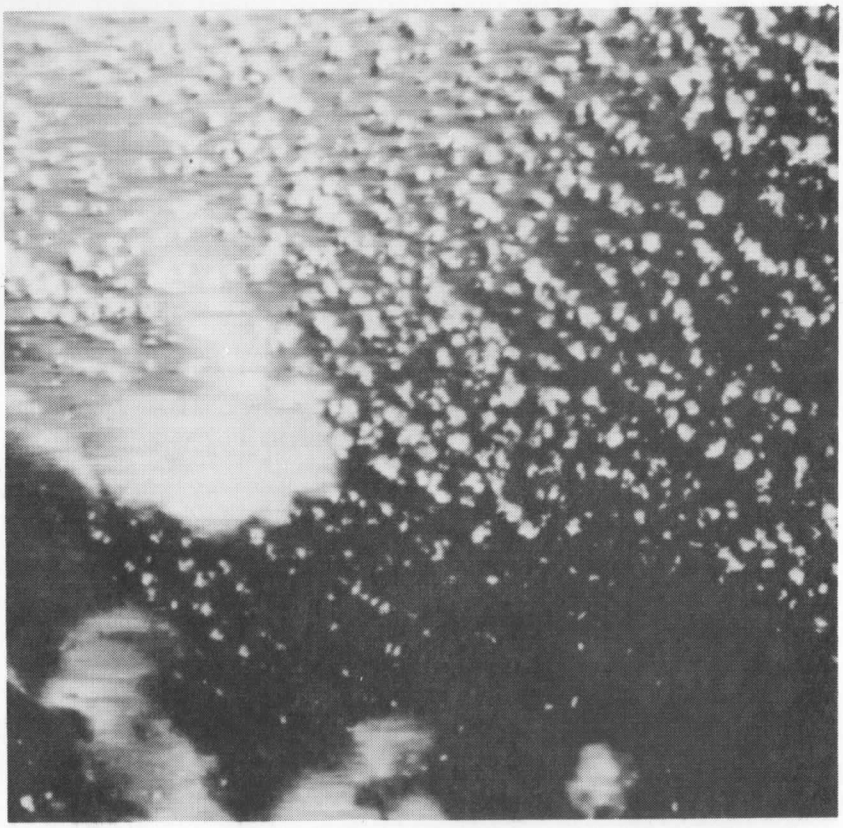

Apollo AS6-2-877 (LRQ)
Second-order Interpolator
6-bit linear output code

Apollo AS6-2-934 (URQ)
Second-order Interpolator
6-bit linear output code

Apollo AS6-2-1430 (CRQ)
Second-order Interpolator
6-bit linear output code

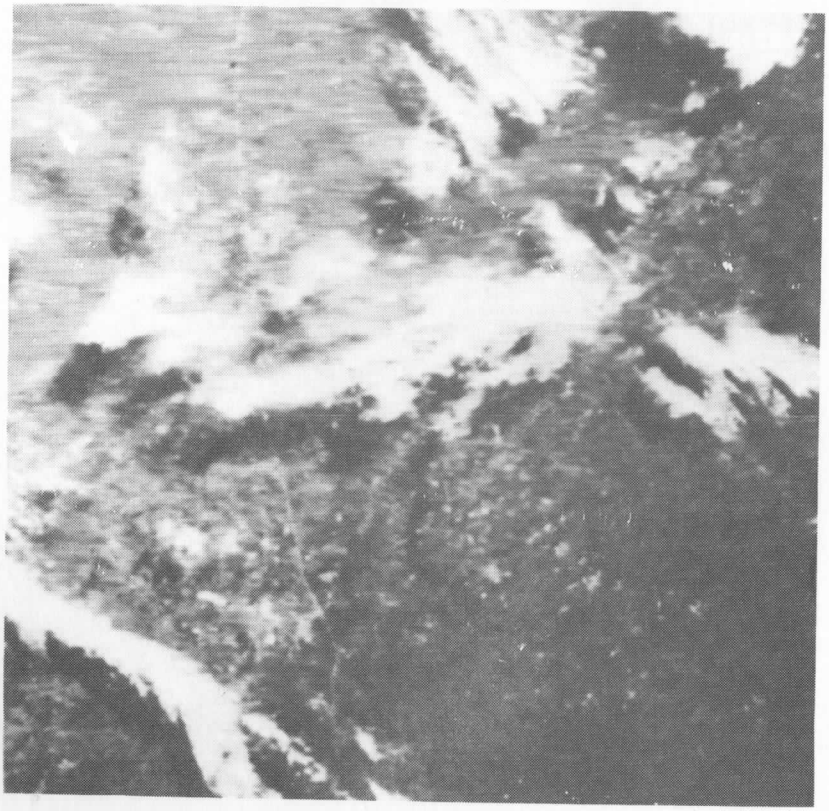

Apollo AS6-2-1467 (LRQ)
Second-order Interpolator
6-bit linear output code

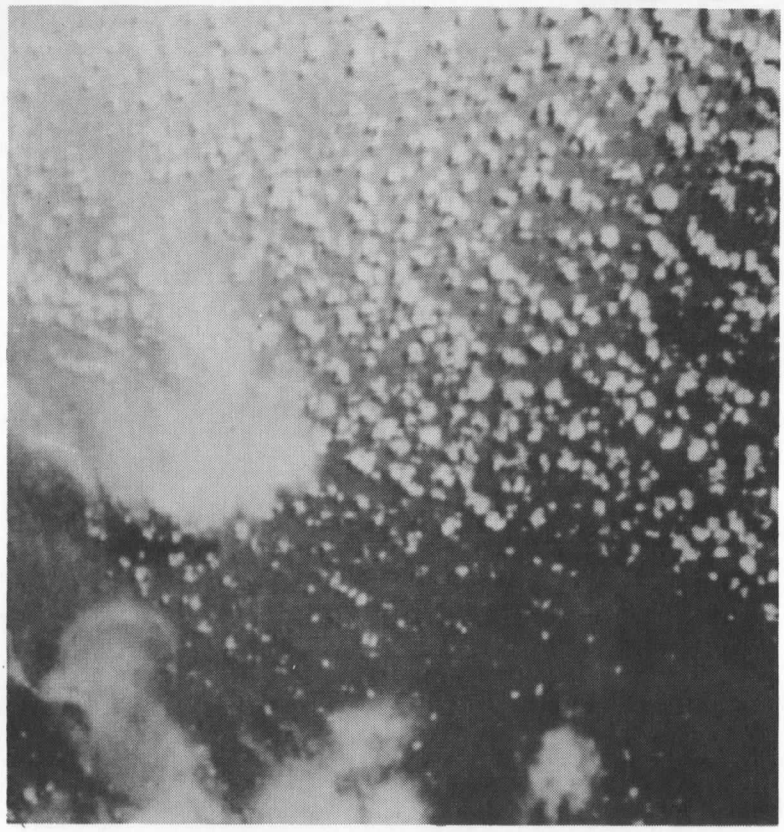

Apollo AS6-2-877 (LRQ)
8 x 8 Walsh, 25 coefficients
6-bit piecewise-linear code

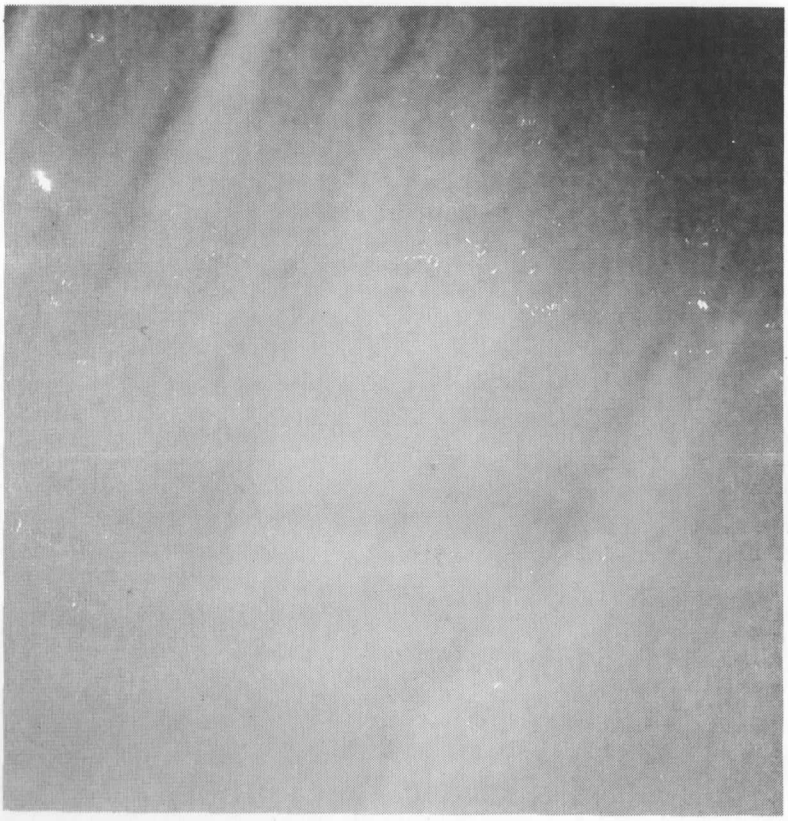

Apollo AS6-2-934 (URQ)
8 x 8 Walsh, 25 coefficients
6-bit piecewise linear code

Apollo AS6-2-1430 (CRQ)
8 x 8 Walsh, 25 coefficients
6-bit piecewise linear code

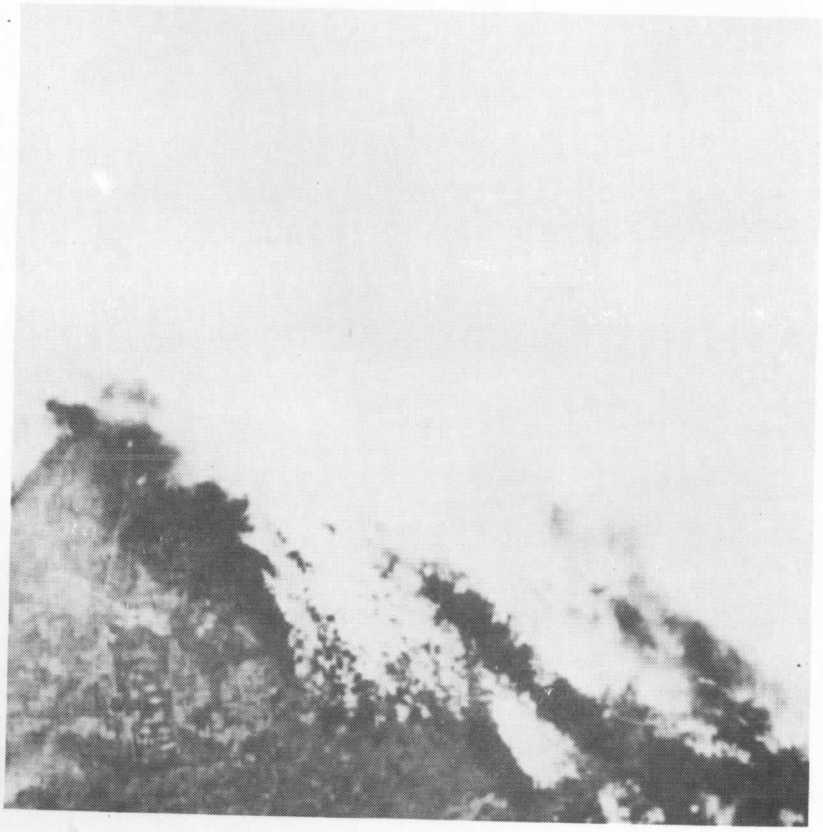

Apollo AS6-2-1469 (LRQ)
8 x 8 Walsh, 25 coefficients
6-bit piecewise linear code

VI

CONCLUSIONS AND RECOMMENDATIONS

Our studies of possible encoding methods for meteorological satellite designs in the near future demonstrate the use of a 4-bit first-order DPCM system with a stand-by accumulator is a first choice. This type of system provides a savings of 33 % in bandwidth over the present SMS and is simple to implement, multiplex and maintain. The stand-by accumulator assures that there are no long-term errors. Short-term errors are present when very sharp cloud edges are encountered , but our studies indicate the loss in resolution is not much greater than about two samples. Wind measurements are virtually unaffected by these errors.

The first-order DPCM system permits a "back-up"mode which is easy to implement. Disabling the delay and accumulator units and increasing the multiplex rate by 50 % (i.e., to the 6-bit rate), the system is returned to a conventional 6-bit system such as the one presently being used. The first-order DPCM system requires one initial sample per scan line. When a scan is completed, the visual scanner is shut off and the delay and accumulator units are cleared. When the scanner comes on, the background intensity will be fairly low (a scan angle of 21° is presently used and the diameter of the earth subtends about 18°). This means the first 4-bit sample can be taken by truncating the 6-bit input code from the left, giving 6-bit intensity resolution in the lowest 25% of the range.

A second choice which involves greater complexity is using the two-dimensional Walsh transform coding. Savings of 60-70 % in bandwidth can be realized using this type of encoding. The method is self-multiplexing and errors tend to be non-localized in the reconstructed picture but spread in

blocks (8x8 in our case). These effects can be minimized with a proper quantization rule for the coefficients.

The second-order interpolator, while efficient in one-dimensional picture reconstructions [6], is not as efficient as the 8x8 Walsh in the two-dimensional reconstructions. It also has the drawback in that it is difficult to multiplex several channels efficiently using this method. Therefore it is more suited to single-scanner systems.

The DPCM system gives the best performance in picture reconstruction but requires the most bandwidth. The 8x8 Walsh is slightly poorer in overall performance because of the "block" effect, but this can be minimized by proper choice of coefficient quantization rule. The second-order interpolator is decidedly the poorest in comparison to the other two methods. The DPCM system yields better wind measurement surfaces which can give more accurately defined winds. The other two systems give about equal performance in this respect. The 8x8 Walsh is more tolerant to additive noise effects because these effects are distributed over an area of 8x8 picture elements. The 8x8 Walsh has a definite advantage in the efficiency of bandwidth used.

Finally, it should be mentioned we have investigated several other types and combinations of systems and have, in fact, run some picture reconstructions and wind measurement surfaces using them. However, the above three systems show the most promise within the design constraints and performance criteria chosen.

VII
REFERENCES

1. Stremler, F.G., G.R. Redinbo et al., "Visual Channel Data Analysis for a Synchronous Meteorological Satellite", NOAA Final Report on NG-26-72, 1 July 1973, Space Science and Engineering Center, The University of Wisconsin, Madison, Wis. 53706.

2. Stremler, F.G. and G.R. Redinbo, "A Study of Applicable Encoding Methods for a Geostationary Orbiting Experimental Satellite", NOAA Interim Report on Grant 3-35372, Space Science and Engineering Center, The University of Wisconsin, Madison, Wis. 53706.

3. Jain, A.K.,"Image Modeling for Unification of Transform and DPCM Coding of Two-Dimensional Images", Proc. NEC (Chicago), 28 Oct. 1973, pp.280-285

4. O'Neal, J.B. Jr.,"Predictive Quantizing Systems (DPCM) for the Transmission of Television Signals", BSTJ, 45, May-June 1966, pp.689-721.

5. Millard, J.B. and H.I. Maunsell, "The PICTUREPHONE System: Digital Encoding of the Video Signal", BSTJ, 50, February 1971, pp.459-479.

6. Kortman, C.M.,"Redundancy Reduction--A Practical Method of Data Compression", Proc. IEEE, 55, Mar. 1967, pp.253-262.

7. Andrews, C.A., J.M. Davies, and G.R. Schwartz, "Adaptive Data Compression", Proc. IEEE, 55, Mar. 1967, pp.267-277.

8. Connor, D.J., R.F.W. Pease and W.G. Scholes, "Television Coding using Two-dimensional Spatial Prediction", BSTJ, 50, March 1971, pp.1049-1061.

9. Sakrison, D.J. and V.R. Algazi, "Comparison of Line-by-Line and Two-Dimensional Encoding of Random Images", IEEE Trans. Info. Theory, IT-17, July 1971, pp.286-398.

10. Landau, H.J. and D. Slepian, "Some Computer Experiments in Picture Processing for Bandwidth Reduction", BSTJ, 50, May-June 1971, pp.1525-1540.

11. Lackey, R.B., "Walsh Functions Inside-Out", Proc. NEC 28, Oct. 1973, pp.267-270.

12. Harmuth, H.F., Transmission of Information by Orthogonal Functions, Second Ed., Springer-Verlag, Berlin/N.Y., 1972.

13. Pratt, W.K., J. Kane and H.C. Andrews, "Hadamard Transform Image Coding", Proc. IEEE, 57, Jan. 1969, pp.58-68.

14. Wintz, P.A., "Transform Picture Coding", Proc. IEEE, 60, July 1972, pp.809-820.

15. Fontaine, A.B., "Simple Dyadic and Sequency Fortran Mechanizations of the Fast Walsh Transform", Proc. NEC, 28 Oct. 1973, pp.271-273.

16. Ahmed, N., D.H. Lenhert and T. Natarajan, "On the Orthogonal Transform Processing of Image Data", Proc. NEC, 28 Oct. 1973, pp.274-279.

17. Blachman, N.M., "Sinusoids versus Walsh Functions", Proc. IEEE, 62 March 1974, pp.346-354.

18. Habbibi, A., W.K. Pratt et al., "Real Time Redundancy Reduction using Transform Coding Techniques," ICC Conf. Record, 18A1-8, Minneapolis, June 17-19, 1974.

19. "Video Compression May Help Jam-Proof RPV Communications", Electronics, June 27, 1974, pp.33-34.

20. Smith, E. and D. Phillips, "WINDCO: An Interactive System for Obtaining Accurate Cloud Motions from Geostationary Satellite Spin Scan Camera Pictures", NASA Annual Report on NAS5-11542, February 1972, Space Science and Engineering Center, The University of Wisconsin, Madison, Wis. 53706.

21. Computer Sciences Corp. Synchronous Meteorological Satellite Image Quality Analysis, Final Report, Sept. 1972.

APPENDIX A

HISTOGRAM DATA OF SAMPLED APOLLO VI PHOTOGRAPHS

Based on comments from NOAA* on earlier work [1] with selected photographs from the Apollo VI mission, some newly-obtained third-generation NASA transparencies** were digitized. These were digitized to 8-bit independent samples in a 1024×1024 format by the DicoMed Corporation.*** The concern which arose in our earlier digitized pictures was whether some of the levels were "clipped" in the digitization process. Therefore, DicoMed was instructed to make certain no saturation occurred.

To check the work, we ran histograms of the intensity levels for all ten pictures shown in an earlier report [1]. The histograms, which are approximations to the probability density functions of the brightness levels, were computed using all samples in each picture (2^{20} sample values).

Let x be the intensity level of a given photograph; x_i is the value of x at point i digitized to a linear scale at intensity level L. The histogram approximation to the probability density function evaluated at the given level L is:

$$p(L) \approx h(L) = \frac{\sum_{i=1}^{N} x_i | L}{\sum_{i=1}^{N} x_i} \qquad \text{(A-1)}$$

where $x_i | L$ represents the x_i samples at the level L, and N is the total number of samples (2^{20} in our case).

---

* Joseph Silverman, David Small, Charles Bristol.

** Courtesy of R. D. Bratton, Earth Resources Research Data Facility, NASA-JSC, Houston, Texas 77058.

*** DicoMed Corporation, 9700 Newton Avenue South, Minneapolis, Minnesota 55431.

The sample-average statistics of the picture data are computed from:

$$\text{Mean:} \qquad \bar{x} = \frac{1}{N} \sum_{i=1}^{N} x_i \tag{A-2}$$

$$\text{Std. Dev.:} \qquad \sigma_x = \left[\frac{1}{N} \sum_{i=1}^{N} (x_i - \bar{x})^2 \right]^{1/2} . \tag{A-3}$$

These computed statistics are listed in Table A.1.

Table A.1. Standard Deviations of Apollo VI Data

Apollo VI Picture	Picture Data	First Differences	Second Differences
877	34.7	10.60	7.33
934	33.3	5.31	5.14
948	26.7	7.81	5.23
1064	60.0	15.17	10.35
1429	63.9	17.14	11.30
1430	45.7	18.80	12.20
1467	41.0	9.24	7.14
1468	36.1	7.47	5.55
1469	31.2	5.53	3.68
1484	41.4	14.90	9.27

When the transparencies are digitized, the scale is adjusted automatically for the range of transmissivities. This does not give a relative basis for comparisons. Therefore the transmissivity of each transparency was measured using a spot densitometer. Among the ten pictures sampled, the maximum and minimum levels were found to be in Apollo AS6-2-877 and AS6-2-1064 respectively. These were taken as references and several levels were allowed for tolerance. The values of all ten transparencies were then scaled linearly by the computer to fit this range.

Following a suggestion made by David Small at NOAA, we plot this data as histograms to a logarithmic scale. In this way we obtain a large dynamic range in our plots. Plots of the log-histograms of the picture intensity levels

are shown in Fig. A.1 for the ten Apollo transparencies chosen. (Photographic replicas of these pictures appear in Ref. 1, p. 2-3 ff.)

The average entropy is calculated by computing:

$$\varepsilon = - \sum_{i=1}^{N} h(L) \log_2 [h(L)] \qquad \text{(A-4)}$$

over the statistics for each picture. These values are listed in Table A.2. They give us some idea of the relative information content of the sampled picture data.

Table A.2. Computed Entropy (in bits) of Apollo VI Data

Apollo VI Picture #	Picture Data (scaled)	PMT Noise Added (scaled)	First Differences	Second Differences
877	6.58	6.68	5.20	4.62
934	4.19	5.99	4.18	3.77
948	3.45	5.53	4.31	3.63
1064	7.29	7.40	5.69	5.09
1429	5.83	6.84	5.66	5.06
1430	6.89	7.19	6.14	5.51
1467	5.34	6.82	5.05	4.41
1468	4.75	6.44	4.47	3.83
1469	3.94	5.94	3.53	2.94
1484	4.80	6.52	5.58	4.88

The statistics obtained in the above manner are based on photographic data and therefore do not include effects of photomultiplier tube (PMT) noise. To simulate the effects of a typical PMT, a zero-mean conditional Gaussian noise source was added using the experimentally-determined relation:

$$\sigma_{mv} = 1.76\sqrt{S_{mv}} \quad . \qquad \text{(A-5)}$$

Here σ is the standard deviation of the noise and S is the signal level, both expressed in millivolts.

Assuming a linear dynamic range of 5,000 mv for the PMT to correspond to the 8-bit range (0,255), the data samples for inclusion of PMT noise are:

$$w_i = x_i + n_i \tag{A-6}$$

where n_i is zero-mean Gaussian with standard deviation σ_i of:

$$\sigma_i = 0.397\sqrt{x_i} \quad . \tag{A-7}$$

Because the addition of this noise can cause the picture data to exceed the 8-bit capability, all picture datawere re-scaled. The scaling was determined so the minimum and maximum light levels with the PMT noise added would not exceed the 8-bit (0-255) range with a probability of more than 10^{-5} (i.e., within the accuracy of the plots).

Plots of the log-histograms of the picture intensity levels with PMT noise added are shown in Fig. A.2 for the ten Apollo transparencies chosen.

For investigation into possible encoding methods, the statistics of the first- and second-order differences in the picture data are also of interest. The first-order difference between adjacent picture samples in a scan line is defined as:

$$y_i = \begin{cases} x_i & \text{if } x_i \text{ is first sample of scan} \\ x_i - x_{i-1} & \text{otherwise} \end{cases} \tag{A-8}$$

The second-order difference is defined as:

$$z_i = \begin{cases} y_i & \text{if } x_i \text{ is first, second sample of scan} \\ y_i - y_{i-1} & \text{otherwise} \end{cases} \tag{A-9}$$

After the initial few samples in a scan line, Eq. A-9 can be rewritten using Eq. A-8 so that:

$$z_i = x_i - 2x_{i-1} + x_{i-2} \quad . \tag{A-10}$$

Figure A.3 shows plots of the log-histograms of the first-order differences (cf. Eq. A-8) and the second-order differences (cf. Eq. A-10) for the ten Apollo VI photographs.

Conclusions from these histograms are that taking first-order differences does narrow the spread of level values considerably and reduces the average entropy. Second-order differences decrease the spread even more but the relative reduction is not as dramatic. Data reduction of around 40% simply by taking first-order differences would appear to be reasonable from these data. Significant improvements beyond that point by using differences will depend on narrowing the specified uses of the data to tailor the data to the user or by use of adaptive techniques to tailor the encoding to the picture.

Another measure of some interest, particularly in variable-length codes, is run lengths, i.e., how many consecutive samples in a given picture are within specified numerical bounds. Run lengths were tabulated for Apollo AS6-2-877 (2^{20} sample values) and are summarized in Fig. A.4.

FIGURE A.1. LOG-HISTOGRAMS OF BRIGHTNESS LEVELS (SCALED) OF APOLLO VI TRANSPARENCIES.

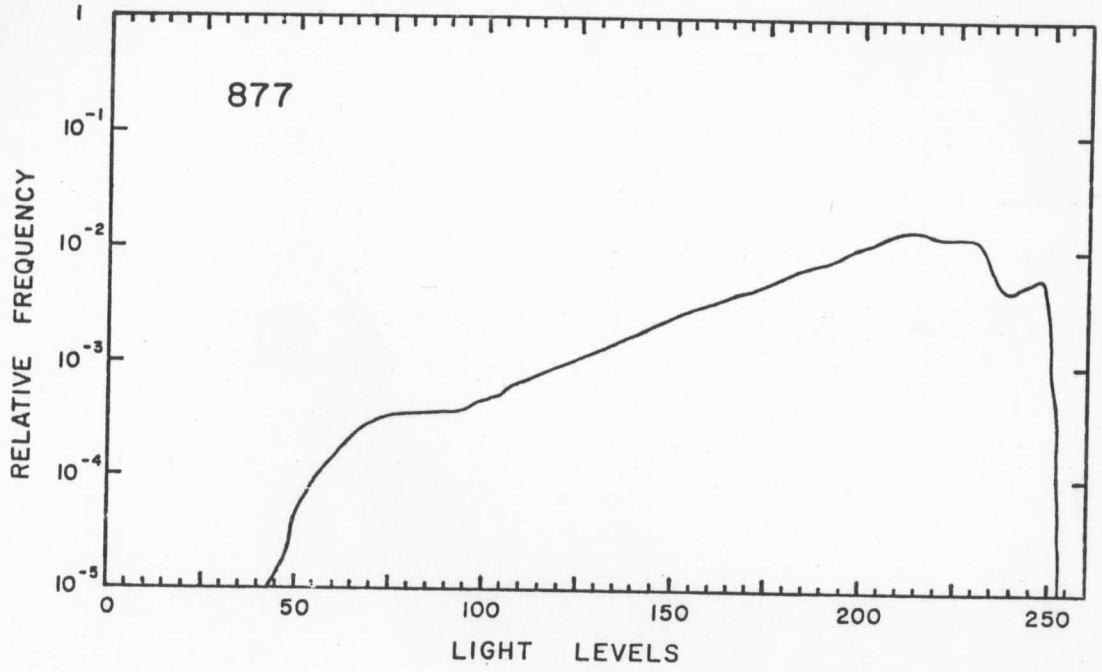
877
RELATIVE FREQUENCY
1
10^{-1}
10^{-2}
10^{-3}
10^{-4}
10^{-5}
0
50
100
150
200
250
LIGHT LEVELS

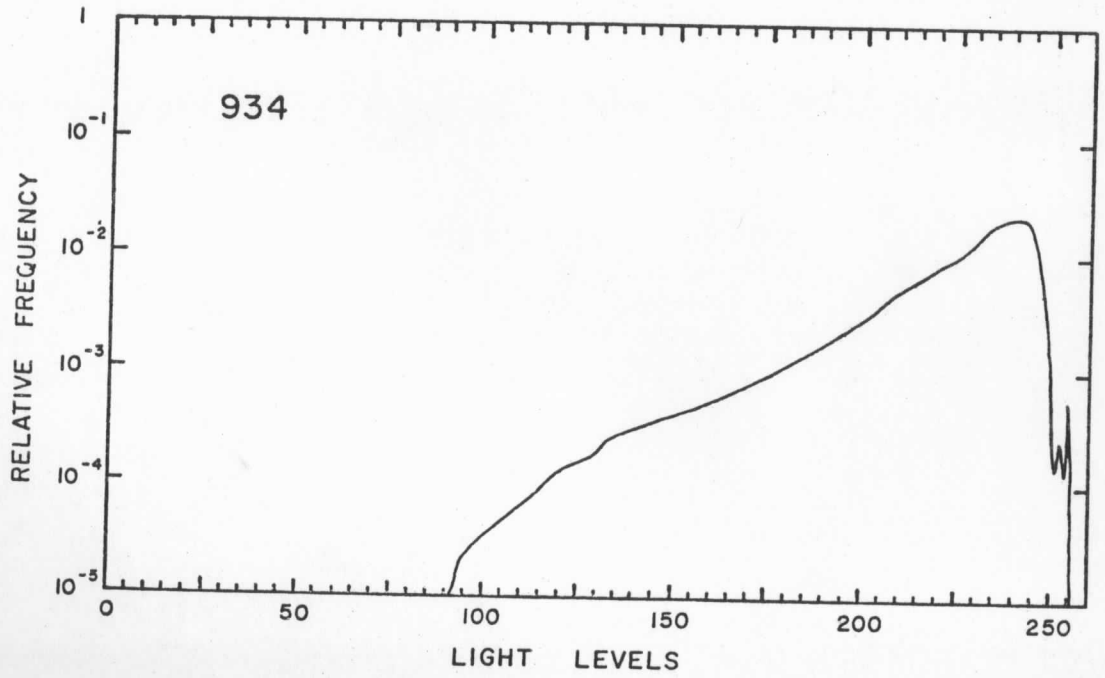
934
RELATIVE FREQUENCY
1
10^{-1}
10^{-2}
10^{-3}
10^{-4}
10^{-5}
0
50
100
150
200
250
LIGHT LEVELS

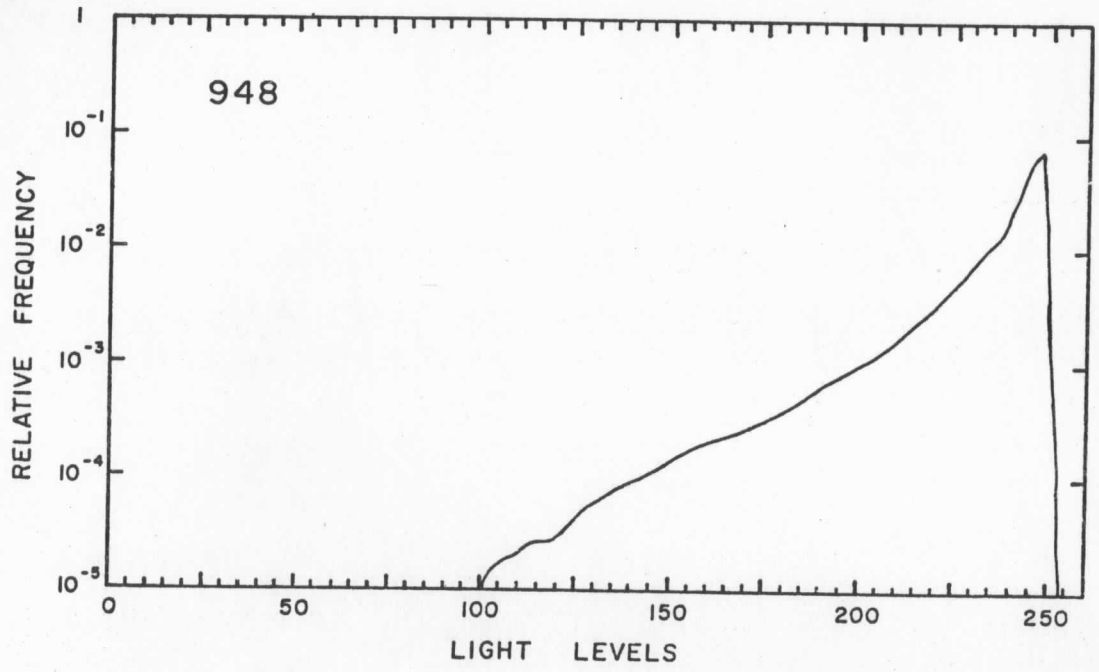
948
RELATIVE FREQUENCY
1
10^{-1}
10^{-2}
10^{-3}
10^{-4}
10^{-5}
0
50
100
150
200
250
LIGHT LEVELS

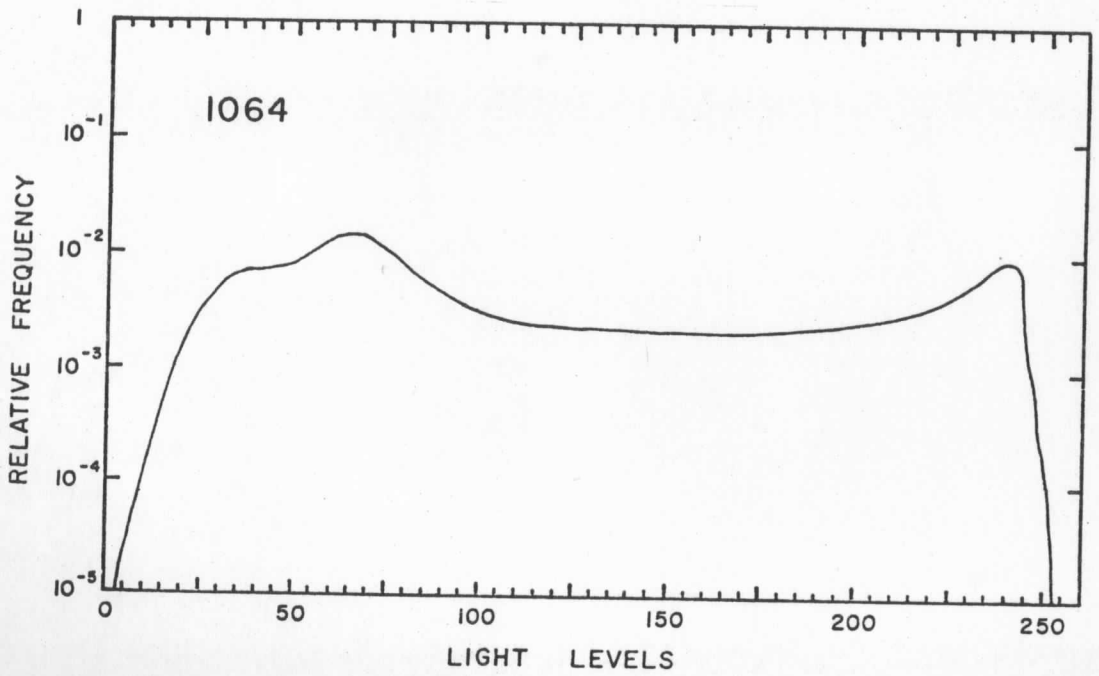
1064
RELATIVE FREQUENCY
1
10^{-1}
10^{-2}
10^{-3}
10^{-4}
10^{-5}
0
50
100
150
200
250
LIGHT LEVELS

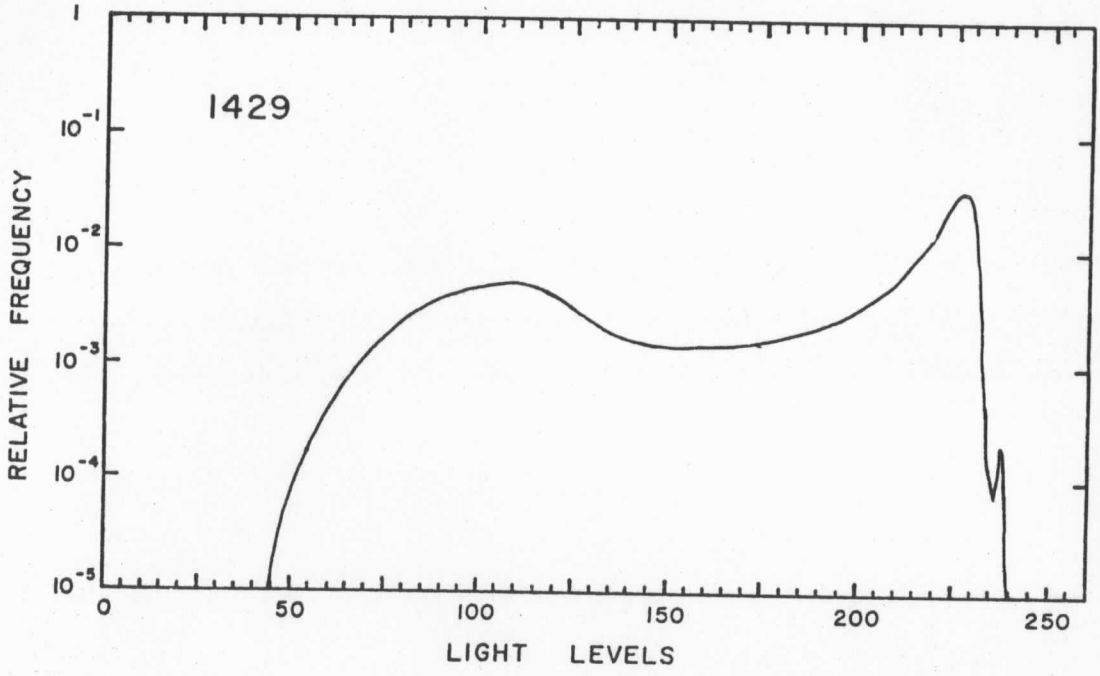
1429
RELATIVE FREQUENCY
1
10^{-1}
10^{-2}
10^{-3}
10^{-4}
10^{-5}
0
50
100
150
200
250
LIGHT LEVELS

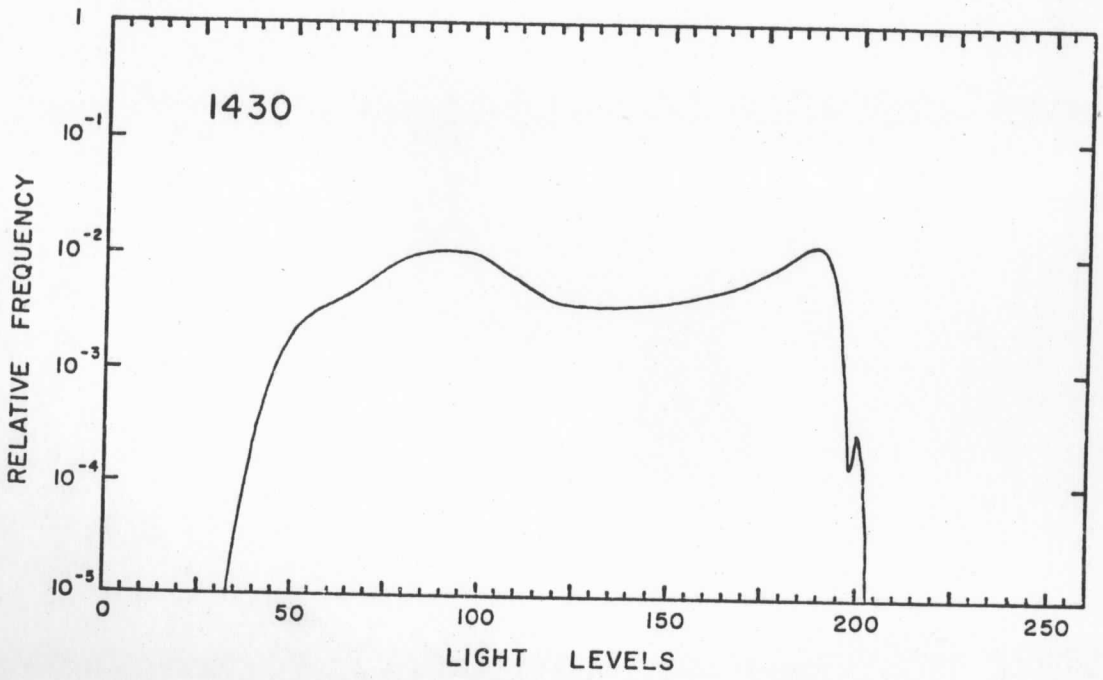
1430
RELATIVE FREQUENCY
1
10^{-1}
10^{-2}
10^{-3}
10^{-4}
10^{-5}
0
50
100
150
200
250
LIGHT LEVELS

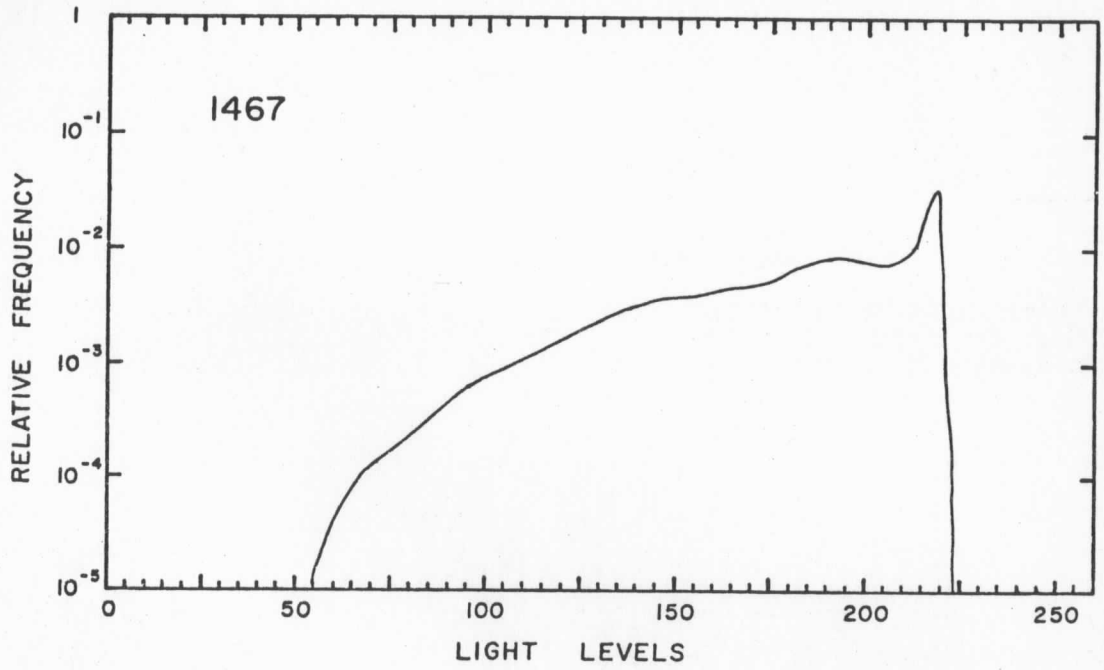
1467
RELATIVE FREQUENCY
1
10^{-1}
10^{-2}
10^{-3}
10^{-4}
10^{-5}
0
50
100
150
200
250
LIGHT LEVELS

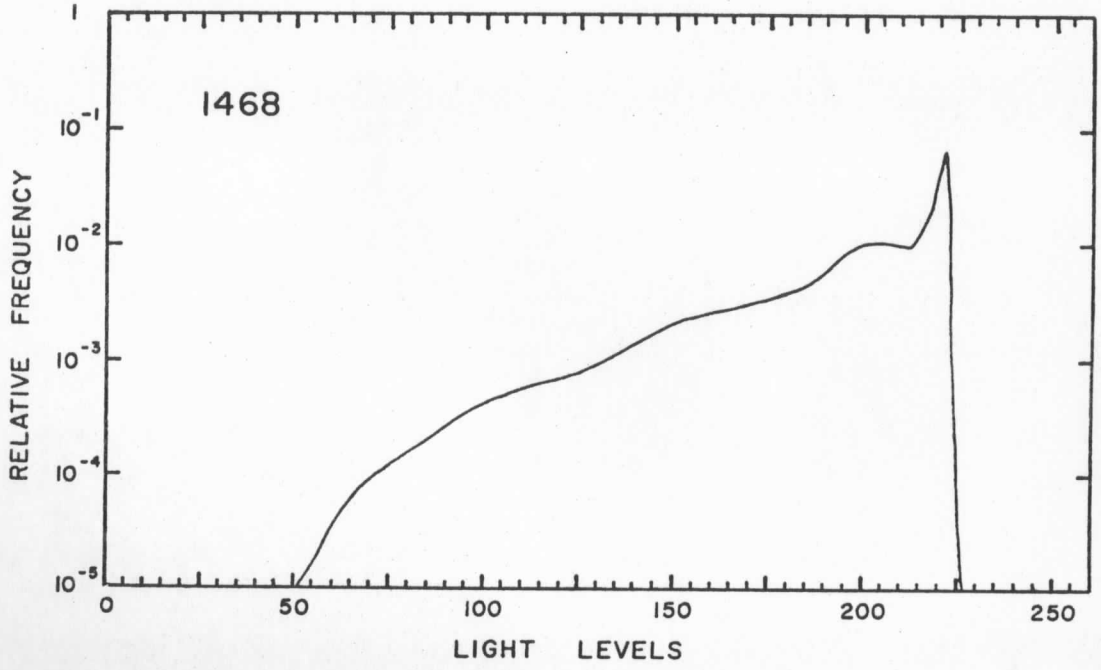
1468
RELATIVE FREQUENCY
1
10^{-1}
10^{-2}
10^{-3}
10^{-4}
10^{-5}
0
50
100
150
200
250
LIGHT LEVELS

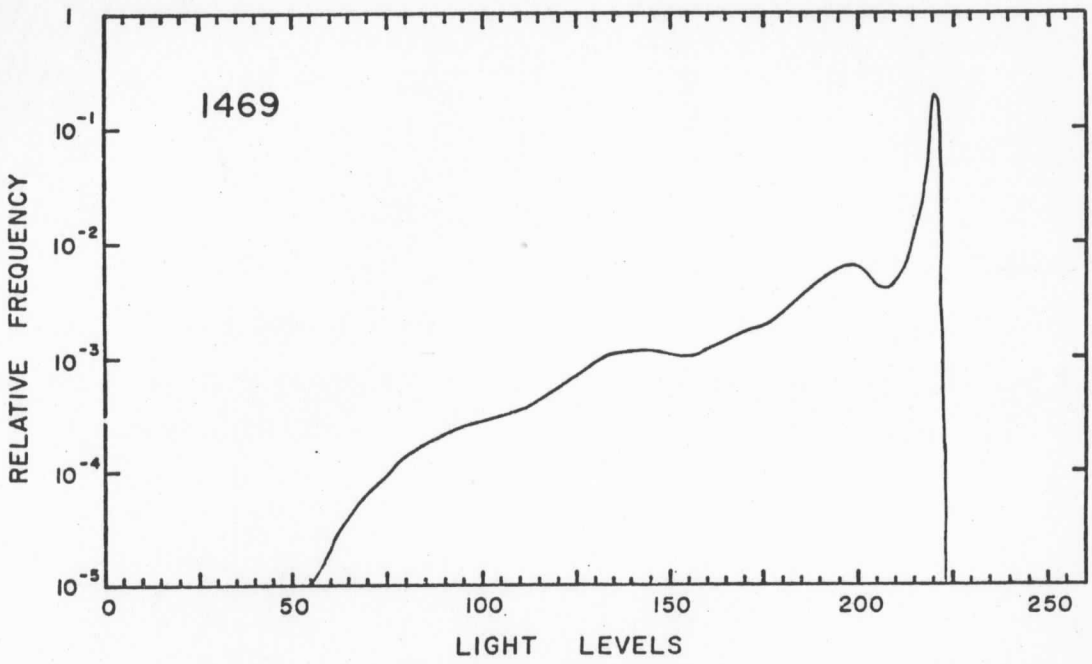
1469
RELATIVE FREQUENCY
1
10^{-1}
10^{-2}
10^{-3}
10^{-4}
10^{-5}
0
50
100
150
200
250
LIGHT LEVELS

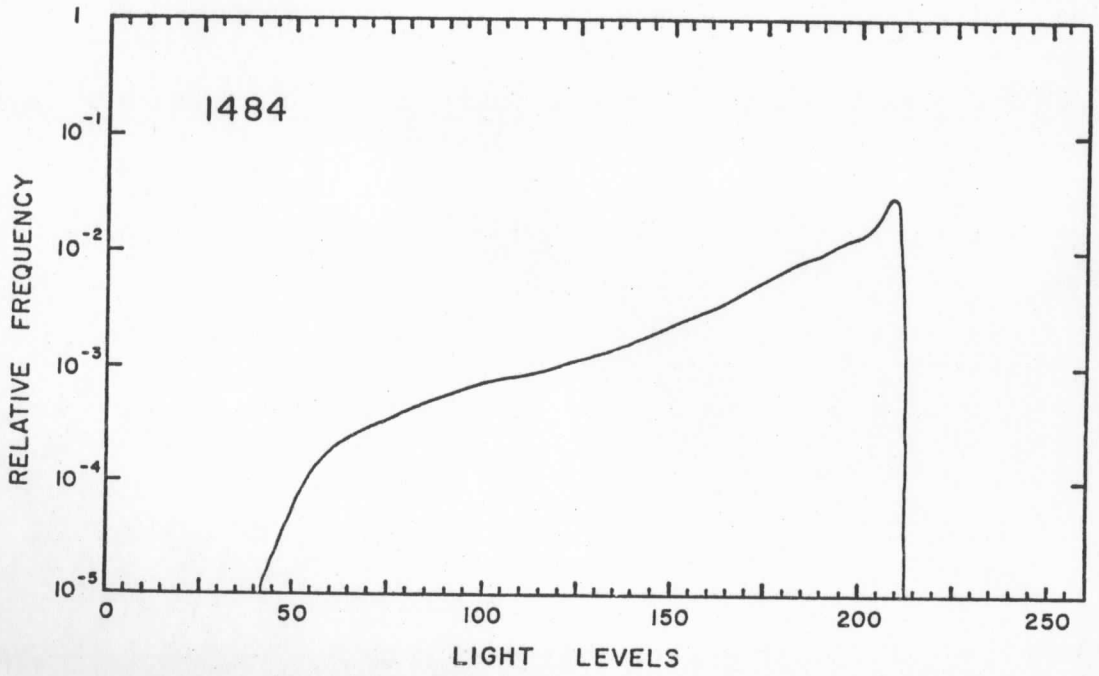
1484
RELATIVE FREQUENCY
1
10^{-1}
10^{-2}
10^{-3}
10^{-4}
10^{-5}
0
50
100
150
200
250
LIGHT LEVELS

FIGURE A.2. LOG-HISTOGRAMS OF BRIGHTNESS LEVELS (SCALED AND SIMULATED PMT NOISE ADDED) OF APOLLO VI TRANSPARENCIES.

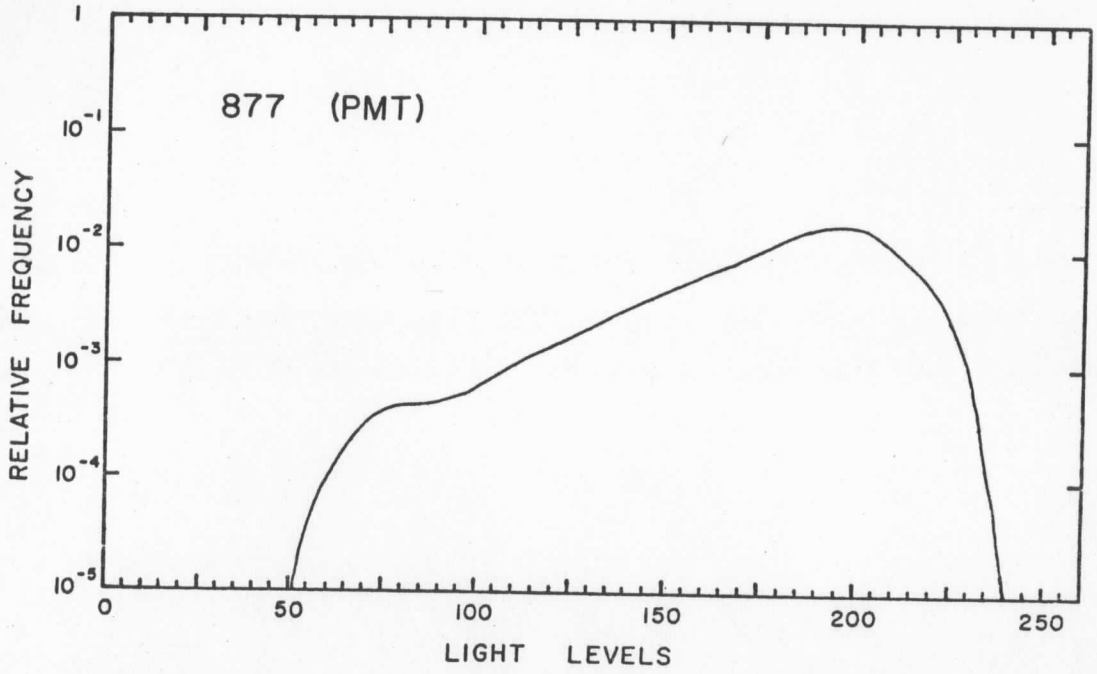
877 (PMT)
RELATIVE FREQUENCY
1
10^{-1}
10^{-2}
10^{-3}
10^{-4}
10^{-5}
0
50
100
150
200
250
LIGHT LEVELS

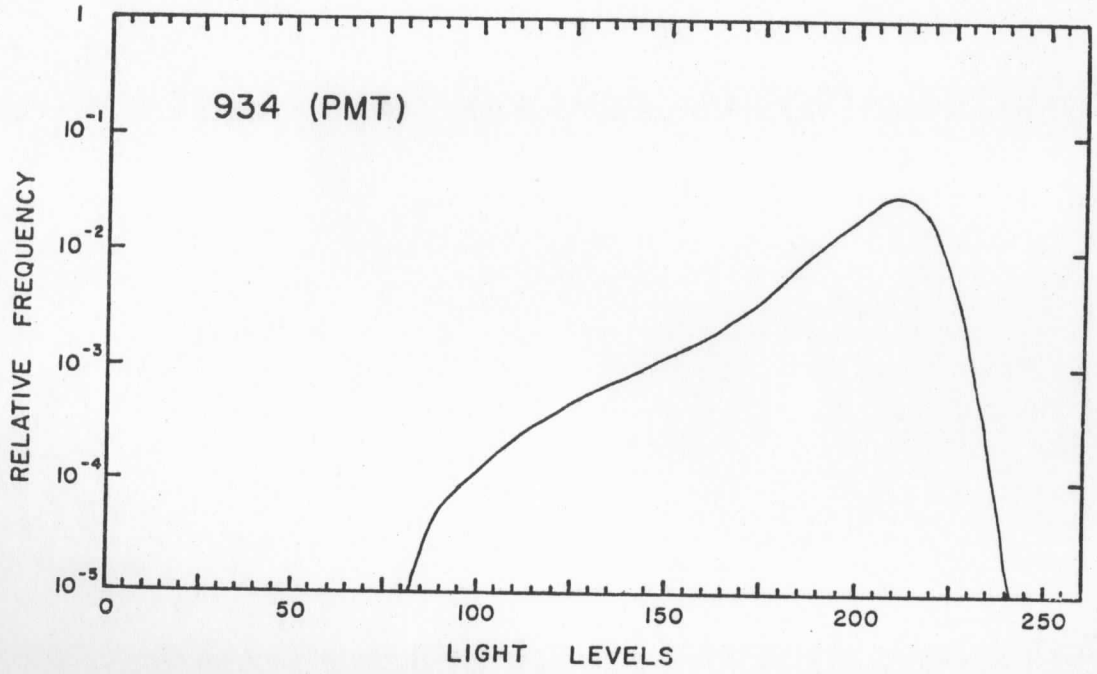
934 (PMT)
RELATIVE FREQUENCY
1
10^{-1}
10^{-2}
10^{-3}
10^{-4}
10^{-5}
0
50
100
150
200
250
LIGHT LEVELS

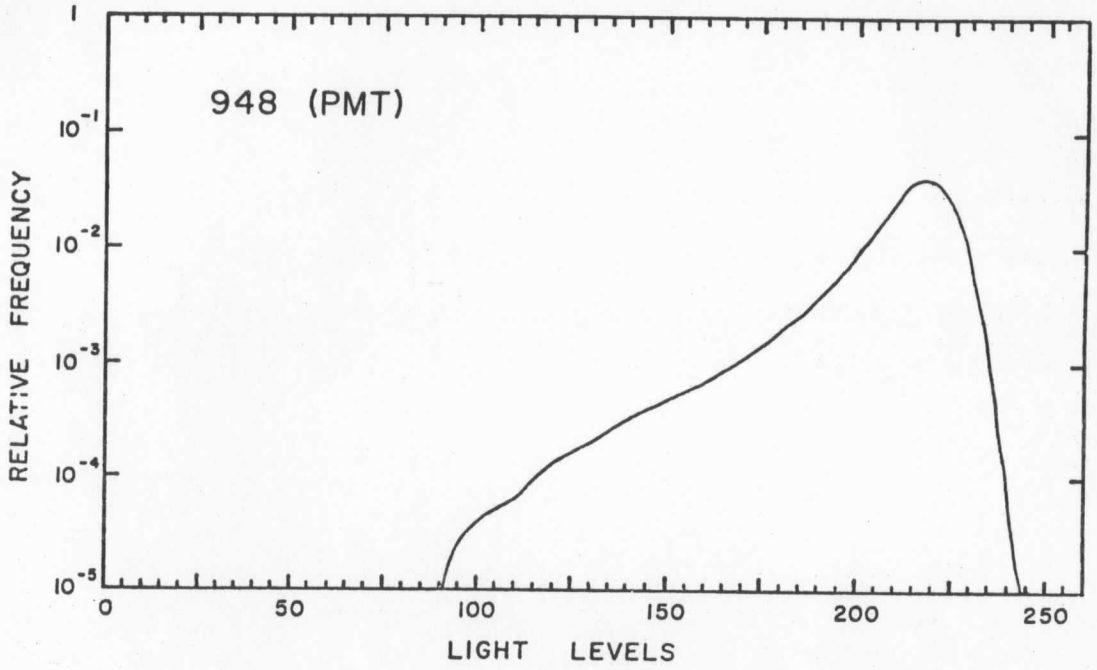
948 (PMT)
RELATIVE FREQUENCY
1
10^{-1}
10^{-2}
10^{-3}
10^{-4}
10^{-5}
0
50
100
150
200
250
LIGHT LEVELS

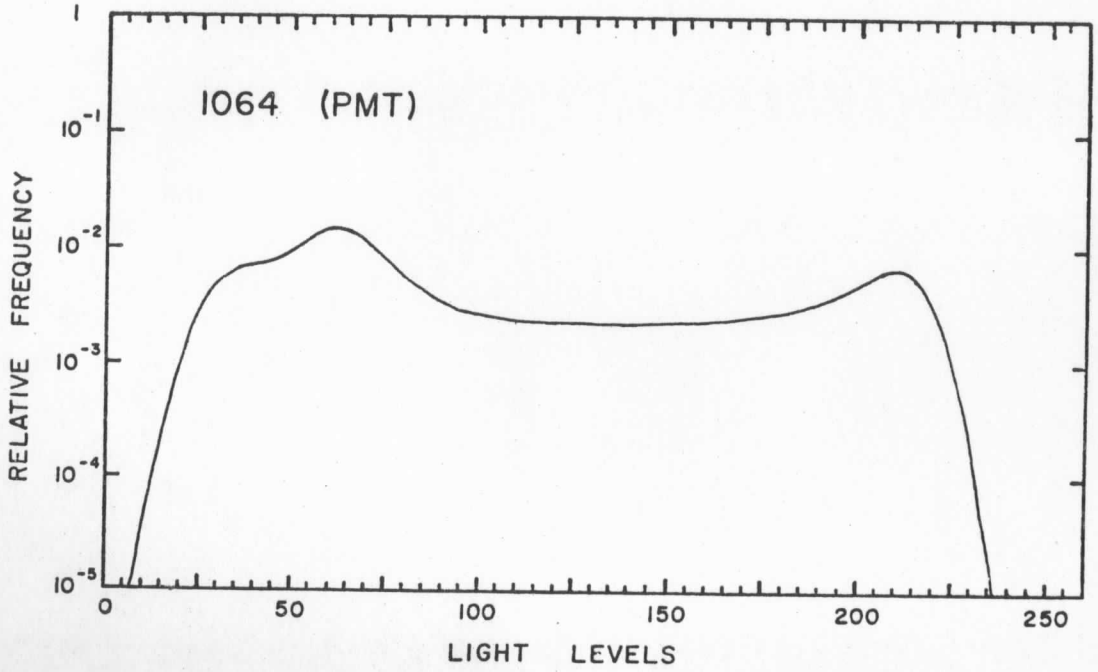
1064 (PMT)
RELATIVE FREQUENCY
1
10^{-1}
10^{-2}
10^{-3}
10^{-4}
10^{-5}
0
50
100
150
200
250
LIGHT LEVELS

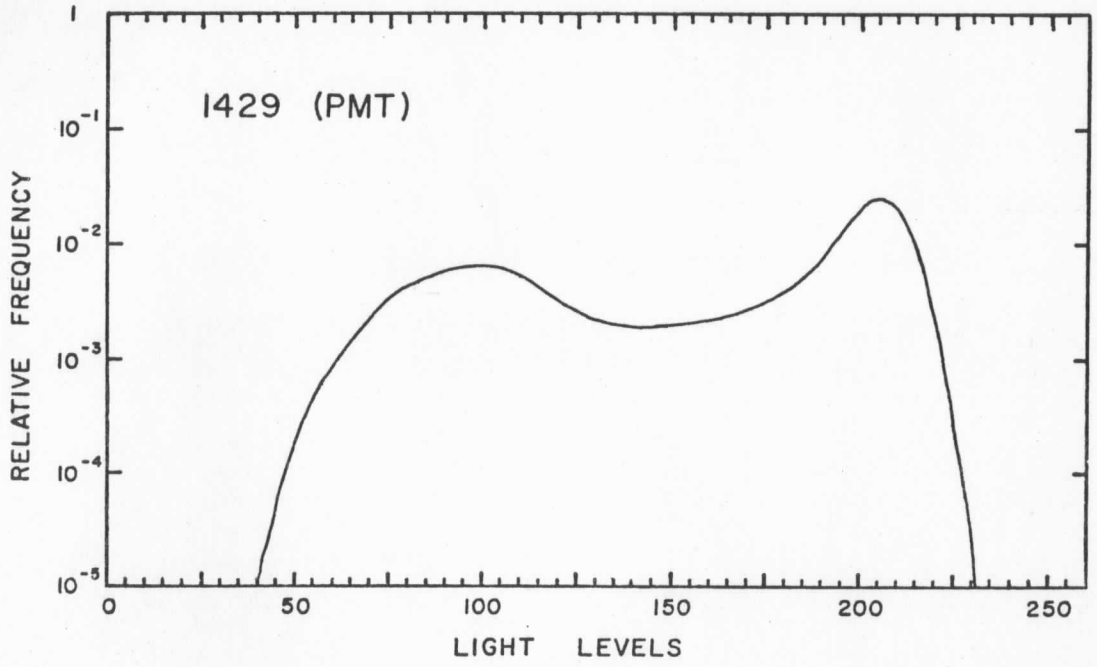
1429 (PMT)
RELATIVE FREQUENCY
1
10^{-1}
10^{-2}
10^{-3}
10^{-4}
10^{-5}
0
50
100
150
200
250
LIGHT LEVELS

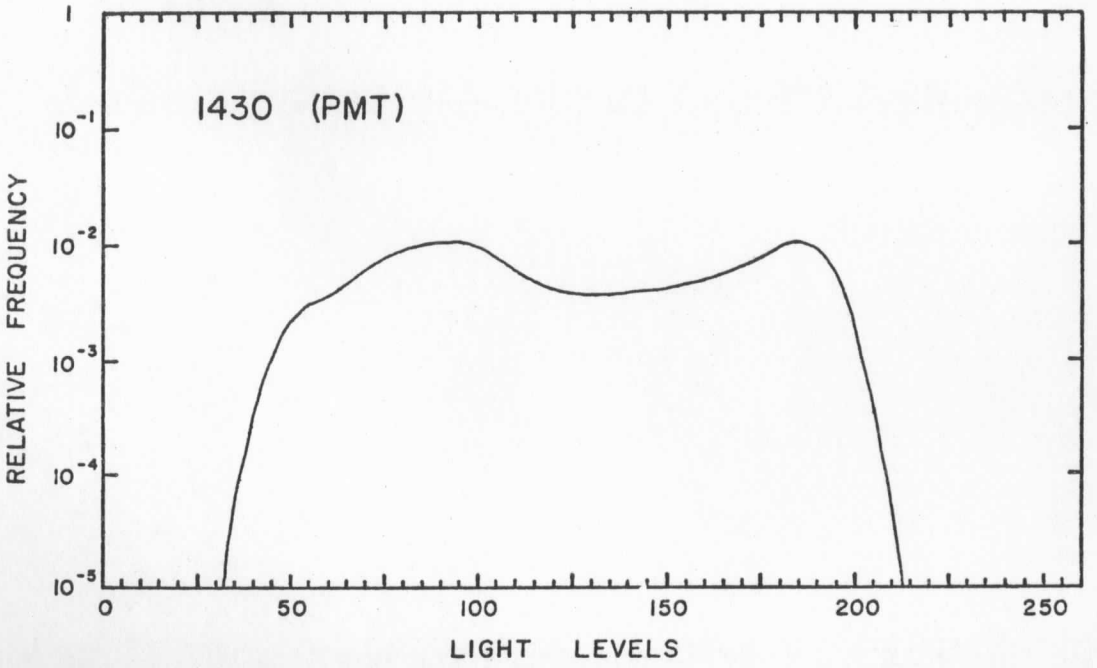
1430 (PMT)
RELATIVE FREQUENCY
1
10^{-1}
10^{-2}
10^{-3}
10^{-4}
10^{-5}
0
50
100
150
200
250
LIGHT LEVELS

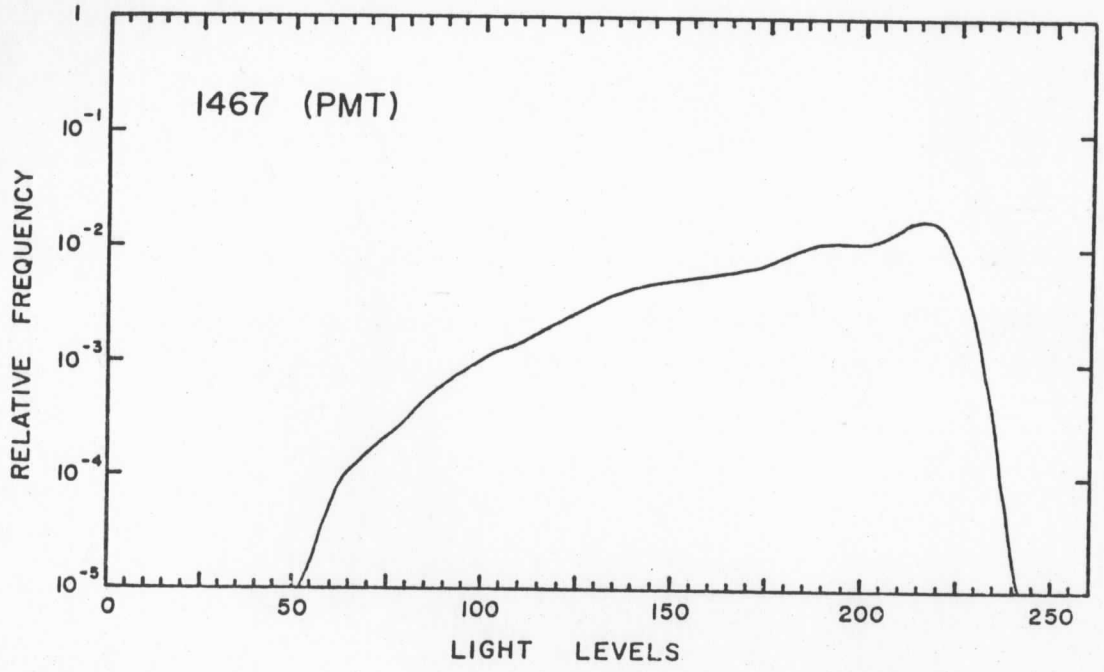
1467 (PMT)
RELATIVE FREQUENCY
1
10^{-1}
10^{-2}
10^{-3}
10^{-4}
10^{-5}
0
50
100
150
200
250
LIGHT LEVELS

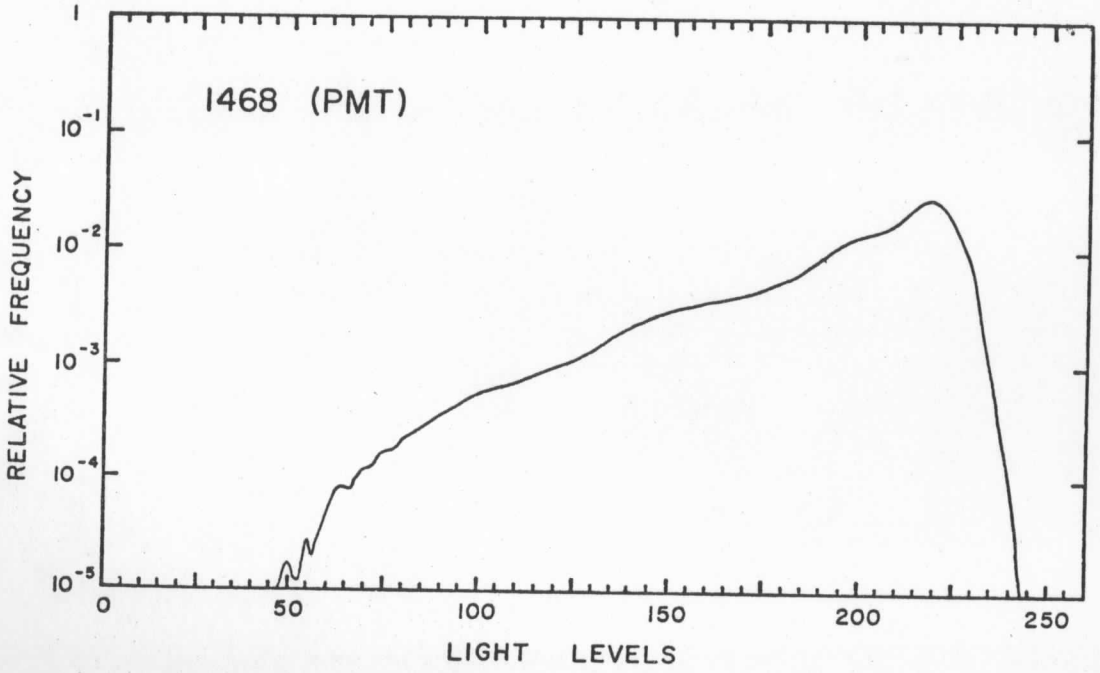
1468 (PMT)
RELATIVE FREQUENCY
1
10^{-1}
10^{-2}
10^{-3}
10^{-4}
10^{-5}
0
50
100
150
200
250
LIGHT LEVELS

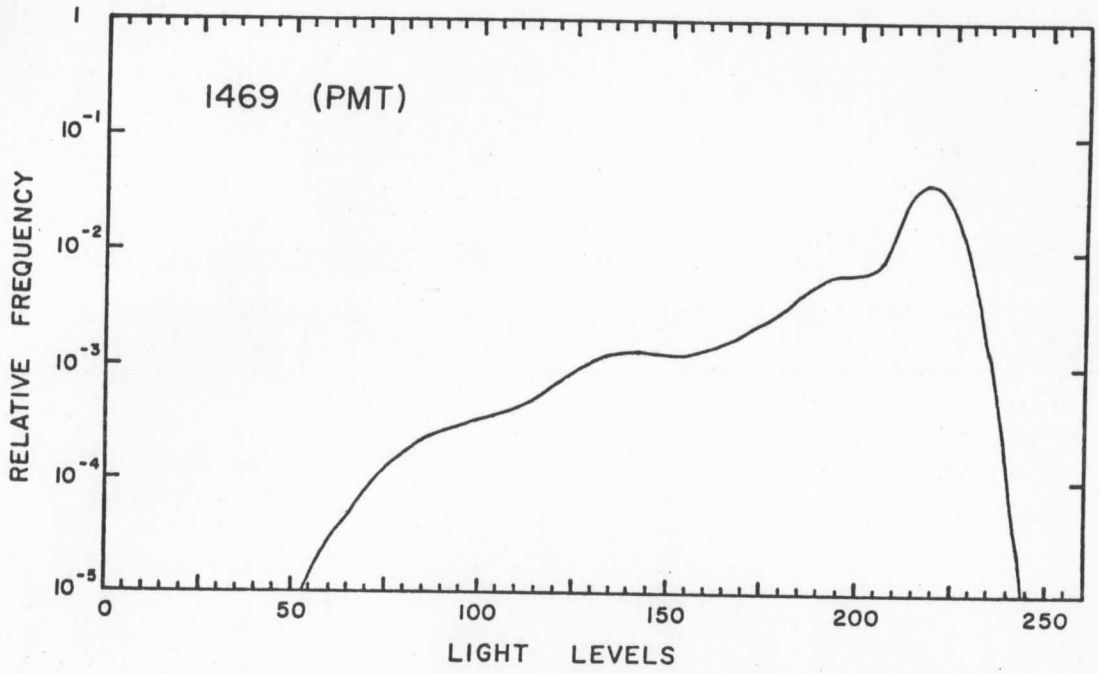
1469 (PMT)
RELATIVE FREQUENCY
1
10^{-1}
10^{-2}
10^{-3}
10^{-4}
10^{-5}
0
50
100
150
200
250
LIGHT LEVELS

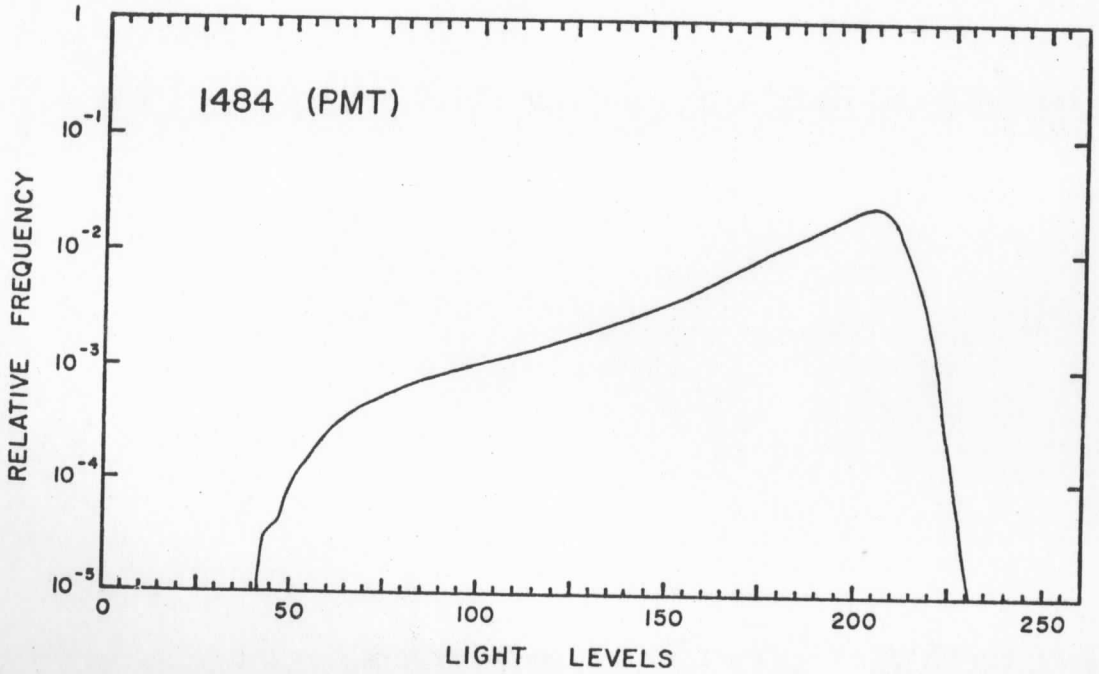
1484 (PMT)
RELATIVE FREQUENCY
1
10^{-1}
10^{-2}
10^{-3}
10^{-4}
10^{-5}
0
50
100
150
200
250
LIGHT LEVELS

FIGURE A.3. LOG-HISTOGRAMS OF DIFFERENCES OF BRIGHTNESS LEVELS OF APOLLO VI TRANSPARENCIES.

Notes: 1. Solid line denotes histograms of first differences.

2. Dashed line denotes histograms of second differences.

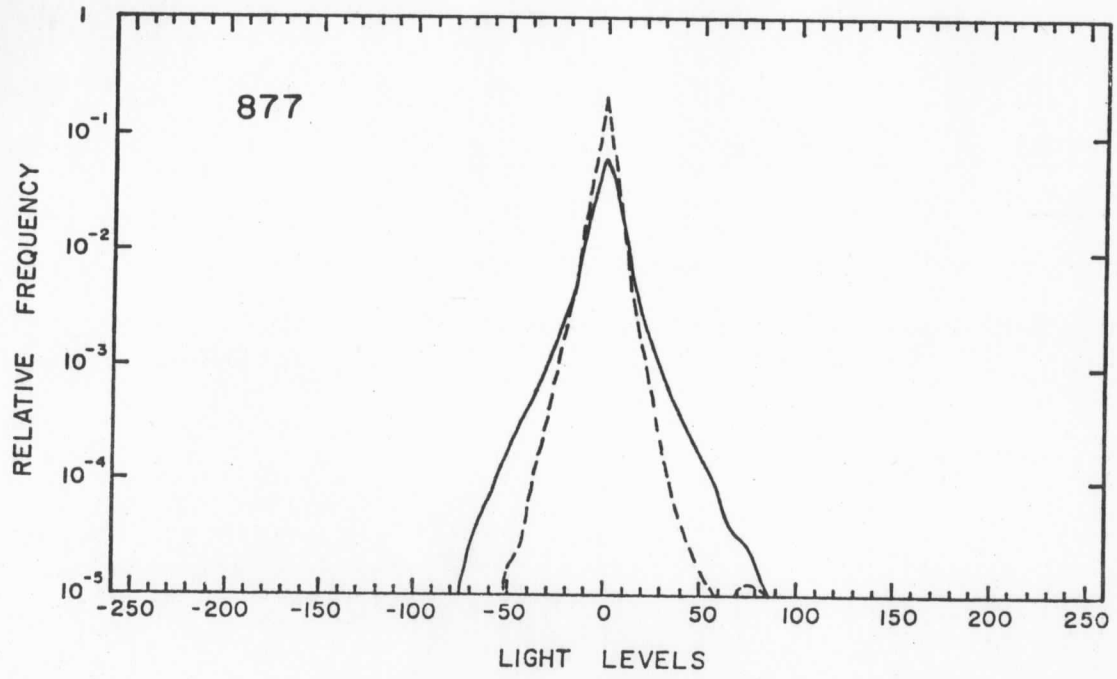
877
RELATIVE FREQUENCY
1
10^{-1}
10^{-2}
10^{-3}
10^{-4}
10^{-5}
-250 -200 -150 -100 -50 0 50 100 150 200 250
LIGHT LEVELS

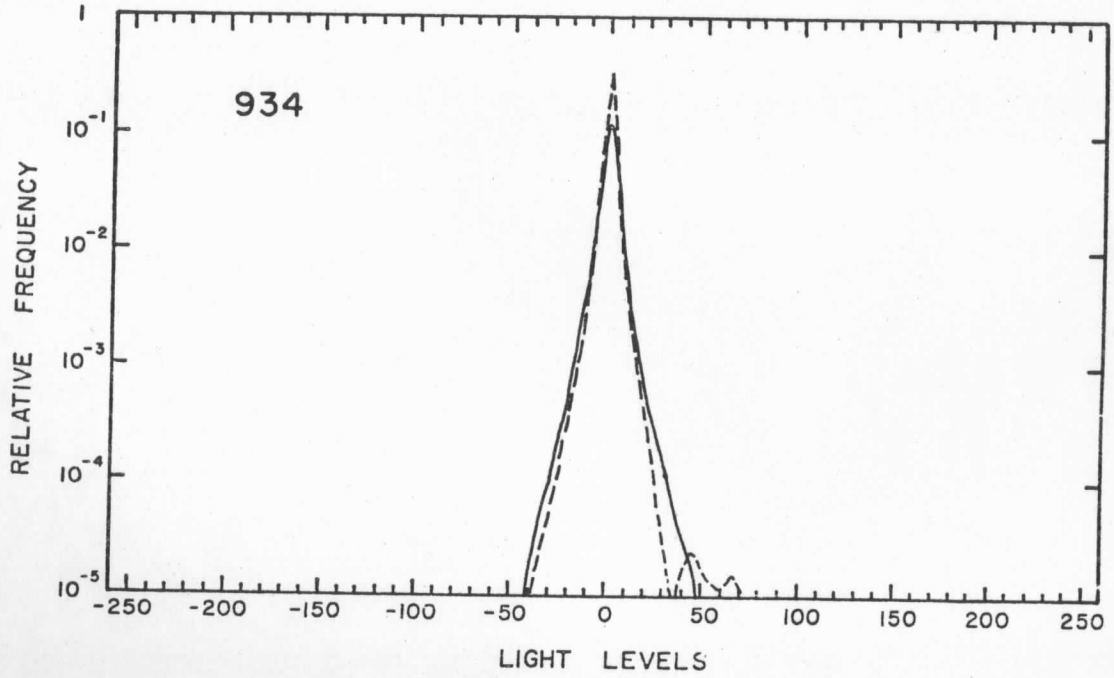
934
RELATIVE FREQUENCY
1
10^{-1}
10^{-2}
10^{-3}
10^{-4}
10^{-5}
-250 -200 -150 -100 -50 0 50 100 150 200 250
LIGHT LEVELS

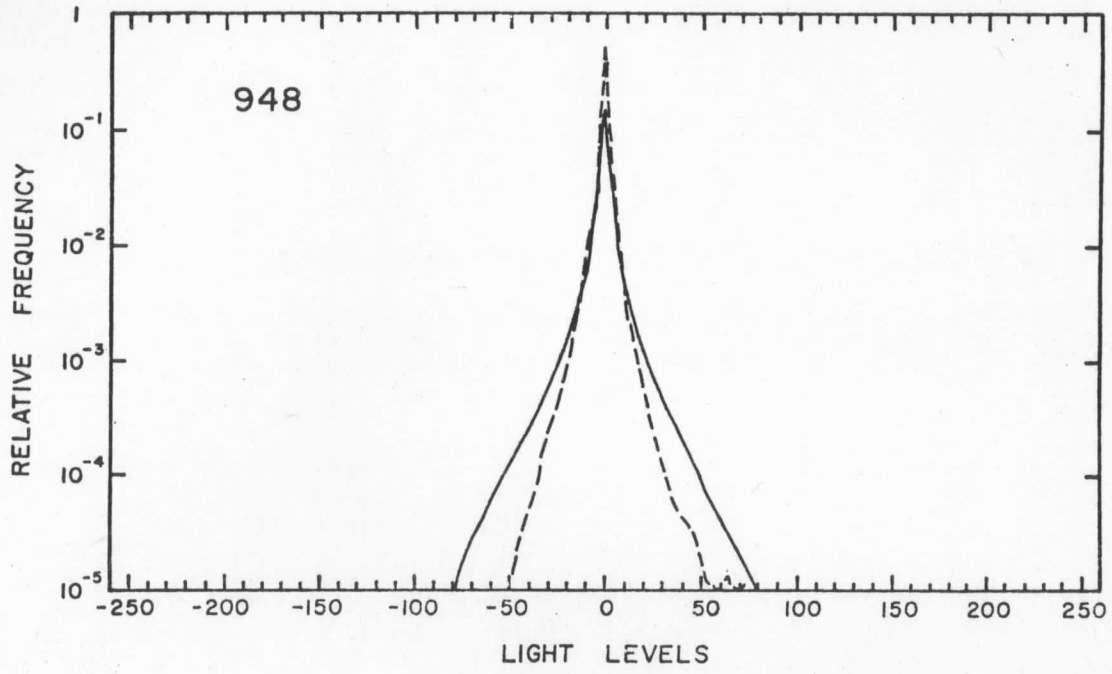
948
RELATIVE FREQUENCY
1
10^{-1}
10^{-2}
10^{-3}
10^{-4}
10^{-5}
-250 -200 -150 -100 -50 0 50 100 150 200 250
LIGHT LEVELS

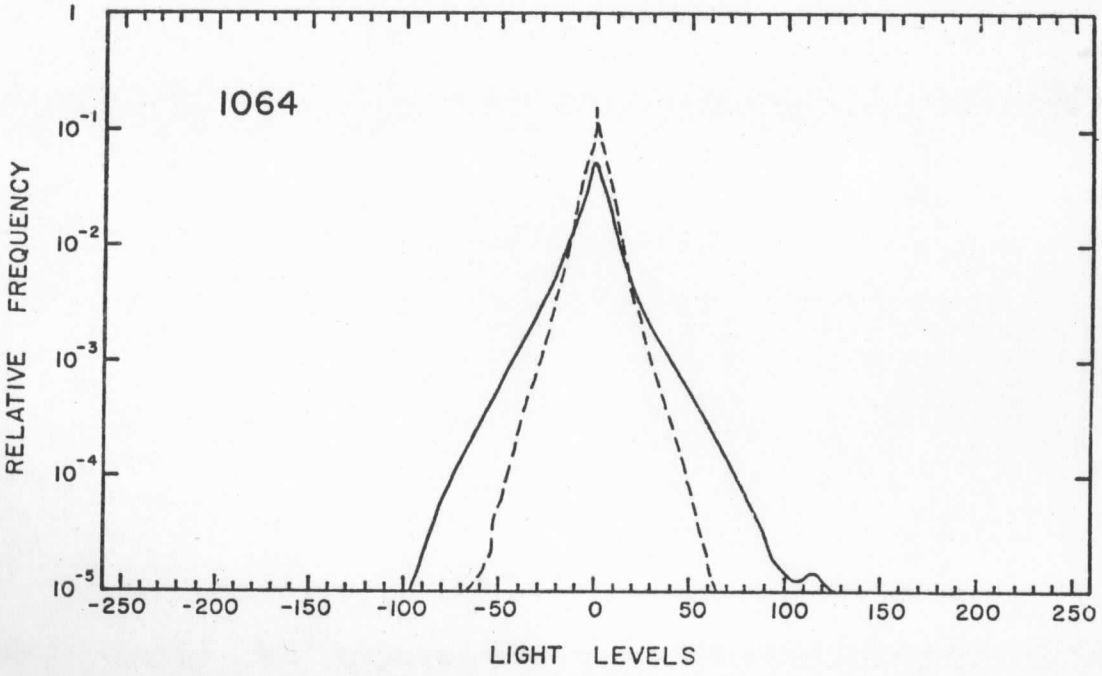
1064
RELATIVE FREQUENCY
1
10^{-1}
10^{-2}
10^{-3}
10^{-4}
10^{-5}
-250 -200 -150 -100 -50 0 50 100 150 200 250
LIGHT LEVELS

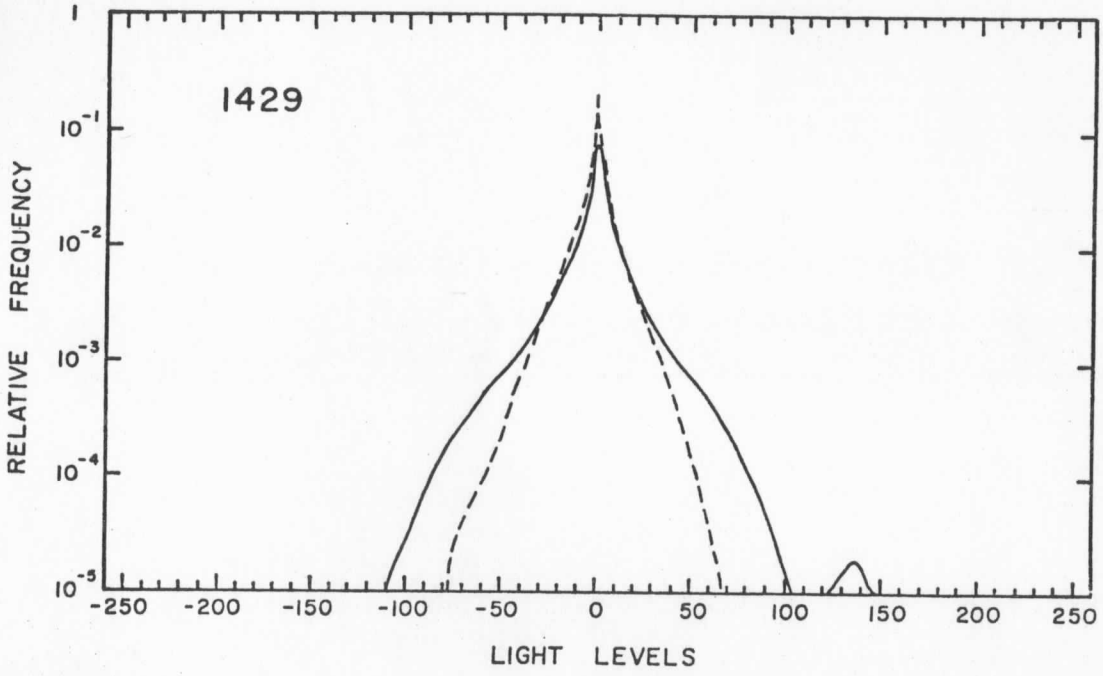
1429
RELATIVE FREQUENCY
1
10^{-1}
10^{-2}
10^{-3}
10^{-4}
10^{-5}
-250 -200 -150 -100 -50 0 50 100 150 200 250
LIGHT LEVELS

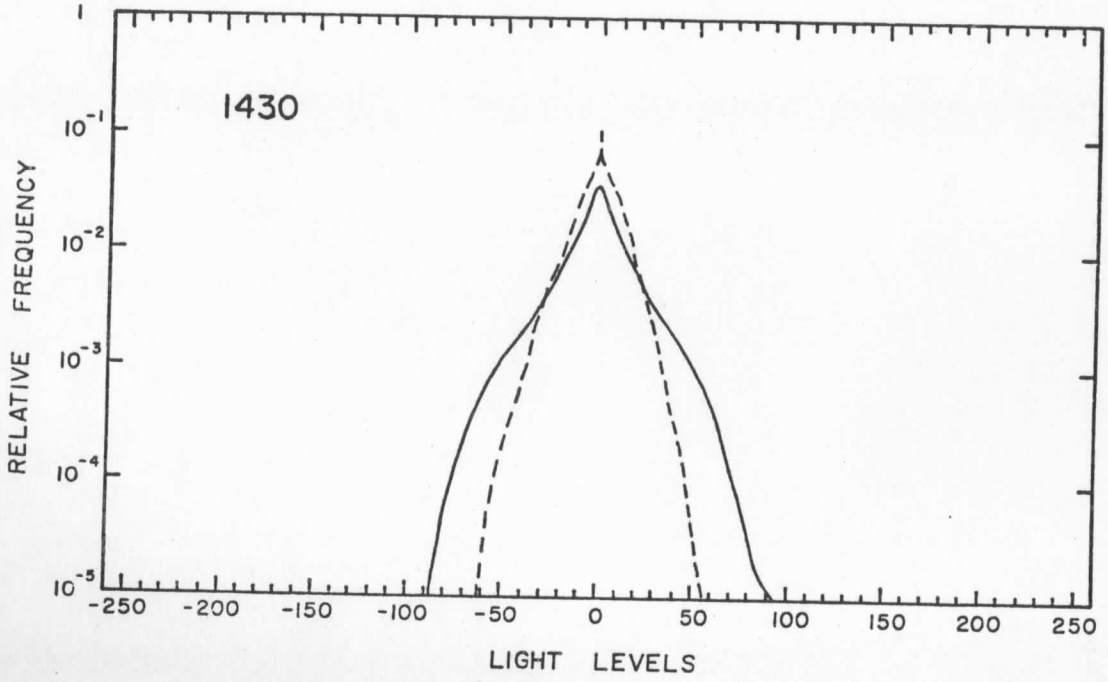
1430
RELATIVE FREQUENCY
1
10^{-1}
10^{-2}
10^{-3}
10^{-4}
10^{-5}
-250 -200 -150 -100 -50 0 50 100 150 200 250
LIGHT LEVELS

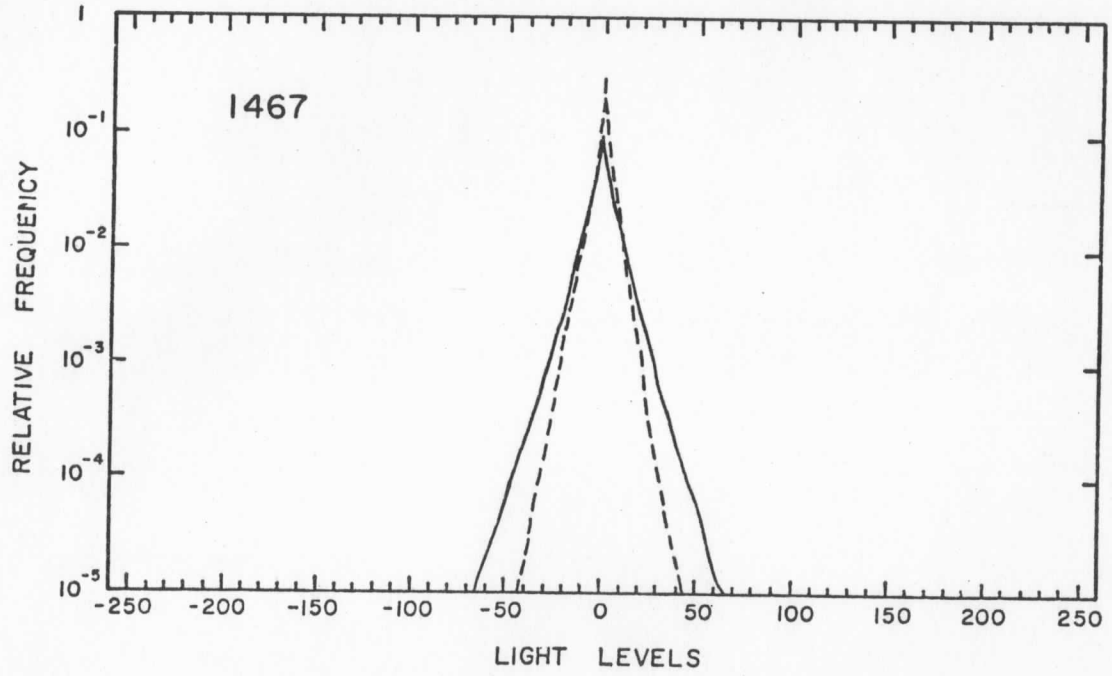
1467
RELATIVE FREQUENCY
1
10^{-1}
10^{-2}
10^{-3}
10^{-4}
10^{-5}
-250 -200 -150 -100 -50 0 50 100 150 200 250
LIGHT LEVELS

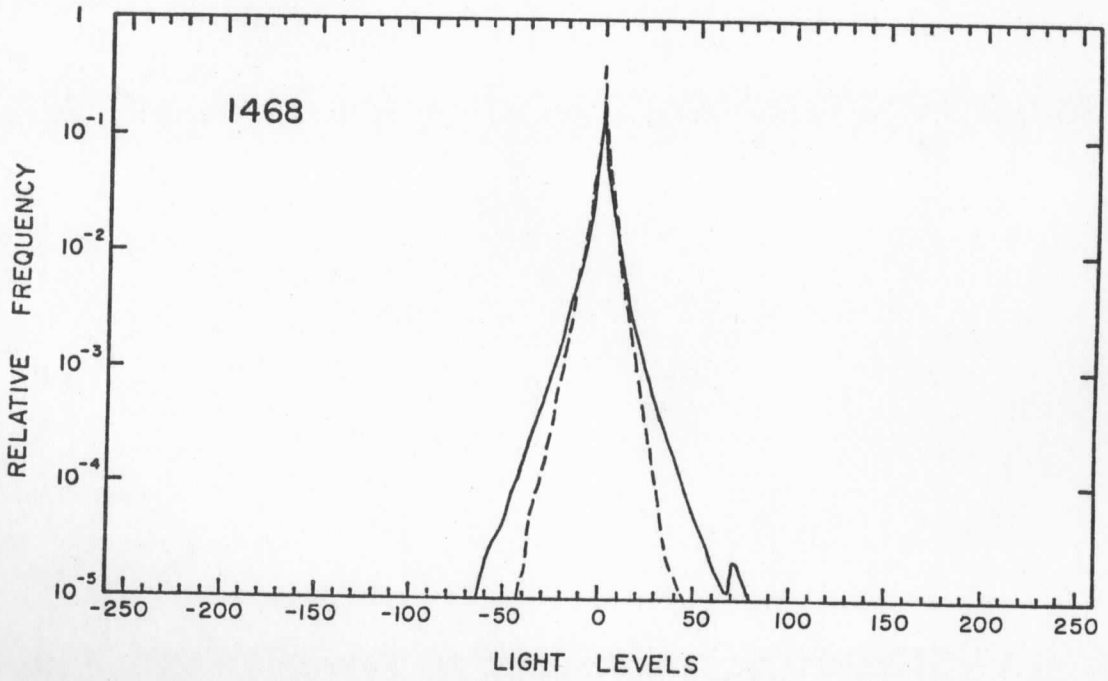
1468
RELATIVE FREQUENCY
1
10^{-1}
10^{-2}
10^{-3}
10^{-4}
10^{-5}
-250 -200 -150 -100 -50 0 50 100 150 200 250
LIGHT LEVELS

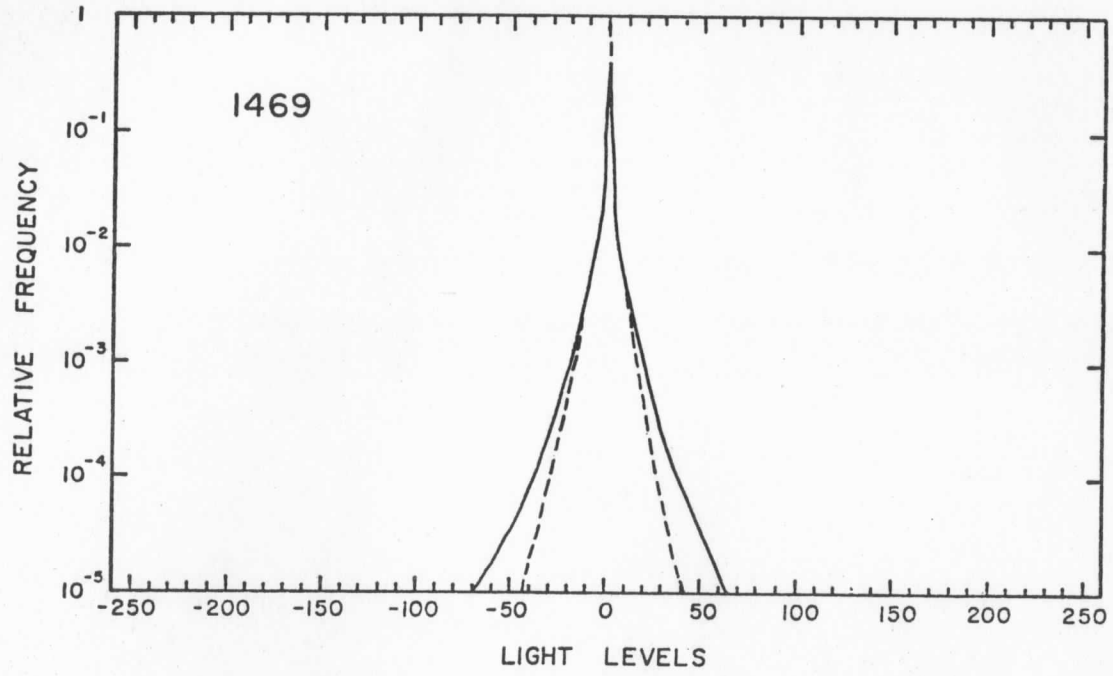
1469
RELATIVE FREQUENCY
1
10^{-1}
10^{-2}
10^{-3}
10^{-4}
10^{-5}
-250 -200 -150 -100 -50 0 50 100 150 200 250
LIGHT LEVELS

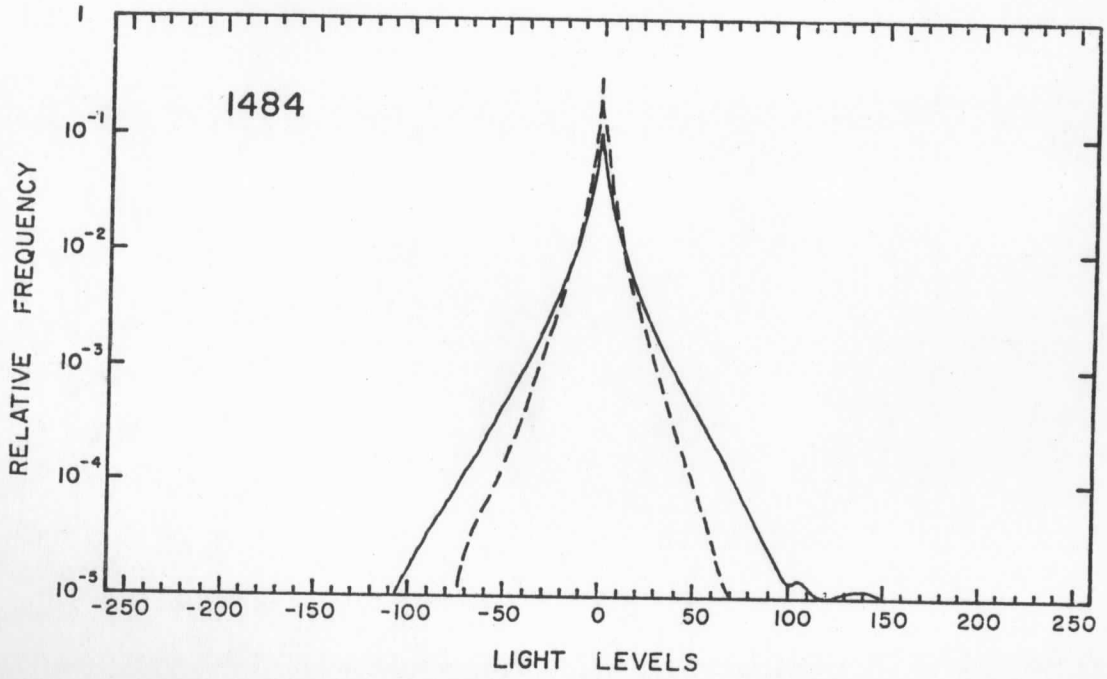
1484
RELATIVE FREQUENCY
1
10^{-1}
10^{-2}
10^{-3}
10^{-4}
10^{-5}
-250 -200 -150 -100 -50 0 50 100 150 200 250
LIGHT LEVELS

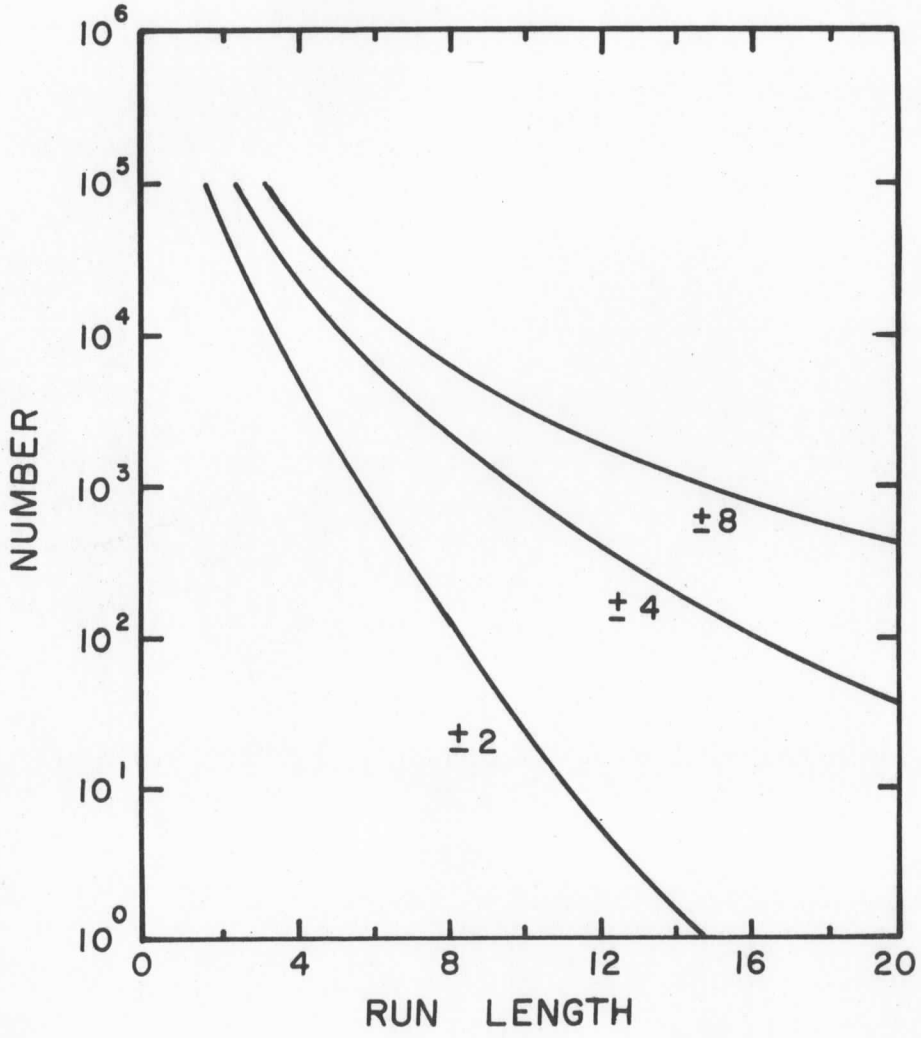

FIGURE A.4. RUN LENGTH STATISTICS FOR APOLLO AS6-2-877
(data digitized to 8 bits, 1024×1024 samples;
total number of samples is $2^{20} \cong 10^6$).

APPENDIX B

THE SMS SIMULATION PROGRAM

To simulate the present SMS optical weighting function, we have taken the optics impulse response as reported in Ref. 21 and scaled it to the sampling scale of our Apollo VI photographs. This particular response is for a 42 μ-radian diameter raised-cosine blur circle plus a 23 μ-radian IGFOV. The resulting relative weighting pattern is shown in Figure B.1.

The weighting pattern shown in Fig. B.1 is passed over a sampled Apollo VI photograph. Each point in the picture data array is weighted by this pattern and normalized by the sum of the weights (1541 for this pattern). Basically this is a two-dimensional convolution. Because the procedure is lengthy, we have performed this operation only on selected quarter-picture segments (512×512). To avoid edge effects, we use circular convolution so the last lines are used in the weighting pattern for the first lines, etc. This subroutine is called "SMSOPT".

The resulting spatial resolution is reduced, on an rms basis, from one sample to 4.65 samples using this program. The data can be independently sampled again by taking every fifth point. This closely corresponds to the present SMS optics and data sampling rate.

A block diagram of the organization of our satellite visual channel simulation on the Univac 1110 computer is shown in Fig. B.2. Processing of the data from all ten of the Apollo VI photographs would be quite expensive, particularly for the SMSOPT program. Therefore we have used the lower right-hand quarter of Apollo AS6-2-877 for our studies.

0	0	0	1	1	1	1	1	1	1	0	0	0
0	1	1	2	4	4	5	4	4	2	1	1	0
0	1	3	5	9	11	11	11	9	5	3	1	0
1	2	5	10	15	18	20	18	15	10	5	2	1
1	4	9	15	21	28	30	28	21	15	9	4	1
1	4	11	18	28	35	38	35	28	18	11	4	1
1	5	11	20	30	38	41	38	30	20	11	5	1
1	4	11	18	28	35	38	35	28	18	11	4	1
1	4	9	15	21	28	30	28	21	15	9	4	1
1	2	5	10	15	18	20	18	15	10	5	2	1
0	1	3	5	9	11	11	11	9	5	3	1	0
0	1	1	2	4	4	5	4	4	2	1	1	0
0	0	0	1	1	1	1	1	1	1	0	0	0

FIGURE B.1. SMSOPT OPTICAL WEIGHTING PATTERN

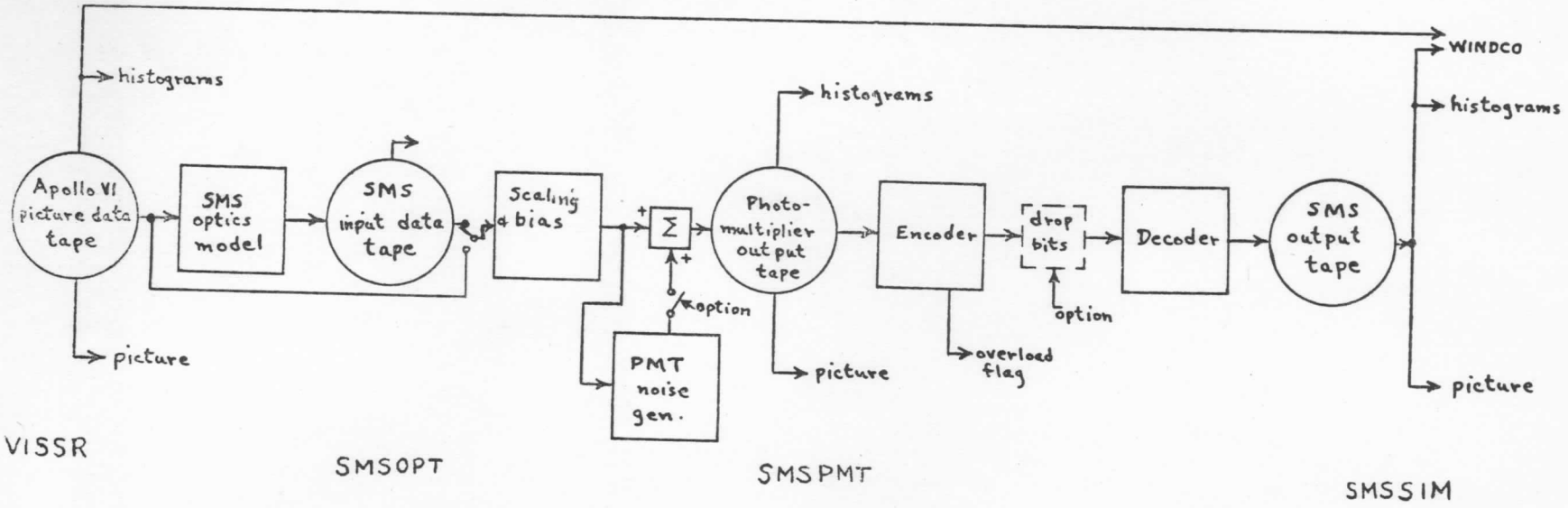

FIGURE B.2. SMS ENCODING/DECODING SIMULATIONS

APPENDIX C

ENCODING OF SMS DATA USING TRANSFORM CODING

The advantages of encoding coefficients of the discrete two-dimensional Walsh series expansion of the original SMS data rather than a transmission of the SMS data itself are discussed in Chapter 3. To achieve a significant bit reduction (or bandwidth compression), the fewest possible Walsh coefficients that will give rise to pictures of acceptable quality need to be encoded after quantizing them as finely as possible to 6-bits or less. This appendix suggests a method for the selection of the essential Walsh coefficients containing significant information and also the quantization procedures for them based on their first and second order statistics over four different Apollo pictures of varying content. It also reviews the earlier methods of encoding and outlines the modifications that are being done and the ones that will be done in the near future, giving considerations to their implementation and optimality (or suboptimality).

A reasonable basis for selecting a Walsh coefficient is it should have a fairly large magnitude (i.e., a large contribution to a particular sequency and also to the picture energy) and also a large "spread" (a large standard deviation or "sigma" over all the subpictures, implying a large amount of information) over the different 8×8 subpictures of varying details normally encountered while the satellite scans the earth. The same coefficient may convey a different amount of information from one picture to the other, thus depending on the particular picture. Thus the selection of coefficients (i.e., Walsh domain filtering) and their subsequent quantization, both adapted to individual subpictures and coefficients, will involve a large amount of "bookkeeping" information (i.e., which coefficients correspond to which type of

subpicture, etc.). This is difficult to implement even though such methods may give rise to bit rates close to the rate distortion bound for a given criterion. Hence only nonadaptive Walsh filtering and quantization methods using only one quantizer, preferably symmetrical about zero, are used to encode the pictures.

The above methods require the first and second order statistics (mean and variance respectively) of the coefficients of the particular picture to be encoded. A sample mean and a sample variance for each coefficient is computed over an ensemble of 4 pictures (4x128x128 - 65,536 subpictures of 8x8 size) of varying details. In the future, variance values of coefficients obtained by fitting a curve of the form: $\sigma^2(u,v) = S \exp\left(-\frac{u^2+v^2}{p}\right)$,* where S and p are to be determined or some other suitable curve to the actual variances calculated from picture data, will be used so no a priori knowledge of the variances is required.

For the pictures reconstructed for our earlier interim report, the coefficients to be encoded were selected on the basis of their values over about 1000 8x8 subpictures of picture # 877. It is inferred all the coefficients except the zero sequency, or "D.C.", one are nearly equal to their corresponding transpose in the 8x8 Walsh coefficient matrix, and are approximately symmetrical about zero. The Walsh coefficients take a wide range of values (for example, for the picture 877, the coefficient (1,1)**, or "D.C.", has a range [70,255], coefficients (1,2) and (2,1) have a range [-40,40], and higher sequency coefficients have smaller ranges). Therefore the "D.C." term was divided by 50, the rest by 5, and a uniform quantizer with 64 levels (6-bit words) and symmetrical about zero was used.

---

* Symmetry in the picture statistics is assumed, so p is the same for both coordinates.

** The numbers within the parentheses refer to the position in the 8x8 Walsh coefficient matrix, i.e., row and column numbers respectively.

A better and more efficient encoding method is to subtract the mean from each "pel" (picture element), divide each coefficient by its respective ensemble standard deviation computed over all the subpictures of a picture, and then use a symmetrical uniform or nonuniform quantizer. But such a method requires a priori knowledge of the "sigma" values of the coefficients. The first procedure described above and used in our interim report [2] quantizes coarsely the relatively high sequency components of the ones chosen for encoding. Thus in subpictures containing cloud edges, the edges cannot be expected to be "sharp". A slight improvement over the above method was done by subtracting from each 8-bit "pel" the number 175 and then dividing the "D.C." term by 20 and the rest of the selected coefficients by 4 so all the coefficients including the "D.C." term span the interval (-4,4). Sixty uniformly-spaced levels were allotted for the range (-4,4) symmetrically about zero plus two levels (one each at -5 and -6) below -4 and similarly two levels (one each at 5 and 6) above 4. Apollo pictures #877 (LRQ), 934 (URQ), 1430 (CRQ) and 1468 (LRQ) were reconstructed using the above procedure. Some specific original and reconstructed (dashed curve) lines are shown in Figs. C.1a and b for pictures 877 and 934. The quantization error in the above scheme is slightly less than that in the previous one.

To determine what can be best done for bit reduction once the first and the second order statistics of the coefficients of different pictures are known, the mean and sigma values of each of the 64 coefficients were computed over all the sub-pictures for each of the four above-mentioned pictures. The coefficients were ordered in descending order of their respective "sigmas" and the first few significant ones are shown in Table C.1. From this table, the ones having the largest "sigmas" for the four pictures are chosen for encoding. It is observed the "sigmas" of the coefficients exhibit a symmetry about

Table C.1.

The Standard Deviation of the Walsh Coefficients
for the Four Apollo Pictures AS6-2-877, -934, -1430, -1469.

Picture # 877		Picture # 934		Picture # 1430		Picture # 1469	
Coef-ficient	Sigma	Coef-ficient	Sigma	Coef-ficient	Sigma	Coef-ficient	Sigma
(1,1)	35.50	(1,1)	32.33	(1,1)	36.60	(1,1)	30.33
(1,2)	6.33	(1,2)	2.20	(2,1)	12.73	(1,2)	3.21
(2,1)	6.12	(2,1)	1.85	(1,2)	10.14	(2,1)	3.06
(1,3)	3.80	(1,4)	1.42	(2,2)	7.32	(2,2)	1.79
(2,2)	3.77	(1,3)	1.27	(3,1)	7.27	(1,3)	1.62
(3,1)	3.38	(2,2)	1.06	(1,3)	6.28	(1,4)	1.61
(1,4)	3.04	(4,1)	1.05	(4,1)	5.83	(3,1)	1.59
(4,1)	2.77	(1,5)	1.01	(3,2)	5.17	(4,1)	1.54
(2,3)	2.59	(1,8)	0.98	(1,4)	5.07	(3,2)	1.27
(3,2)	2.51	(1,7)	0.95	(2,3)	5.01	(2,3)	1.22
(2,4)	1.95	(2,3)	0.95	(2,4)	3.82	(4,2)	0.98
(4,2)	1.93	(1,6)	0.94	(3,3)	3.76	(2,4)	0.95
(1,7)	1.89	(3,1)	0.91	(4,2)	3.66	(3,3)	0.89
(3,6)	1.83	(2,4)	0.81	(7,1)	3.28	(1,5)	0.84
(1,6)	1.81	(3,2)	0.79	(6,1)	3.09	(1,6)	0.83
(1,5)	1.69	(4,2)	0.77	(1,6)	3.07	(1,7)	0.83
(1,8)	1.56	(3,3)	0.77	(1,5)	3.03	(1,8)	0.83
(7,1)	1.56	(7,1)	0.75	(1,7)	2.99	(5,1)	0.76
(6,1)	1.46	(2,5)	0.73	(3,4)	2.87	(3,4)	0.76
(3,4)	1.44	(5,1)	0.68	(5,1)	2.87	(6,1)	0.76
(4,3)	1.42	(3,4)	0.68	(4,3)	2.77	(7,1)	0.76
(5,1)	1.34	(6,1)	0.66	(8,1)	2.65	(8,1)	0.75
(8,1)	1.31	(5,2)	0.65	(6,2)	2.49	(4,3)	0.72
(2,6)	1.27	(4,3)	0.65	(2,5)	2.48	(2,5)	0.70
(2,5)	1.25	(4,4)	0.65	(2,6)	2.47	(2,6)	0.67
(2,7)	1.23	(8,1)	0.64	(5,2)	2.42	(6,2)	0.66

the diagonal of the 8×8 "sigma" matrix and have circular symmetry [i.e., "sigmas" of coefficients (1,5) and (3,4) are nearly equal -- note $\sqrt{1^2+5^2} \cong \sqrt{3^2+4^2}$] and all except the "D.C." term have zero mean. Two sets of coefficients to be encoded in the future work are shown in Figs. C-2a and b. In order to quantize these coefficients efficiently, the histograms of the coefficients in Fig. C-2a were calculated over the picture # 877 and a few representative ones are shown in Figs. C-3a, b, c and d. It is observed from Fig. C-3 that the histogram of the "D.C." term resembles a Rayleigh density and is not symmetrical about its non-zero mean, while that for each of the other coefficients is symmetrical about zero (mean) and resembles a two-sided exponential. It is also observed the histogram of coefficient (1,2) and of coefficient (2,1) look almost the same. It is to be noted the small spikes in the histograms about $\pm 2.5\sigma$ are due to the rough approximation of the histogram over the range (2.5 , 7.5) by relative frequency counts at only 18 discrete levels, and also due to the subpictures near picture edges where the "D.C." term is usually small and the rest of the coefficients assume large values. From these histograms, the probability density function of the input to the single quantizer is obtained after dividing each coefficient by its respective sigma, and is shown in Fig. C-4. It is observed in Fig. C-4 that the histogram is not symmetrical about zero and also the statistical mean (expected value) is not zero. This is due to the asymmetry of the histogram of the "D.C." term about its mean.

Based on the histogram in Fig. C-4, a suboptimum symmetrical quantizer that gives rise to: (a) the maximum output entropy; or, (b) minimum mean-square error, is being designed using 64 (6-bit words) and 32 (5-bit words) levels. These equal-length codes can also be used to address a "read only memory" (ROM) which can output a corresponding variable-length Huffman code generated from the histogram in Fig. C-4. Picture # 877 (LRQ) will be

reconstructed using the above quantization scheme. The above scheme is adapted to picture #877 and the histogram of the input to the quantizer based on the subpicture data over all four pictures will be computed. Also the "sigma" of each coefficient computed based on the subpicture data over all four pictures will be used to divide each coefficient before its entry to the quantizer. Alternatively, the "sigma" data taken from a least-square fit of a suitable curve to the actual data obtained over all four pictures can be used so the "sigma" matrix of the coefficients need not be known a priori. The resulting suboptimum quantizer will be used to reconstruct pictures 877, 934, 1430 and 1469.

It is also worth while to find out whether the assumption of symmetry of the Walsh coefficients about the main diagonal is valid or not by reconstructing pictures based on the above assumption because the histograms and the "sigma" values exhibit such a symmetry. Of course, this "large-scale" symmetry need not be valid for an individual 8×8 coefficient matrix. Also, one-dimensional transform coding will be tried to find out how much bit reduction it can achieve. It is also equally important to recognize the difficulties associated with the real-time implementation of the transform coding technique, keeping in mind what the present day technology can offer and also the conditions prevailing in a satellite.

FIGURE C.1. GRAPHS OF A RECONSTRUCTED LINE FROM APOLLO AS6-2-877 and AS6-2-934 USING AN 8×8 WALSH TRANSFORM.

Notes:
1. Solid line is the original scan line (8-bit data, unsmoothed).
2. Dashed line is the reconstructed line after quantizing 25 of the 64 Walsh coefficients to 6-bit accuracy using a linear quantizer and then taking the inverse Walsh transform.
3. Scan lines taken are noted.

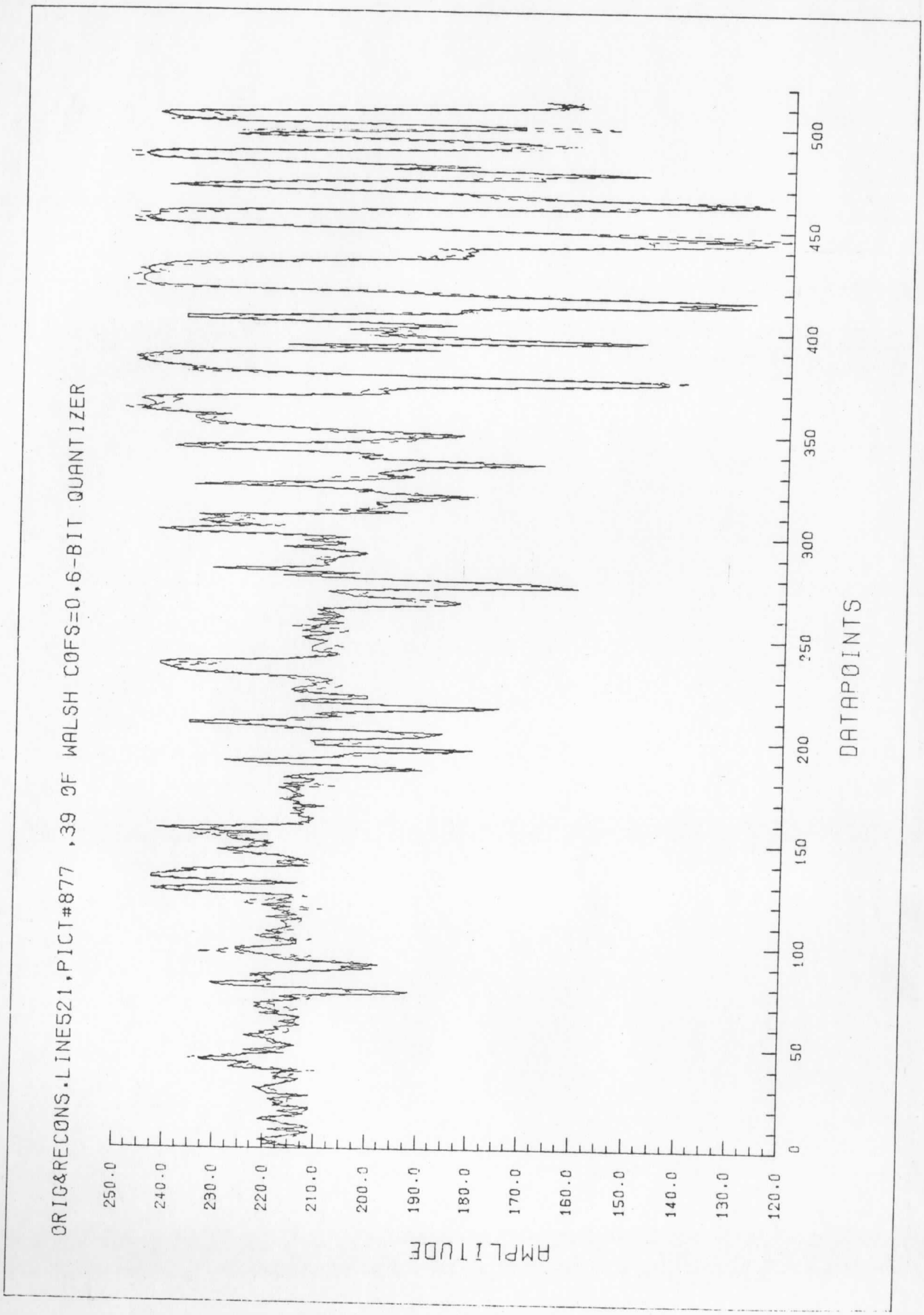
ORIG&RECONS.LINE521,PICT#877 ,39 OF WALSH COFS=0,6-BIT QUANTIZER
AMPLITUDE
250.0
240.0
230.0
220.0
210.0
200.0
190.0
180.0
170.0
160.0
150.0
140.0
130.0
120.0
0
50
100
150
200
250
300
350
400
450
500
DATAPOINTS

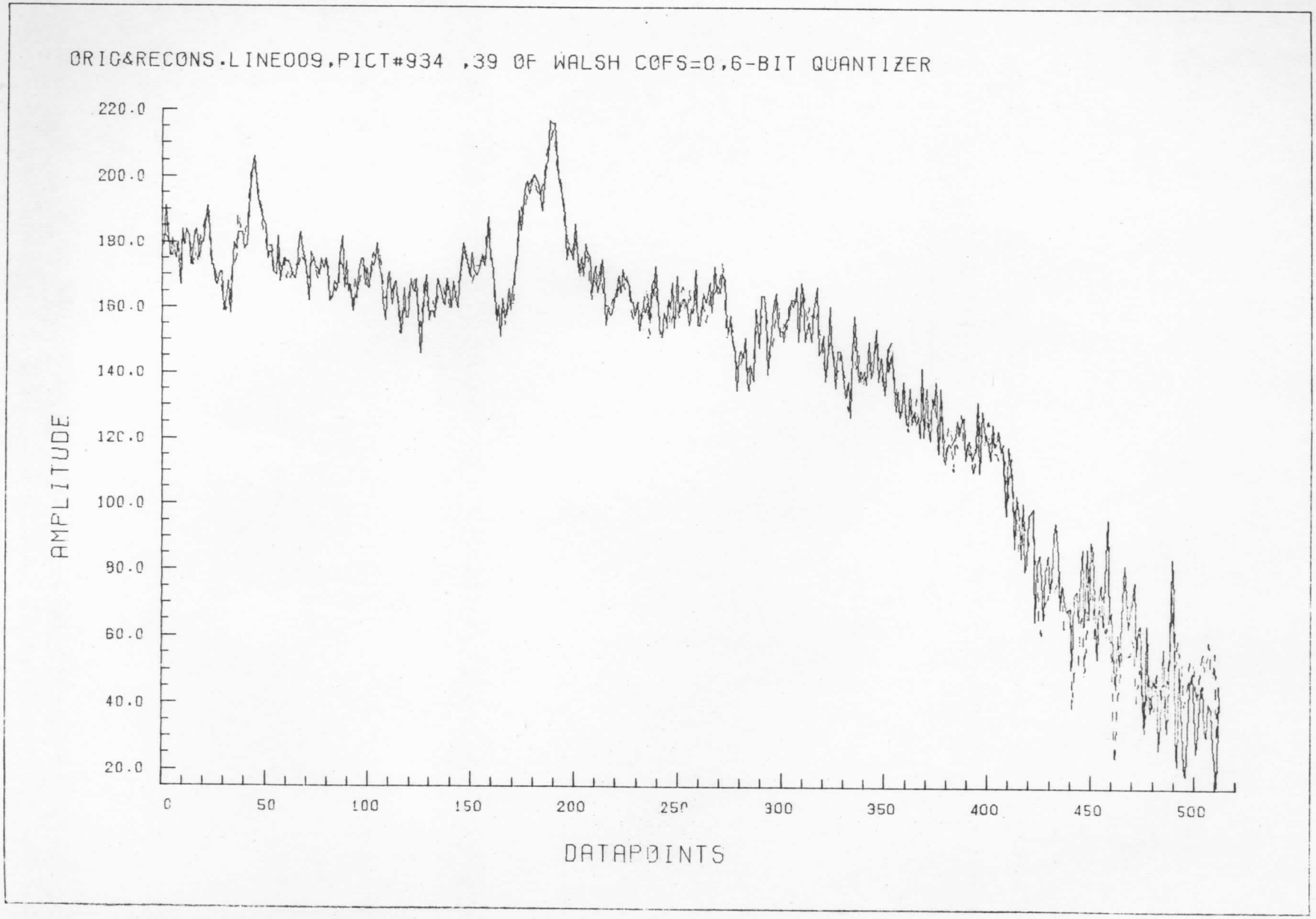
ORIG&RECONS.LINE009,PICT#934 ,39 OF WALSH COFS=0,6-BIT QUANTIZER
220.0
200.0
180.0
160.0
140.0
120.0
100.0
80.0
60.0
40.0
20.0
AMPLITUDE
0
50
100
150
200
250
300
350
400
450
500
DATAPOINTS

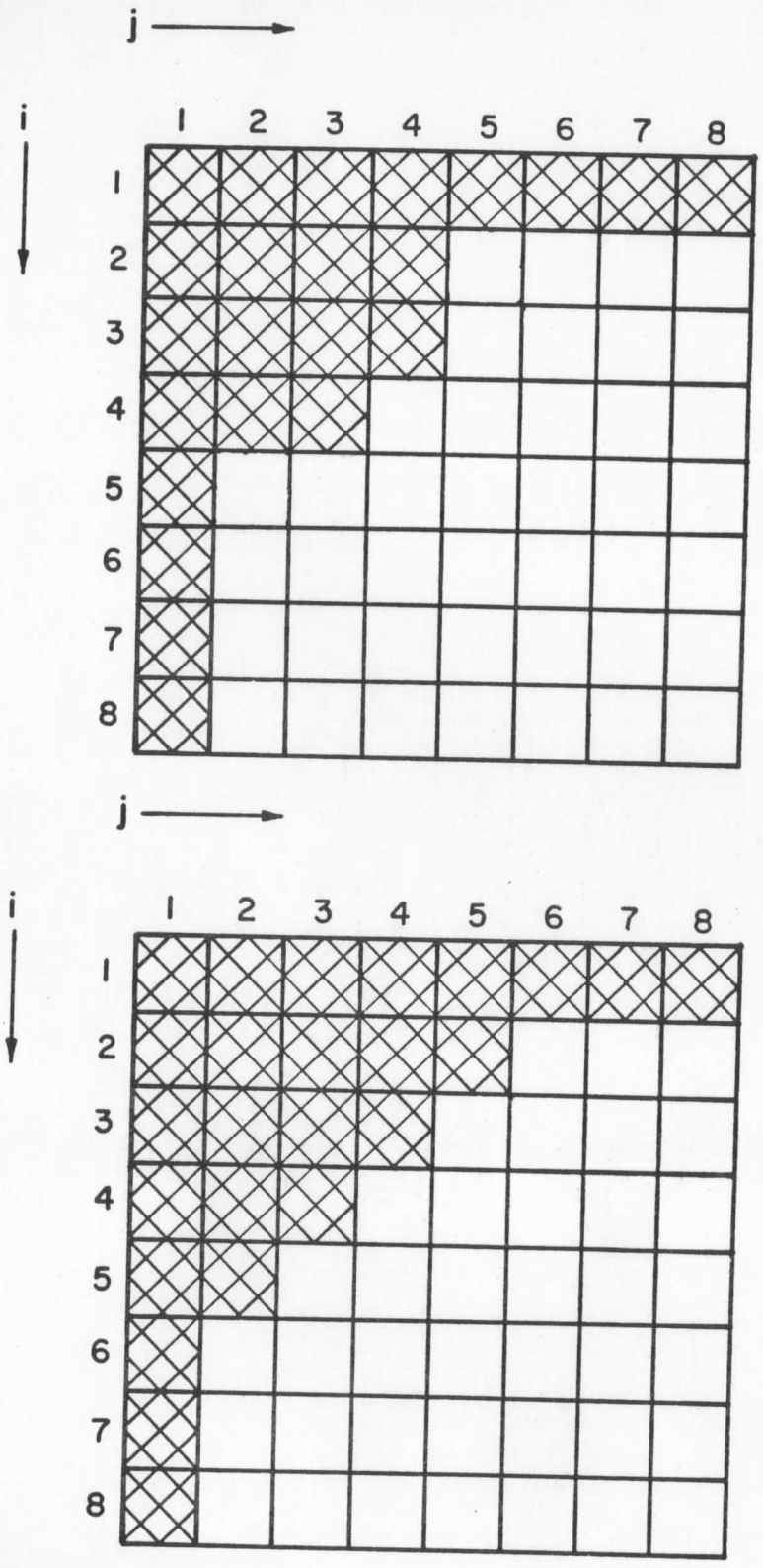

Figure C.2. Diagrams of the Walsh Coefficient Array:
(a) Array to be used for Apollo AS6-2-877, -934, -1430, -1469; coefficients chosen after computing the Walsh coefficients and retaining most significant ones [2];
(b) A symmetrical array under consideration for future work.

FIGURE C.3. HISTOGRAMS OF SOME SELECTED 8×8 WALSH COEFFICIENTS FOR APOLLO AS6-2-877.

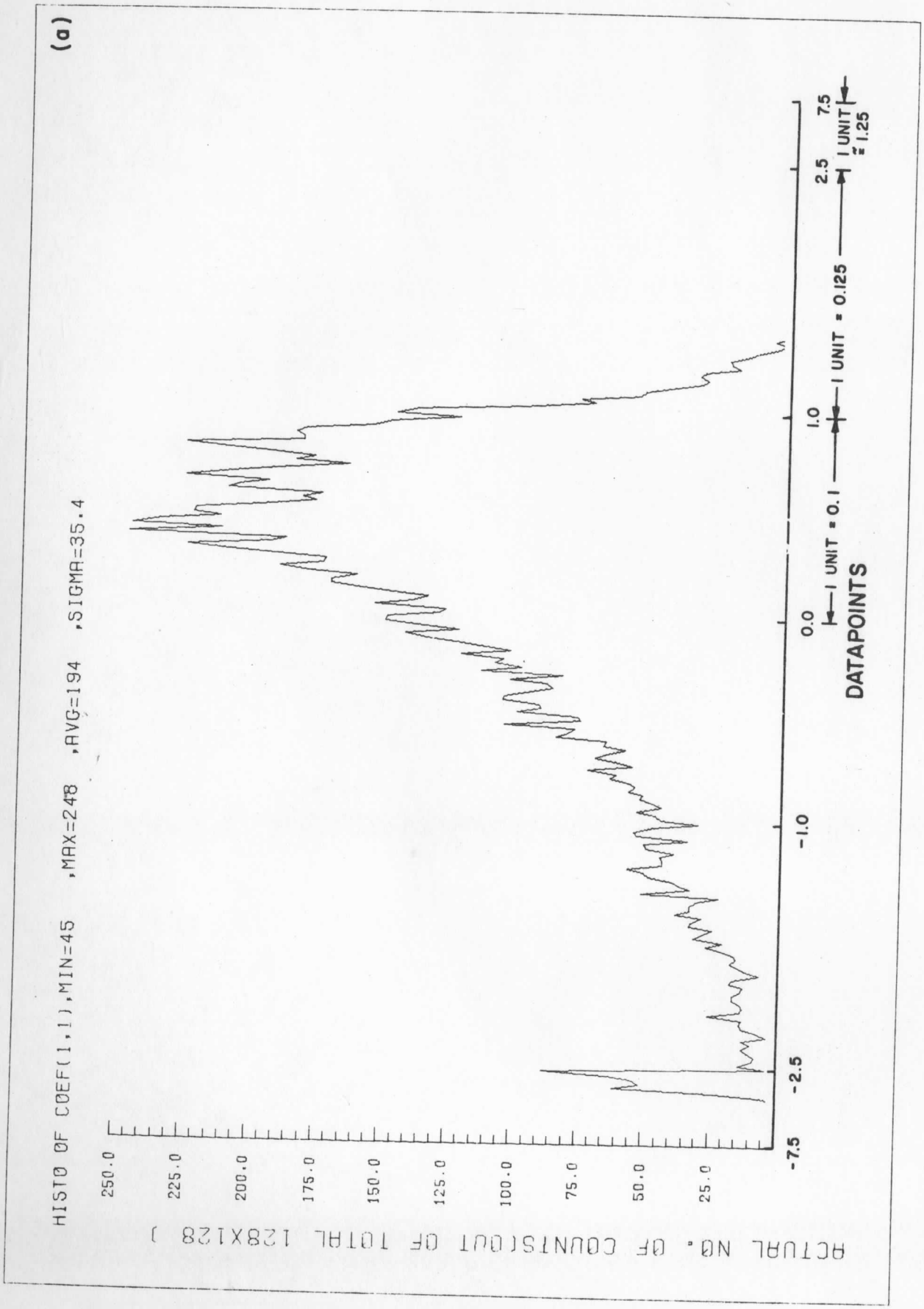
(a)
HISTO OF COEF(1,1),MIN=45 ,MAX=248 ,AVG=194 ,SIGMA=35.4
ACTUAL NO. OF COUNTSCOUT OF TOTAL 128X128)
250.0
225.0
200.0
175.0
150.0
125.0
100.0
75.0
50.0
25.0
-7.5
-2.5
-1.0
0.0
1.0
2.5
7.5
1 UNIT = 0.1
1 UNIT = 0.125
1 UNIT = 1.25
DATAPOINTS

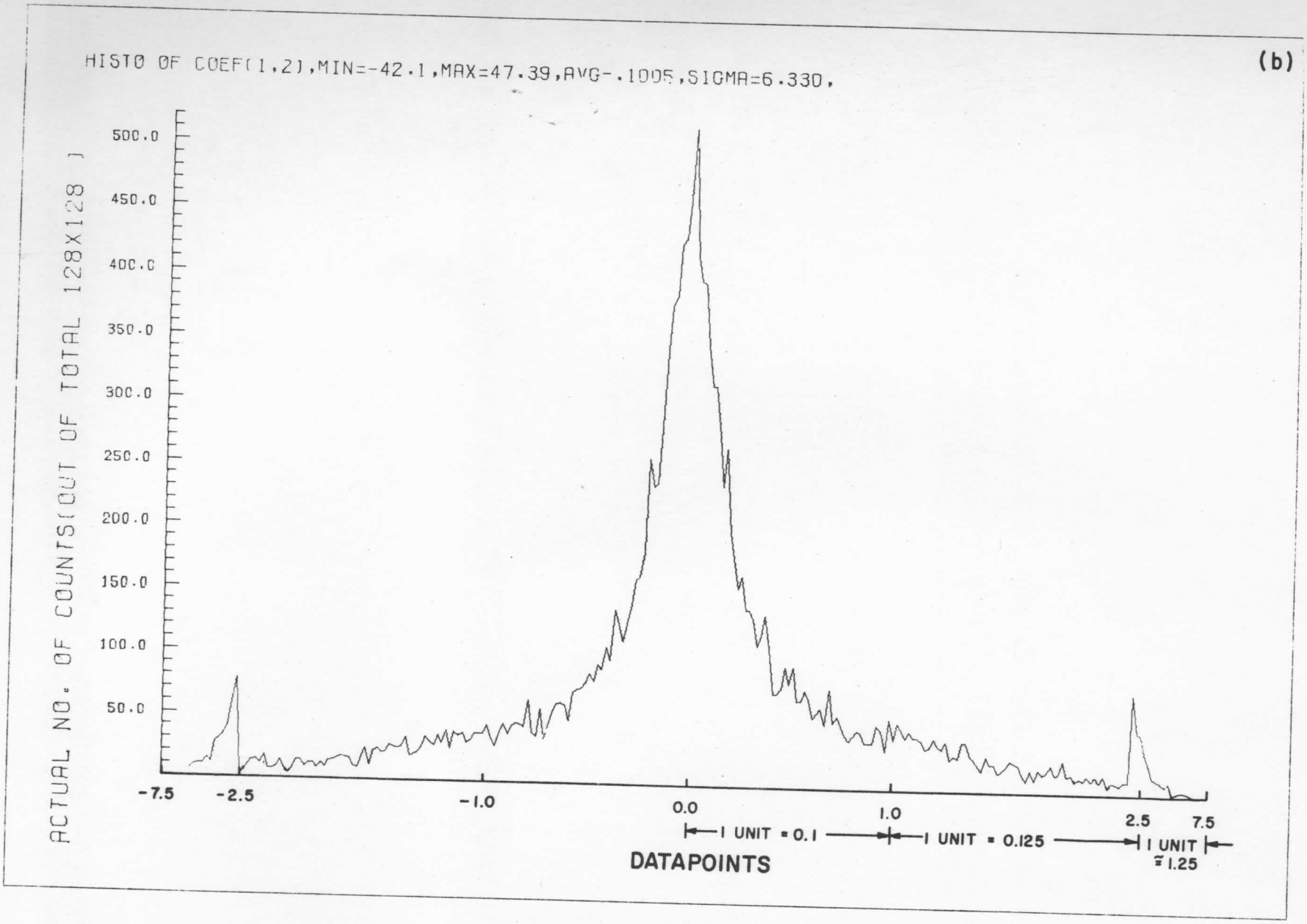
HISTO OF COEF(1,2),MIN=-42.1,MAX=47.39,AVG=-.1005,SIGMA=6.330,
(b)
ACTUAL NO. OF COUNTS(OUT OF TOTAL 128X128)
500.0
450.0
400.0
350.0
300.0
250.0
200.0
150.0
100.0
50.0
-7.5
-2.5
-1.0
0.0
1.0
2.5
7.5
1 UNIT = 0.1
1 UNIT = 0.125
1 UNIT ≈ 1.25
DATAPOINTS

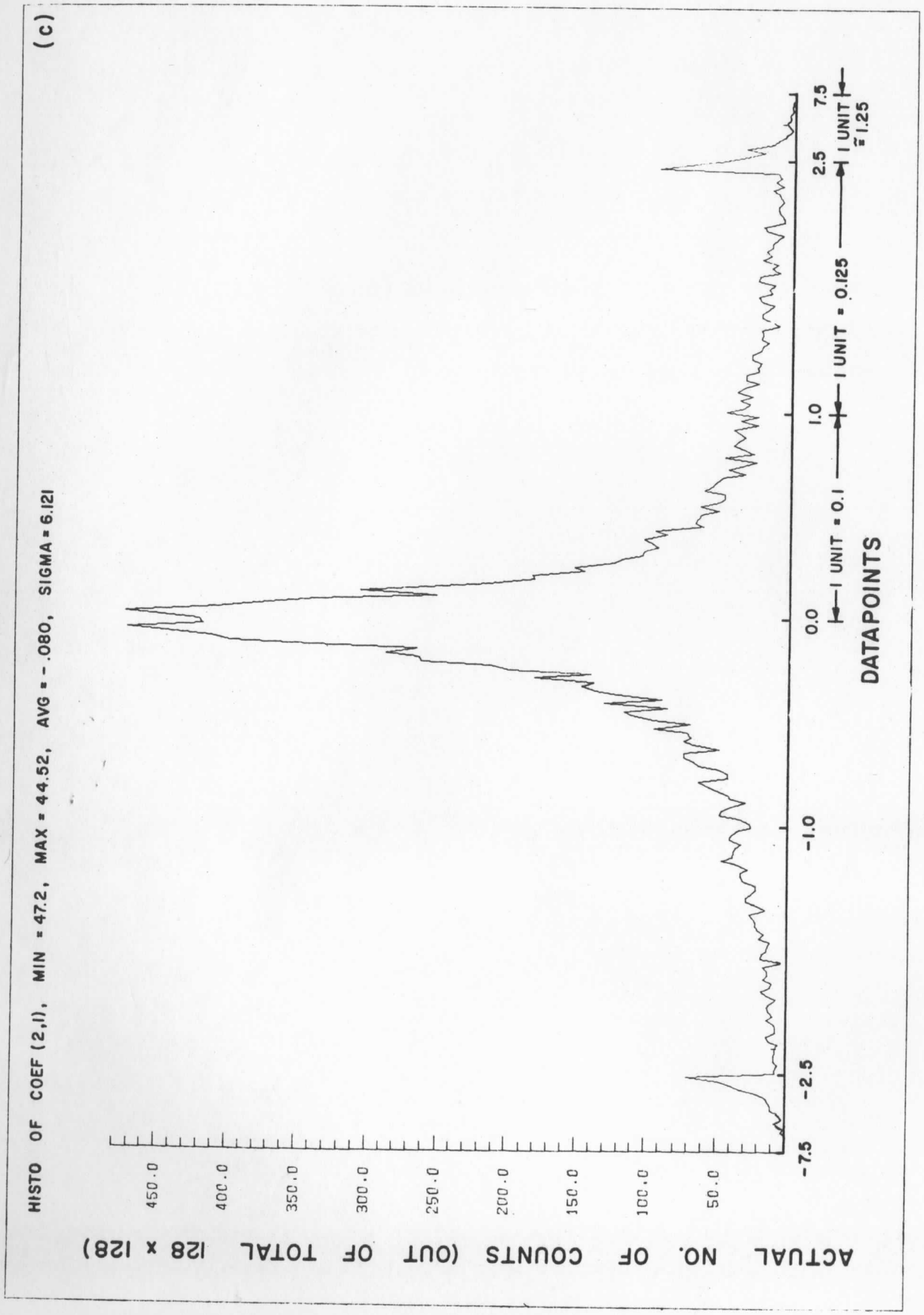
(c)
HISTO OF COEF (2,1), MIN = 47.2, MAX = 44.52, AVG = -.080, SIGMA = 6.121
ACTUAL NO. OF COUNTS (OUT OF TOTAL 128 x 128)
450.0
400.0
350.0
300.0
250.0
200.0
150.0
100.0
50.0
-7.5
-2.5
-1.0
0.0
1.0
2.5
7.5
1 UNIT = 0.1
1 UNIT = 0.125
1 UNIT = 1.25
DATAPOINTS

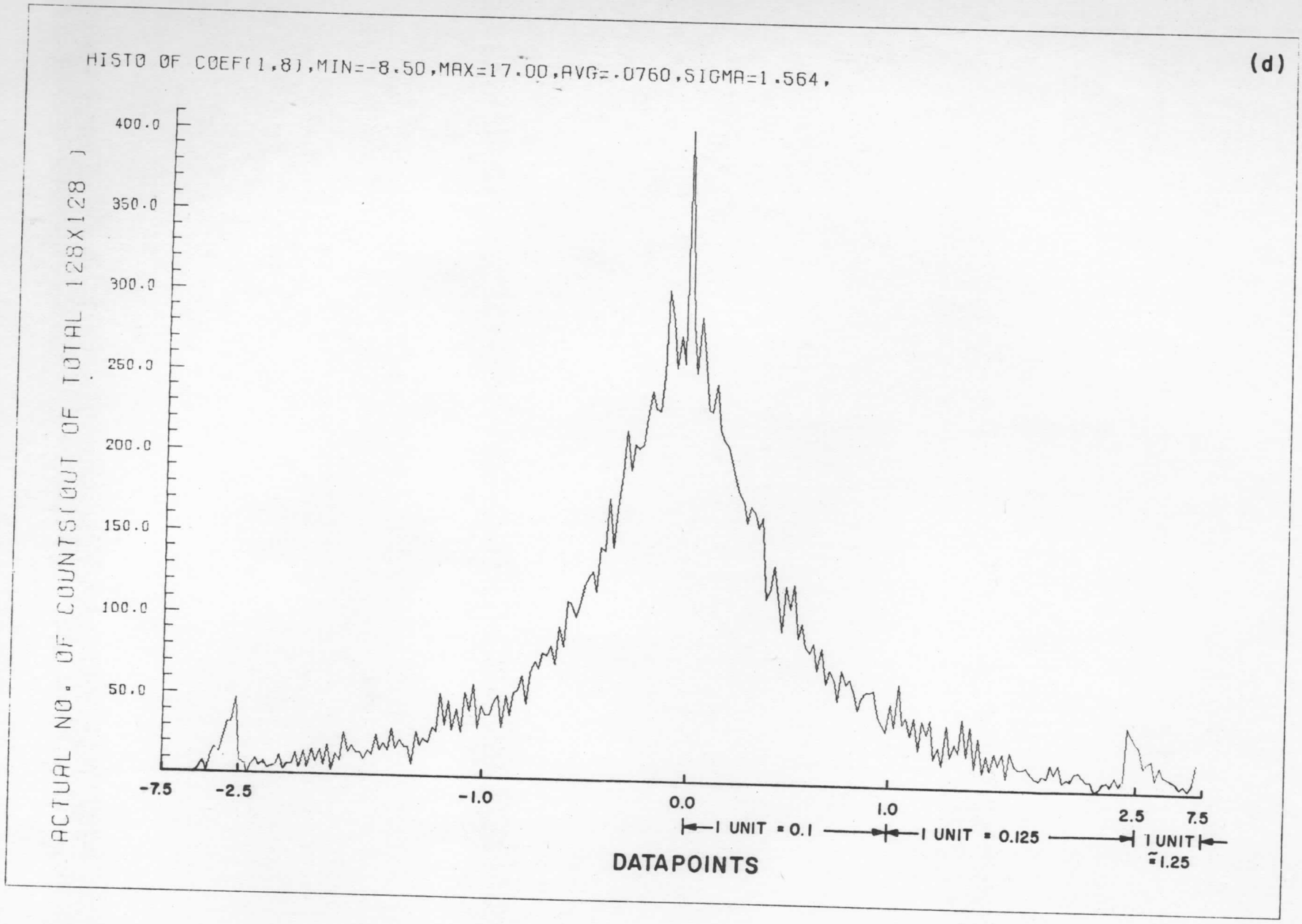
HISTO OF COEF(1,8),MIN=-8.50,MAX=17.00,AVG=.0760,SIGMA=1.564,
(d)
ACTUAL NO. OF COUNTS(OUT OF TOTAL 128X128)
400.0
350.0
300.0
250.0
200.0
150.0
100.0
50.0
-7.5
-2.5
-1.0
0.0
1.0
2.5
7.5
1 UNIT = 0.1
1 UNIT = 0.125
1 UNIT ≈1.25
DATAPOINTS

FIGURE C.4. PROBABILITY DENSITY FUNCTION AT INPUT
OF COEFFICIENT QUANTIZER FOR APOLLO AS6-2-877

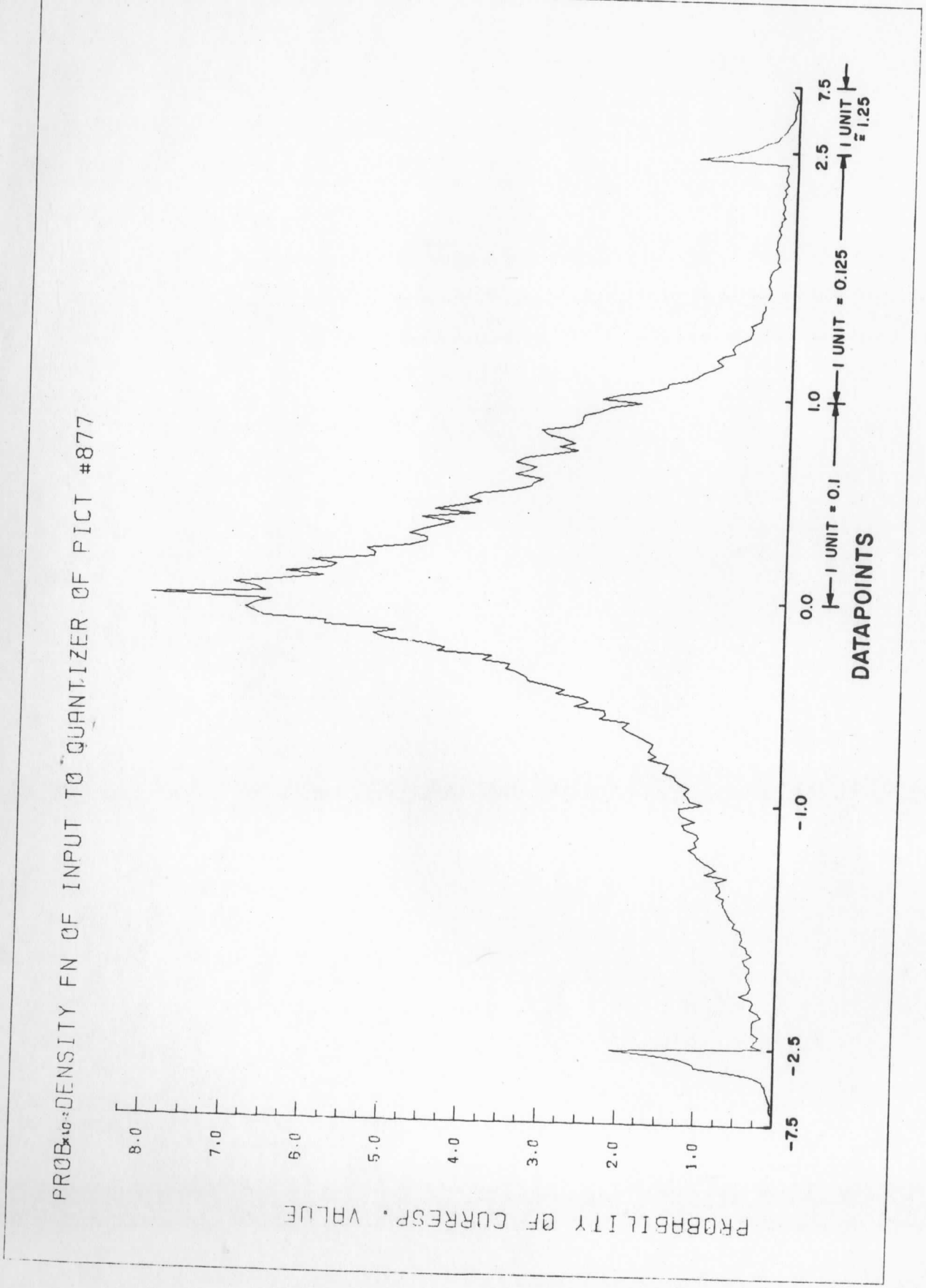
PROB10:DENSITY FN OF INPUT TO QUANTIZER OF PICT #877
PROBABILITY OF CURRESP. VALUE
8.0
7.0
6.0
5.0
4.0
3.0
2.0
1.0
-7.5
-2.5
-1.0
0.0
1.0
2.5
7.5
1 UNIT = 0.1
1 UNIT = 0.125
1 UNIT = 1.25
DATAPOINTS

APPENDIX D
CORRELATION SURFACES FOR THE SMS SYSTEM

We include here some wind measurement surfaces obtained using a correlation metric. Use of this metric generally gives lower secondary peaks and surfaces at the expense of increased computational capacity. Therefore these plots were run on the Univac 1108 rather than the McIDAS system.

Fig. D.1 shows wind measurement surface plots when selected areas in the lower right quarter of Apollo AS6-2-877 were correlated against themselves (autocorrelation). Fig. D.2 shows wind measurement surface plots when the same selected areas were cross-correlated with the output of the SMS simulation program described in Appendix B (but without PMT noise). Note the loss in resolution of the SMS system causes some small cloud indicators to be lost in the measurement. (The small constant shift in the plots in Fig. D.2 results from delays introduced in the SMS filtering and are of no consequence here.) The point scaling is 0.08 n.mi./sample.

FIGURE D.1. SELECTED AUTOCORRELATION MEASUREMENT SURFACES FOR APOLLO AS6-2-877.

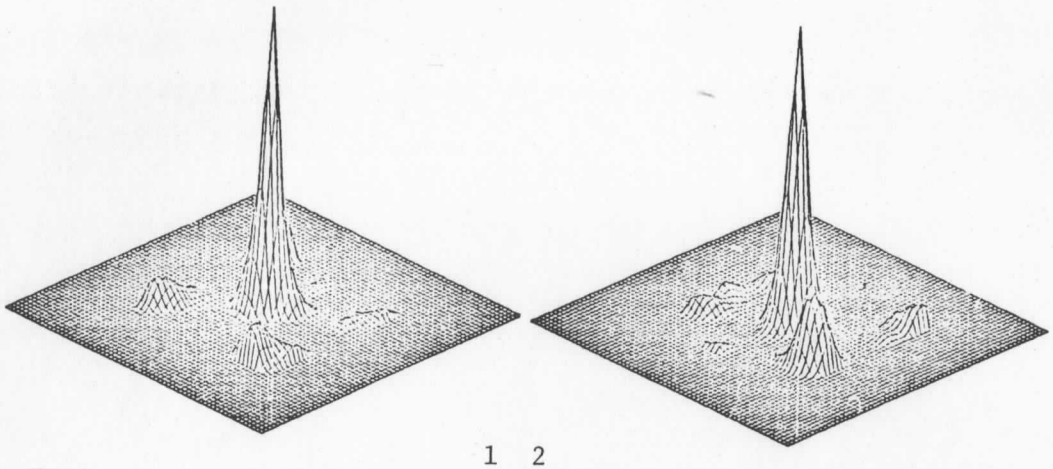

1 2

3 4

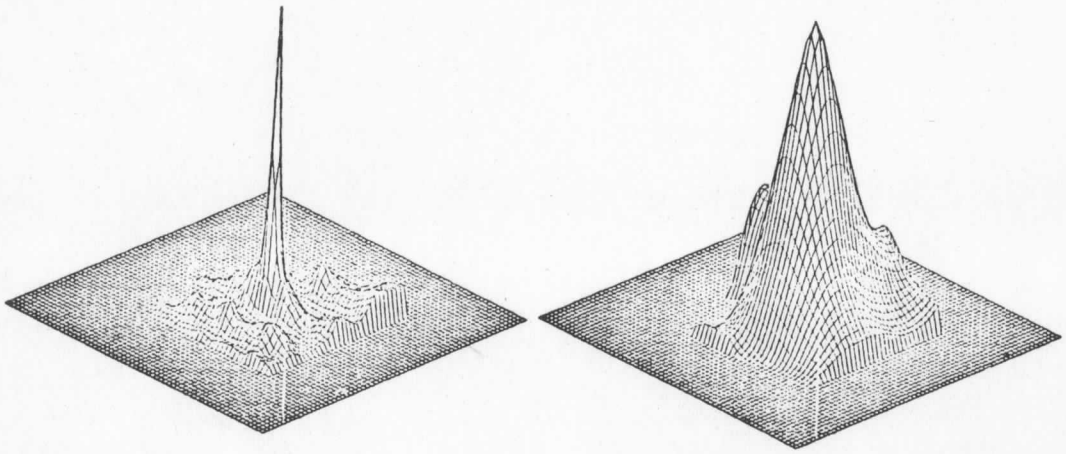

Apollo AS6-2-877
Correlation metric
Original data (8-bit)

FIGURE D.2. CROSS-CORRELATION MEASUREMENT SURFACES FOR APOLLO AS6-2-877 AFTER SMS SIMULATION

Notes: 1). Plot numbers correspond to those in Figure D.1.

2). Scale fixed to that used in Figure D.1.